StruSoft

StruSoft FEM-Design

FEM-Design

Theory of Plastic Shells
Reinforced Concrete and Steel

version 1.1
2024

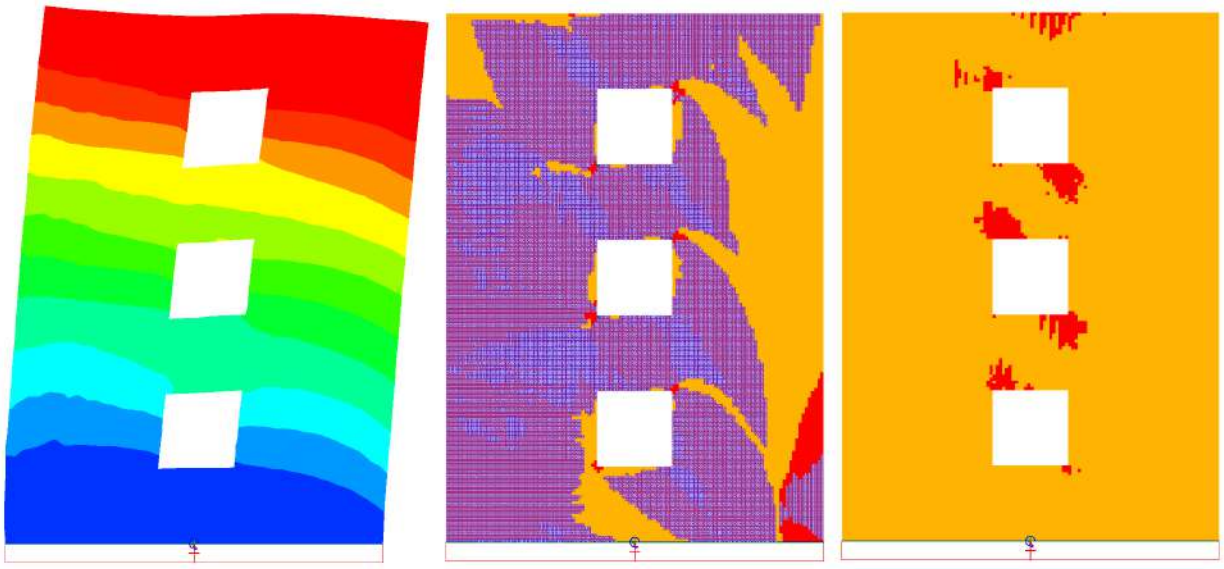

StruSoft AB
Visit the StruSoft website for company and FEM-Design information at
www.strusoft.com

Theory of Plastic Shells
Reinforced Concrete and Steel

Trademarks
FEM-Design is a registered trademark of StruSoft.

Edited by
Zoltán I. Bocskai, Ph.D.
Zoltán Juhász, Ph.D.
StruSoft Ltd., Hungary

Contents

Download link to the example files:

Link to verification example files

List of symbols

Scalars

Latin upper case letters

A_s	area of the reinforcement
A,B,C	constants of parabola fitting
E	elastic modulus in isotropic case
E_c	elastic modulus of concrete
E_s	elastic modulus of steel
E_{Ti}	tangent elastic modulus of the ith hardening section
E_{Ts}	tangent elastic modulus of the steel reinforcement
G	shear modulus in isotropic case
G_{12} ; G_{13} ; G_{23}	shear moduli in the symmetry planes of the orthotropy
G_f	fracture energy of concrete
H_i	hardening modulus of the ith hardening section
I_1	first scalar invariant of the in-plane stresses
J_2	second deviatoric scalar invariant of the in-plane stresses
L	length of the specimen

Latin lower case letters

$a_{s,k}$	specific area of the reinforcement
b	width
d	denotes differential changes, or depth in the verification examples
f	flow field
f_c	compressive strength
f_t	tensile strength
f_y	yield strength
h	height
k_{TS}	parameter of the tension stiffening rules
m_x ; m_y ; m_{xy}	specific bending moments
n	exponent of the parabola function of non-linear concrete section based on EC

n_x ; n_y ; n_{xy} specific normal forces

q_x ; q_y specific transverse shear forces

t total thickness of the shell/plate

z_k^{mid} thickness coordinate of the kth layer

$z_{s,k}$ effective height of the kth steel layer

Greek upper case letters

Δ denotes changes between iterative steps

$\Theta_{s,k}$ angle of the steel layer

Greek lower case letters

α material parameter of the compression flow rule for concrete

β material parameter of the compression flow rule for concrete

β_s shear reduction factor

γ_{yz} ; γ_{xz} ; γ_{xy} engineering shear strains

ε_{0x} ; ε_{0y}; γ_{0xy} mid-plane strains

ε_x ; ε_y ; ε_z normal strains

ε_1 ; ε_2 in-plane principal total strains

$\varepsilon^{cr}{}_n$; $\varepsilon^{cr}{}_m$ crack strains normal to the crack surfaces

ε_{c2} strain at the top of the parabola in the compressed concrete material model

ε_{eq} equivalent strain

$\varepsilon^p{}_{eq}$ equivalent plastic strain

ε_m tension cut-off strain

ε_s reinforcement total strain

$\varepsilon^p{}_s$ reinforcement plastic strain

ε_t strain at crack initiation

ε_u ultimate strain

κ_x ; κ_y ; κ_{xy} curvatures

λ plastic multiplier

ν Poisson's ratio

ν' effectiveness factor of cracked concrete

ρ_x, ρ_y reinforcement ratio in x and y directions

σ_x ; σ_y ; σ_z	normal stresses
σ_1 ; σ_2	in-plane principal stresses
σ_n; σ_m	crack stresses normal to the crack surfaces
σ_0	equivalent effective stress
σ_c	compression stress
σ_e	equivalent stress
σ_y	yield stress
σ_s	reinforcement stress
τ_{yz} ; τ_{xz} ; τ_{xy}	shear stresses

Vectors, Matrices, Tensors

$\boldsymbol{\sigma}$	stress tensor with the in-plane stress components
ε_{ij} ; $\underline{\underline{\varepsilon}}$; $\boldsymbol{\varepsilon}$	strain tensor with different notations
$\boldsymbol{\varepsilon}$; $\boldsymbol{\varepsilon}^e$; $\boldsymbol{\varepsilon}^p$	total,elastic and plastic strain vector of the in-plane strains
$\boldsymbol{\varepsilon}_0$	vector of ε_{0x}, ε_{0y}, γ_{0xy} total mid-plane strains
$\boldsymbol{\varepsilon}_k$; $\boldsymbol{\varepsilon}^e{}_k$; $\boldsymbol{\varepsilon}^p{}_k$	vector of total elastic and plastic mid-plane strains of the k^{th} layer
$\boldsymbol{\kappa}$	vector of κ_x, κ_y, κ_{xy} total curvatures
$\boldsymbol{\gamma}$	vector of γ_{xz}, γ_{yz} total transverse shear strains
a	plastic flow vector
m	vector of specific moments
n	vector of specific normal forces
D	in-plane elastic material stiffness matrix
$\mathbf{D}^{ep}$	in-plane elasto-plastic material stiffness matrix in the local CS
$\overline{\mathbf{D}}$	bending stiffness matrix in the local CS
$\overline{\mathbf{B}}$	eccentricity (coupling) stiffness matrix in the local CS
$\overline{\mathbf{A}}$	membrane stiffness matrix in the local CS
$\underline{\underline{T}}_{(3x3)}$	transformation matrix to the in-plane stiffnesses from local to global CS
$\mathbf{K}_e$	element tangent stiffness matrix in local CS
$\overline{\mathbf{K}}_e^{glob}$	element tangent stiffness matrix in global CS
$\mathbf{F}_e^{int}$	internal nodal forces on element level
$\mathbf{F}_e^{ext}$	external nodal forces on element level

$\mathbf{U}_e$	element displacement matrix
$\mathbf{B}_b$; $\mathbf{B}_m$; $\mathbf{B}_s$	strain-displacement matrices

Abbreviations

CS	Coordinate System
EC	EuroCode
ESLM	Equivalent Single Layer Method
FE	Finite Element
FSDT	First-order Shear Deformation Theory
LM	Layer-wise Model
LPSM	Layered Plastic Shell Model
RC	Reinforced Concrete

Preface

In the first part of this paper we will show the theoretical background of the implemented layered plastic shell model (LPSM). This serves in FEM-Design to model plastic reinforced concrete (RC) and structural steel shells. In the second part the application of the theory and the new LPSM Finite Element (FE) will be shown across verification examples.

To formulate the new plastic shell elements complex techniques have been combined. This makes the FEM-Design 3D Structure module capable to handle plasticity by the linear (standard) and the quadratic (fine) FE shells. The coupled membrane and bending behaviour is covered, as well the ability to model complex yielding through the cross section by a layered or layer-wise model (LM), see Refs. [1] [2] [3] [4] [5].

The LPSM is fully compatible with all the existing elements as it keeps the same equation number of the discretized structure regardless the number of layers by using the same kind of stiffness matrix homogenization as the laminated FE shells Ref. [5].

Another advantage is that the LM is applicable in a general commercial structural finite element (FE) software with arbitrary geometry of shell regions and boundary conditions with additional solid, shell and bar elements, because the degrees of freedom are compatible to each other.

The LPSM shell uses the first-order shear deformation shell theory (FSDT) or in other name the Reissner-Mindlin theory, see Ref. [6]. This is in accordance with the former regular orthotropic shells in FEM-Design Refs. [7] [8]. As a general structural analysis tool, the calculation results of the LPSM shells are the displacements and internal forces, which provide an appropriate result to design check. The in-plane stresses are calculated based on an elasto-plastic manner according to Ref. [9], whereas the out-of-plane components are based on elastic theory. Moreover results about the failure mode of the finite elements like concrete crushing, cracking and steel fracture are also available.

Application of the LPSM shells is the analysis calculation of RC and structural steel shells. It means that in the analysis FE calculation some of the design process of reinforced concrete and steel will be involved into the calculation directly due to the complex plastic material model, with the failure of the structure can be captured.

Speaking about shell model the proposed calculation method is mainly valid in the following dimension range: $0.01 < t/L < 0.1$, where t is the thickness of the LPSM shell and L is the average span length.

The precondition of using this new plastic shell calculation is a deep knowledge of shell theory Refs. [6] [7], and understanding the basics of elasto-plastic theory Refs. [1] [9].

Basic definition

A **plate/shell** is a structural element, its geometric configuration is a three-dimensional solid whose **thickness is small compared to its other dimensions**.

These basic assumptions by the mechanical model of a plate/shell results that when somebody would like to calculate a plate/shell (such as a surface RC structure) the appropriate mechanical model is a plate/shell model instead of a beam model. Thus during the modelling of a surface structure we should use a mechanical model which applicable by a surface structure namely e.g. plate/shell theory. It means that (ignoring some special cases) the beam model is not applicable to calculate a surface structure. If someone uses a beam model to design a surface structure the results can be misleading and the solution could be very uneconomical.

1 Few words about plasticity

1.1 Overview of the solution with the LPSM

In FEM-Design modelling of non-reversible material behaviour is covered by elasto-plastic theory (Fig. 1a). The combination of the material model with the layered FSDT shell element results in the LPSM element, which allows to create elasto-plastic structural models (example shown in Fig. 1b and makes possible to simulate yielding of RC and Structural Steel shells and follow non-linear load-displacement relationship as Fig. 1c shows.

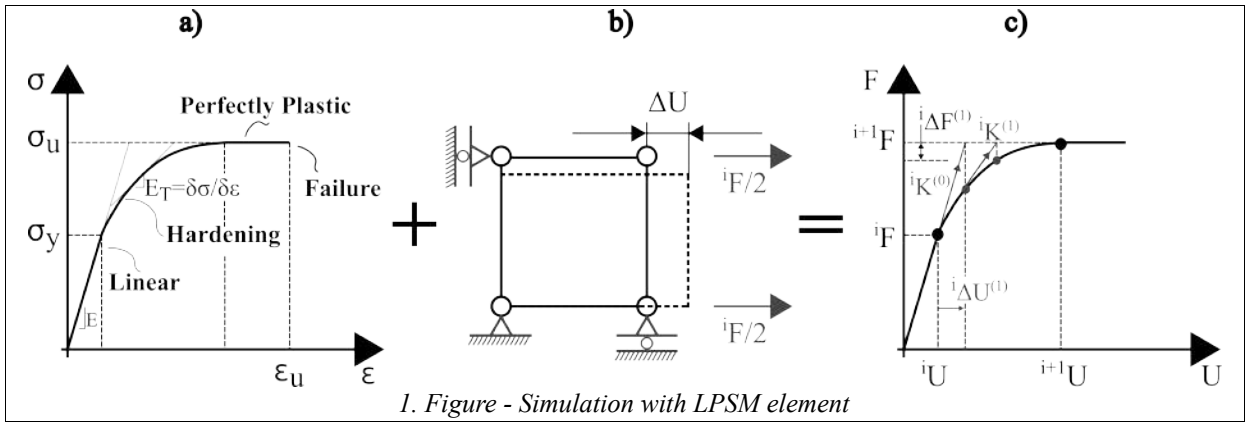

1. Figure - Simulation with LPSM element

To follow the equilibrium path like the one in Fig. 1c iterative method is used. Thus advancing from one equilibrium point to the next load level predictions are made by using the tangent stiffness matrix of the previous solution and the corresponding stress resultants are calculated according to the material law. The difference between the external load level and the stress resultants results the ΔF unbalanced forces which is equilibrable by corrective iterations Ref. [9]. This solution process is equivalent with the plastic beam and connection solution of FEM-Design.

In this solution method the plastic algorithm has three roles during the FE solution:

1. Satisfying the yield condition to ensure the material law,
2. Determination of the elasto-plastic material stiffness matrix to provide input for the FE stiffness matrix calculation,
3. Integration of the stress-strain law to provide the stress resultants.

In the next sections the mathematical background of the plastic algorithm will be briefly outlined.

1.2 The elasto-plastic material stiffness matrix formulation for shells

The elasto-plastic theory for LPSM is applied for the in-plane stress components (σ_x, σ_y, τ_{xy}). This means that throughout this chapter the $\boldsymbol{\sigma}$ and $\boldsymbol{\varepsilon}$ vectors denote vectors containing the three in-plane components in the usual Voigt order.

The flow rule is always composed as the difference of an equivalent stress σ_e and the actual σ_0 yield stress:

$$f(\boldsymbol{\sigma}) = \sigma_e(\boldsymbol{\sigma}) - \sigma_0 \tag{1.1}$$

where σ_e is composed of the in-plane stresses based on appropriate theories, which will be discussed later, and σ_0 is the equivalent effective stress, usually a result of some material failure tests.

The fundamental relation in small strain plasticity is that a small strain increment is composed of an elastic and a plastic part:

$$d\,\boldsymbol{\varepsilon} = d\,\boldsymbol{\varepsilon}^e + d\,\boldsymbol{\varepsilon}^p \tag{1.2}$$

where the plastic strain can be expressed using associative plasticity as follows Ref. [10]:

$$d\,\boldsymbol{\varepsilon}^p = d\,\lambda \frac{\partial f}{\partial \boldsymbol{\sigma}} = d\,\lambda\,\boldsymbol{a} \tag{1.3}$$

where $d\lambda$ is the rate of the plastic multiplicator (a positive multiplier). The prefix d denotes *rate* or in engineering sense *small change* of the prefixed quantity.

With this approximation the material stiffness matrices and the global structural stiffness matrices remain symmetric. This is a time and memory-saving advantage during the calculation, see Ref. [9].

In general plasticity plastic strains occur during yielding when

$$f(\boldsymbol{\sigma}) = 0 \tag{1.4}$$

and

$$\left(\frac{\partial f}{\partial \boldsymbol{\sigma}}\right)^T d\,\boldsymbol{\sigma} = 0 \tag{1.5}$$

where the latter equation is the so called normality rule, which ensures that $d\boldsymbol{\varepsilon}^p$ is normal to the flow field.

If the yield function $f(\boldsymbol{\sigma}) < 0$, then after a small increment the stress state is linear elastic. With geometrical representation this means that the stress state is located inside the flow field. If the yield function $f(\boldsymbol{\sigma}) \geq 0$, then the stress state reached the end of the linear elastic behaviour. In this case a plastic strain increment will arise. According to the normality rule (1.5) the direction of the plastic strain is given if the direction of the stress increment is known. To relate the stress increment of the actual stress state to the total strain increment the additive split of strains (1.2) and the Hooke's law, can be used:

$$d\,\boldsymbol{\sigma} = \boldsymbol{D}\,d\,\boldsymbol{\varepsilon}^e = \boldsymbol{D}\left(d\,\boldsymbol{\varepsilon} - d\,\boldsymbol{\varepsilon}^p\right) = \boldsymbol{D}\,d\,\boldsymbol{\varepsilon} - \boldsymbol{D}\,d\,\boldsymbol{\varepsilon}^p \tag{1.6}$$

where $\mathbf{D}$ is the in-plane linear elastic material stiffness matrix assuming isotropic elasticity:

$$\boldsymbol{D} = \frac{E}{1-\nu^2}\begin{bmatrix} 1 & \nu & 0 \\ \nu & 1 & 0 \\ 0 & 0 & (1-\nu)/2 \end{bmatrix} \tag{1.7}$$

During FE calculation a finite strain and finite stress increment are given in one load-step. Therefore it looks reasonable to rearrange (1.6) to:

$$d\,\boldsymbol{\sigma} = \boldsymbol{D}^{ep}\,d\,\boldsymbol{\varepsilon} \tag{1.8}$$

where $\mathbf{D}^{ep}$ is the so-called elasto-plastic material stiffness matrix, which can be obtained by substituting (1.3) into (1.6) and expressing $d\lambda$ using (1.5) with combination of (1.6) Ref. [9]. All of this results in:

$$\boldsymbol{D}^{ep} = \boldsymbol{D} - \boldsymbol{D}\left(\frac{\boldsymbol{a}\boldsymbol{a}^T\boldsymbol{D}}{\boldsymbol{a}^T\boldsymbol{D}\boldsymbol{a}}\right) \tag{1.9}$$

Based on (1.9) it is obvious that the elasto-plastic material stiffness matrix is symmetric, if the linear elastic perfectly plastic material model is associated (the yield function equivalent to the plastic potential).

1.3 Hardening in the plasticity model

The non-linear hardening section of the characteristic curve of a material (example shown in Fig. 1a) can be described using hardening theories. In FEM-Design the section between linear-elastic and perfectly-plastic zones is approximated by using n number of piecewise linear hardening lines as Fig. 2 shows.

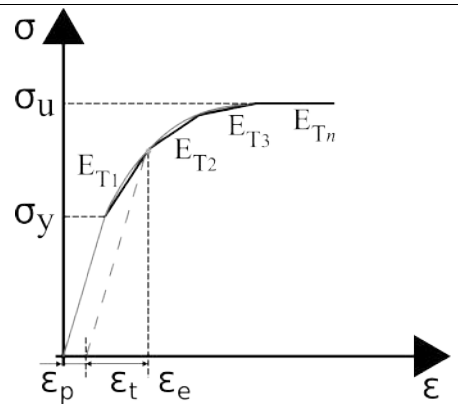

2. Figure - Piecewise linear hardening in one dimension

To follow this path the fixed yield stress in (1.1) is replaced to a function: $\sigma_0(\varepsilon^p_{eq})$, which can be formulated along the first linear piece by using isotropic strain hardening Ref. [9]:

$$\sigma_0\left(\varepsilon^p_{eq}\right) = \sigma_y + H_1\varepsilon^p_{eq} \tag{1.10}$$

where H_1 is the plastic hardening modulus corresponding to the 1^{st} linear section:

$$H_1 = \frac{E_{T1}}{1 - E_{T1}/E} \tag{1.11}$$

For the further sections this can be generalized straightforwardly.

In (1.10) ε^p_{eq} is the equivalent plastic strain, a history variable, which establishes the connection between the uniaxial material laws and the in-plane strain state of the LPSM shells:

$$d\,\varepsilon^p_{eq} = B(\boldsymbol{\sigma})\,d\,\lambda \tag{1.12}$$

where $B(\sigma)$ can be derived based on the corresponding flow rule Ref. [9].
As the yield stress varies during hardening (1.10), the normality condition (1.5) becomes:

$$df = \boldsymbol{a}^T d\boldsymbol{\sigma} - H_i d\varepsilon_{eq}^p \tag{1.13}$$

And repeating the derivation given in Section 1.2 the elasto-plastic tangent matrix can be obtained with hardening included:

$$\boldsymbol{D}^{ep} = \boldsymbol{D} - \boldsymbol{D}\left(\frac{\boldsymbol{a}\boldsymbol{a}^T\boldsymbol{D}}{\boldsymbol{a}^T\boldsymbol{D}\boldsymbol{a} + B(\sigma)H_i}\right) \tag{1.14}$$

1.4 Returning map algorithm

The solution method outlined in Section 1.1 results that after an increment the stress state can move outside the flow field $f(\boldsymbol{\sigma}) > 0$ as Fig. 3 shows.

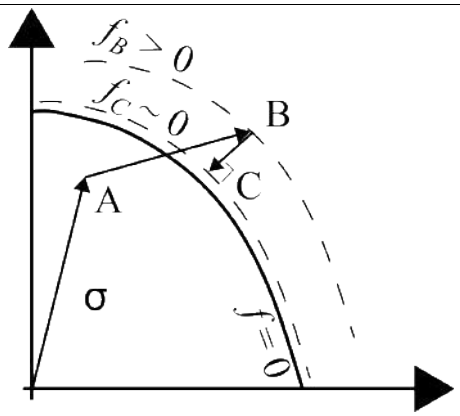

3. Figure. Return to the flow field

This condition is non-admissible therefore to fulfil the plastic flow rule from point B a plastic return has to be applied. In-FEM design this is done by an implicit method Ref. [9]:

$$\boldsymbol{\sigma}_C = \boldsymbol{\sigma}_B - \Delta\lambda\,\boldsymbol{D}\boldsymbol{a}_c \tag{1.15}$$

where $\mathbf{a}_c$ is the normal of the flow field in point C and equals to the direction of the plastic strain according to (1.3). The equation above is solved by using an iterative algorithm where the first estimation is made based on the normal in point B and a corrector step is applied according to the residuum stresses:

$$\boldsymbol{r} = \boldsymbol{\sigma}_C - \boldsymbol{\sigma}_B - \Delta\lambda\,\boldsymbol{D}\boldsymbol{a}_c \tag{1.16}$$

As the normal of the first estimate does not generally equals to the normal in the final point using the residuum further iterations are done until $\boldsymbol{\sigma}_c$ satisfies the flow rule with the prescribed accuracy: $f(\boldsymbol{\sigma}_c) < f_{TOL}$.

2 Calculation with the layered plastic shell model

2.1 Layerwise stresses

To be able to capture the through-thickness variation the FE shells are divided into *n* arbitrary number of layers as Fig. 4. shows.

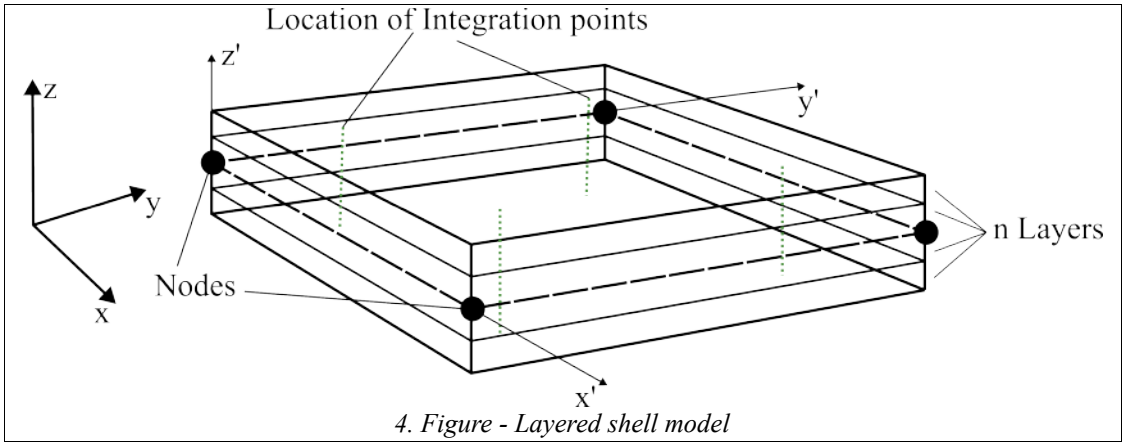

4. Figure - Layered shell model

During the incremental solution of a FE model as shown in Fig. 1, we can express the total shell strains for each shell element in each integration point according to the Reissner-Mindlin or in other name the First Order Shear Deformation plate Theory (FSDT). For this the ${}^{i}\mathbf{U}_{e}$ element nodal solution vector has to be used Ref. [6]:

$$\begin{bmatrix} \boldsymbol{\kappa} \\ \boldsymbol{\varepsilon}_0 \\ \boldsymbol{\gamma} \end{bmatrix} = \begin{bmatrix} \boldsymbol{B}_b \\ \boldsymbol{B}_m \\ \boldsymbol{B}_s \end{bmatrix} {}^{i}\boldsymbol{U}_e \tag{2.1}$$

where on the left side:

$\boldsymbol{\kappa}$ – is the vector of κ_x, κ_y, κ_{xy} total curvatures [rad/m],

$\boldsymbol{\varepsilon}_0$ – is the vector of ε_{0x}, ε_{0y}, γ_{0xy} total mid-plane strains [-].

$\boldsymbol{\gamma}$ – is the vector of γ_{xz}, γ_{yz} total transverse shear strains [-].

calculated in the reference plane of the shell using the local shell coordinate system denoted by the ' sign in Fig. 4. On the right $\boldsymbol{B}_b$, $\boldsymbol{B}_m$, and $\boldsymbol{B}_s$ are the strain-displacement matrices according to the MITC+ theory Ref. [7]. From these shell strains the in-plane strain components of each layer can be expressed at the middle of the layer as:

$$\boldsymbol{\varepsilon}_k = \boldsymbol{\varepsilon}_0 + \boldsymbol{\kappa}\, z_k^{mid} \tag{2.2}$$

where z_k^{mid} is the through thickness coordinate of the middle of the k^{th} layer measured from the reference plane (mid-plane) of the shell as Fig. 5 shows.

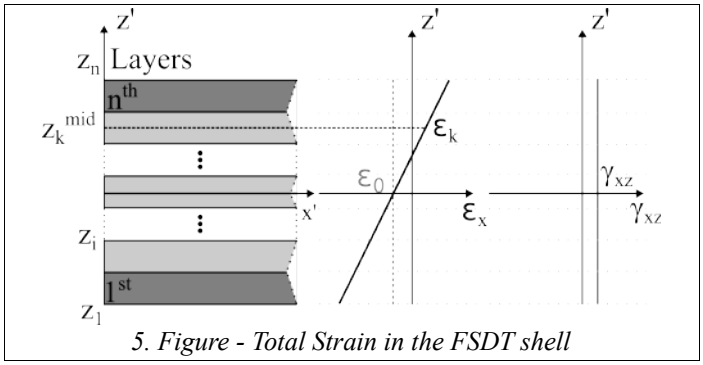

5. Figure - Total Strain in the FSDT shell

$\boldsymbol{\varepsilon}_k$ consists of the three in-plane strain components in engineering sense: ε_x, ε_y, γ_{xy}; in accordance with the in-plane stress components introduced for plastic calculations in Section 1.2. The out-of-plane shear strains (γ_{xz}, γ_{yz}) are considered to be constant through the shell thickness in accordance with the FSDT theory Ref. [6].

If the material point is elastic, the in-plane stresses at the middle of the layer can be calculated as:

$$\boldsymbol{\sigma}_k = \boldsymbol{D}\,\boldsymbol{\varepsilon}_k \tag{2.3}$$

similarly the transverse stresses will be:

$$\begin{bmatrix}\tau_{xz}\\ \tau_{yz}\end{bmatrix} = \begin{bmatrix}G_{13} & 0\\ 0 & G_{23}\end{bmatrix} \cdot \begin{bmatrix}\gamma_{xz}\\ \gamma_{yz}\end{bmatrix} \tag{2.4}$$

where G_{13}, G_{23} are the out-of plane shear moduli and the equation above is valid along the thickness as Fig. 5 shows.

Advancing along the equilibrium path shown in Fig. 1 we will reach the point, where the stresses calculated in the layers based on the total strains will violate the material law (1.4). In this case the stress state will lie outside the flow filed, thus return mapping has to be applied as it was shown in Section 1.4 in Fig. 3. During the return from point B to C the material law is satisfied in each layer by calculating appropriate plastic strains. Thus in plastic state of a material point the stress-strain law for the in-plane components can be formulated as:

$$\boldsymbol{\sigma}_k = \boldsymbol{D}\,\boldsymbol{\varepsilon}_k^e = \boldsymbol{D}\left(\boldsymbol{\varepsilon}_k - \boldsymbol{\varepsilon}_k^p\right) \quad . \tag{2.5}$$

These calculated plastic strains and their increments in (1.2) are serving as a state variable during the solution of the FE system.

An example is shown in Fig. 6, where the top and the bottom layers are already in plastic state. Furthermore Fig. 6 shows the constant stress assumption which states: if the stress in the middle of a layer reaches the yield stress, from that point the whole layer is considered to be in plastic state, hence the stress state will move on the yield surface and will be constant through the thickness of the layer. This means that the equivalent stress in (1.1) in the layer will equal to the yield stress.

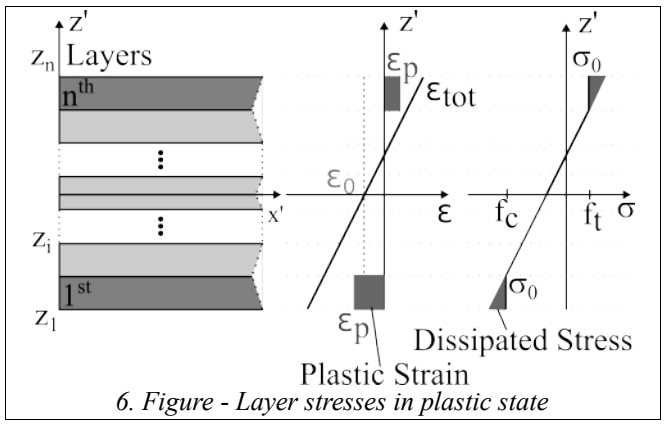

6. Figure - Layer stresses in plastic state

Applying this approach in each layer and each integration point of the FE shell the plastic material model and the corresponding algorithm presented in Sections 1.2-1.4 can be integrated.

2.2 Calculation of stress resultants

After calculation of the stress state in all layers the stress resultants in an integration point can be obtained by simple integration over the thickness layer-by-layer which gives the following form for the in-plane stress-resultants:

$$\begin{bmatrix} \boldsymbol{m} \\ \boldsymbol{n} \end{bmatrix} = \sum_{k=1}^{n} \int_{z_{k-1}}^{z_k} \begin{bmatrix} \boldsymbol{\sigma}_k z \\ \boldsymbol{\sigma}_k \end{bmatrix} dz \tag{2.6}$$

where $\boldsymbol{m}$ is the vector of specific moments and $\boldsymbol{n}$ is the vector of specific normal forces. Similarly the transverse shear forces can be calculated based on the transverse stresses.

In case of elastic state all layers are homogeneous, hence the relationship between stress resultants and strains is the following well known formula:

$$\begin{bmatrix} m_x \\ m_y \\ m_{xy} \\ n_x \\ n_y \\ n_{xy} \end{bmatrix} = \begin{bmatrix} \frac{E t^3}{12(1-\nu^2)} & \frac{\nu E t^3}{12(1-\nu^2)} & 0 & 0 & 0 & 0 \\ \frac{\nu E t^3}{12(1-\nu^2)} & \frac{E t^3}{12(1-\nu^2)} & 0 & 0 & 0 & 0 \\ 0 & 0 & \frac{G t^3}{12} & 0 & 0 & 0 \\ 0 & 0 & 0 & \frac{E t}{1-\nu^2} & \frac{\nu E t}{1-\nu^2} & 0 \\ 0 & 0 & 0 & \frac{\nu E t}{1-\nu^2} & \frac{E t}{1-\nu^2} & 0 \\ 0 & 0 & 0 & 0 & 0 & G t \end{bmatrix} \begin{bmatrix} \kappa_x \\ \kappa_y \\ \kappa_{xy} \\ \varepsilon_{0x} \\ \varepsilon_{0y} \\ \gamma_{0xy} \end{bmatrix}, \tag{2.7}$$

whereas for the out of plane components in case of a homogeneous Reissner-Mindlin shell we can write Ref. [6]:

$$\begin{bmatrix} q_x \\ q_y \end{bmatrix} = \begin{bmatrix} \frac{5}{6} G t & 0 \\ 0 & \frac{5}{6} G t \end{bmatrix} \begin{bmatrix} \gamma_{xz} \\ \gamma_{yz} \end{bmatrix} \tag{2.8}$$

where E, G and ν are the elastic modulus, shear modulus and Poisson's ratio in case of isotropy and t is the thickness of the shell.

On the left sides of (2.7) and (2.8) the values are the internal forces of a shell, namely:

m_x, m_y, m_{xy} – specific bending moments [kNm/m] (elements of $\boldsymbol{m}$),

n_x, n_y, n_{xy} – specific normal forces [kN/m] (elements of $\boldsymbol{n}$),

q_x, q_y – specific transverse shear forces [kN/m] (elements of $\boldsymbol{q}$).

In case, if at least one layer is in plastic condition equation (2.7) has to be adapted according to the constant stress assumption. So the in-plane stress resultant are determined as follows:

$$\begin{bmatrix} \boldsymbol{m} \\ \boldsymbol{n} \end{bmatrix} = \sum_{k=1}^{n} \begin{bmatrix} \boldsymbol{\sigma}_k t_k z_k^{mid} \\ \boldsymbol{\sigma}_k t_k \end{bmatrix} dz \tag{2.9}$$

The transverse shear forces can always be calculated based on (2.8) due to the assumption introduced in Chapter 1, that only the in-plane stresses are involved in plasticity.

The stress resultants calculated in each integration point can be converted to nodal forces simply by using:

$$\boldsymbol{F}_e^{int} = \int \begin{bmatrix} \boldsymbol{B}_b \\ \boldsymbol{B}_m \\ \boldsymbol{B}_s \end{bmatrix}^T \begin{bmatrix} \boldsymbol{m} \\ \boldsymbol{n} \\ \boldsymbol{q} \end{bmatrix} dA \tag{2.10}$$

Converting these vectors from the element local coordinate system to the global and compiling all elements over the whole FE structure the $\Delta \boldsymbol{F}$ unbalanced forces visualized in Fig. 1 can be determined:

$$\Delta \boldsymbol{F} = \boldsymbol{F}^{ext} - \boldsymbol{F}^{int} \tag{2.11}$$

2.3 Homogenization method for the formulation of the element stiffness matrix

As it was discussed the presented plastic material model is fitted into a layered model Ref. [11]. For the iterative solution presented in Section 1.1 the necessary internal forces have already been presented based on the plastic theory. In this section the formulation of the element stiffness matrix will be briefly presented.

To be compatible with other finite elements with respect to number of degrees of freedom and number of equations the well known Equivalent Single Layer Method (ESLM) theory have been applied to formulate a homogenized matrix from all of the layers Ref. [5].

The main modification compared to the standard ESLM theory is to replace the elastic material matrix **D** to the elasto-plastic matrix $\mathbf{D}^{ep}$, which equals either to (1.9) or (1.14) depending on the applied plasticity model. Or it can be $\mathbf{D}^{ep}$=**D** given in (1.7) if the material is in elastic state.

As it was shown in (1.8), that $\mathbf{D}^{ep}$ is a tangent material stiffness matrix which establishes connection between the current stress and strain increments. Fitting these tangent matrices into the homogenization method of the ESLM theory the $\bar{\boldsymbol{D}}$, $\bar{\boldsymbol{A}}$ and $\bar{\boldsymbol{B}}$ bending, membrane and eccentricity (coupling) stiffness matrices can be formulated as:

$$\begin{aligned} \bar{\boldsymbol{A}} &= \sum_{k=1}^{n} \boldsymbol{D}^{ep}{}_k \left(z_{k+1} - z_k \right) \\ \bar{\boldsymbol{B}} &= \frac{1}{2} \sum_{k=1}^{n} \boldsymbol{D}^{ep}{}_k \left(z_{k+1}^2 - z_k^2 \right) \\ \bar{\boldsymbol{D}} &= \frac{1}{3} \sum_{k=1}^{n} \boldsymbol{D}^{ep}{}_k \left(z_{k+1}^3 - z_k^3 \right) \end{aligned} \tag{2.12}$$

where $\mathbf{D}^{ep}$ is the elasto-plastic material stiffness matrix given in the x'-y'-z' local coordinate system according to Fig. 4.

These $\bar{\boldsymbol{D}}$, $\bar{\boldsymbol{A}}$ and $\bar{\boldsymbol{B}}$ homogenized matrices are expressing the current tangent material stiffness in the local coordinate system considering the actual state of all layers in an integration point.

From these matrices the element stiffness matrix can be formulated using numerical integration:

$$\boldsymbol{K}_e = \sum_{i=1}^{int.\ point} \int \boldsymbol{B}_b^T \bar{\boldsymbol{D}}_i \boldsymbol{B}_b + \boldsymbol{B}_m^T \bar{\boldsymbol{A}}_i \boldsymbol{B}_m + \boldsymbol{B}_b^T \bar{\boldsymbol{D}}_i \boldsymbol{B}_m + \boldsymbol{B}_m^T \bar{\boldsymbol{A}}_i \boldsymbol{B}_b + \boldsymbol{B}_s^T \bar{\boldsymbol{S}}_i \boldsymbol{B}_s \, dA \qquad (2.13)$$

where in the last term $\bar{\boldsymbol{S}}$ is the shear matrix which can be calculated similarly as the membrane matrix using the matrix in (2.8) Ref. [5]. Summation in the equation above goes over all of the integration points and the resultant $\boldsymbol{K}_e$ is the element tangent stiffness matrix in the local CS according to the actual plastic state of the LPSM finite element. Based on this tangent stiffness matrix in the local CS, the global element tangent stiffness matrix $\bar{\bar{\boldsymbol{K}}}_e$ can be formulated with the aim of the appropriate transformation matrix from local to global system, $\underline{\underline{T}}_{(3x3)}$.

2.4 Plasticity in use with respect of the LPSM shell element

The discussed element stiffness matrix and stress resultants considering plasticity serves as fundamental building blocks of the LPSM solution. To follow the equilibrium path during a finite element calculation in each iteration a linear prediction is made as discussed in Section 1.1 and shown in Fig. 1. This linearization based on the tangent of the previous point causes drift-off from the equilibrium path, and cause that the internal stress state crosses the flow field as shown in Fig. 3 when we moved from point A to B.
To avoid this drift-off the three roles of the plastic calculation discussed in Section 1.1 has to be applied layer-by-layer in each integration point.

1. An example is shown in Figure 6, where the elastic trial stress exceeds the yield stress in the top and bottom layers, thus the $f(\boldsymbol{\sigma}) \geq 0$ condition activates the plastic algorithm of the LPSM element. The algorithm will first satisfy the flow rule and return the stresses in each layer by calculating the corresponding plastic strains. As it is shown in Fig. 6, during plastic calculation the whole layer is assumed to be plastic. To simplify calculation in this state LPSM uses the strain data in the middle of the layer for calculating the elastic trial stress and the returned stress will be constant through the whole layer. Hence the number of layers determines the resolution of the stress distribution through the thickness for each elements.
2. Next, based on the returned stresses the $\mathbf{D}^{ep}$ stiffness matrices will be generated for each layer and $\boldsymbol{K}_e$ will be evaluated according to Section 2.3.
3. Similarly, the internal forces in the integration points can be calculated according to (2.8) and (2.9) using the layer-wise stresses, and $\Delta\boldsymbol{F}$ can be formulated based on Section 2.2.

Note that transverse shear related quantities are calculated based on elastic theory regardless of the state of the layers. Therefore these stress resultants can always be calculated from the out of plane strains based on the FSDT theory, and similarly the corresponding elements in the stiffness matrix are determined based on the out-of-plane shear moduli of the layers Ref. [12].

Applying these three steps a general non-linear finite element solution can be accomplished as it is shown in Fig. 1 using a traditional Newton-Raphson solution Ref. [9].

3 Constitutive laws of structural steel shells

3.1 General steel behaviour

It is well known that steel exhibits plastic flow under constant stress, which can be modelled by perfectly plastic theory. This assumption is adopted in FEM-Design for modelling structural steel shell. This is an excellent approximation for mild steel, which is the most common steel type due to its relatively low price. The corresponding stress strain curve of a general mild still is shown in Fig. 7. In case of other types of steel like high-carbon or high-tensile steels the perfectly plastic theory is still a good engineering choice, although these types may show some more hardening after yielding Ref. [13].

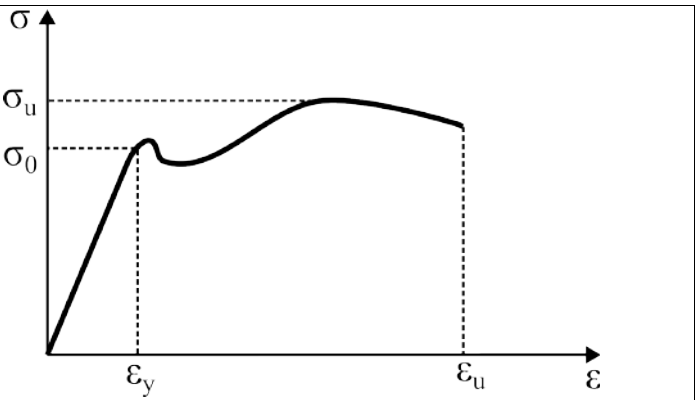

7. Figure - Stress-strain curve of a mild steel

Steels have the remarkable feature that their crystalline structure causes that only the shear stress alone has an effect on the yielding, and plastic volume change is negligible even in case of large plastic deformations. This is why the octahedral shear stress condition of von Mises shows a very good agreement with experimental data and this rule without plastic hardening is generally adopted for establishing the stress-strain law for metals.

3.2 Plasticity in case of structural steel

In FEM-Design plastic yielding of steel shells is covered by the von Mises theory assuming elastic perfectly plastic material. As mentioned before only in-plane plastic flow is considered which results in the following σ_e equivalent stress in the flow rule given by (1.1):

$$\sigma_e = \sqrt{3J_2} = \sqrt{\sigma_x^2 + \sigma_y^2 - \sigma_x \sigma_y + 3\tau_{xy}^2} \tag{3.1}$$

where J_2 is the second scalar invariant of the deviatoric stresses based on the in-plane stress components. The shape of this flow field in the σ_1-σ_2 plane is the well known ellipse shown in Fig. 8.

Substituting the equivalent stress given in (3.1) into (1.1) all the necessary structures for the plastic calculation can be derived based on Section 1.2.

For structural steel perfectly plastic behaviour is assumed, thus the hardening given in Section 1.3 can be omitted during the derivation.

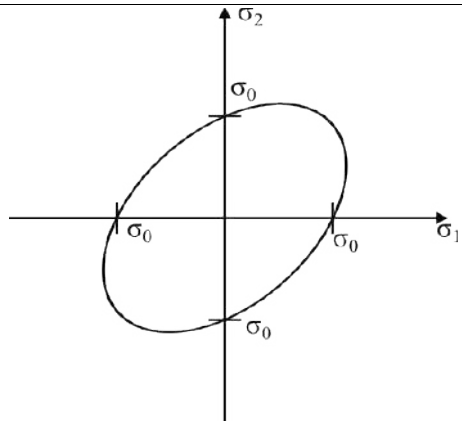

8. Figure - The von Mises flow field

3.3 Fracture of structural steel

Because perfectly plastic behaviour is assumed after reaching the yield stress portions of the structure may suffer displacements without any control, therefore to give a better estimation for the deflection and load bearing capacity the fracture point of the steel is monitored during the simulation. Fig. 9 shows the idealized version of Fig. 8, where the ultimate limit strain is denoted by ε_u. After reaching ε_u fracture in the corresponding layer of the material point is assumed. In case of fracture a sudden release of stresses is assumed and the contribution of that layer in the specific integration point to the structural tangent stiffness is assumed to vanish:

$$\boldsymbol{D}^{ep} = \mathbf{0} \tag{3.2}$$

Applying this damage model the behaviour of the structure can be captured accurately near the end of the load carrying capacity of the structure.

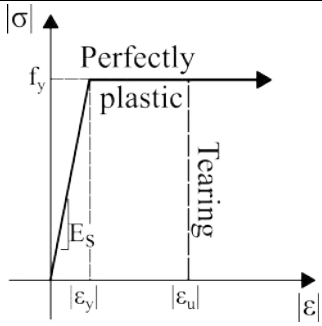

9. Figure - Elastic-Perfectly Plastic material law of steel

To be able to use the fracture strain defined by uniaxial measurements, FEM-Design defines an equivalent total strain which relates the multiaxial strain state to the uniaxial criteria Ref. [9]:

$$\varepsilon_{eq} = \sqrt{3 J_2} = \sqrt{\left(\varepsilon_1^2 - \varepsilon_1 \varepsilon_2 + \varepsilon_2^2\right)} \tag{3.3}$$

where ε_1 and ε_2 are the in-plane total principal strains. Comparing ε_{eq} to ε_u the damage model can be applied to complex loading situations.

This equivalent strain is evaluated based on the $\boldsymbol{\varepsilon}_k$ mid-layer strains except in case of the outermost top and bottom layers, where the strains of the external fibres are used to calculate ε_{eq}.

4 Constitutive laws of reinforced concrete shells

4.1 Concrete

4.1.1 General concrete behaviour

Before discussing the numerical modelling of concrete in finite element environment some typical mechanical properties and experimental stress-strain relations under uniaxial and biaxial states of stress are summarized. Data required for the definition of material model parameters through experimental behaviour is the fundamental basis to develop mathematical models Ref. [3]. Detailed measurement data is especially important in case of concrete which is a very complex composite material consisting of a mixture of aggregate and matrix of mortar. Its stress-strain behaviour is generally determined by the evolution of the initially existing microcracks, which propagation is driven by the external loads. As these phenomena happen on micro-scale, measurement data is essential to develop a phenomenal material model, which captures the macroscopic stress-strain relationship and fits for a continuum FE model.

Uniaxial data is the very basis to create a material model. Typical uniaxial stress-strain curves can be seen in Figs. 10 and 11 representing a 28 days old concrete. Curves are corresponding to concretes having different f_c compression strength. The highly non-linear parabola like behaviour in the compression zone can be seen in Fig. 10. This non-linear behaviour is a result of the existing microcracks especially along the interface of the aggregate particles and mortar. The behaviour in the compression zone is usually assumed to be linear up to 30-40% of the compression strength as until this point the initially existing crack surfaces remain more or less unchanged. Leaving the elastic domain behind the number, width and length of bond cracks increase and form mortar cracks. This is a stable procedure in the compression zone up to the compression strength, but already a damage of the material which is non-reversible. Reaching the maximal compression strength and further increasing the load can lead to evolution of crack zones or internal damage which will cause the degradation of stiffness in form of unstable crack propagation. This last zone is considered to be a mixture of material degradation and the structural behaviour of the specimen. That is why the descending branch cannot be considered to be a pure material behaviour Ref. [13]. This effect was shown by van Mier using specimens with different heights [mm] in a compression test. As Fig. 12 shows the curves are not identical, but their slopes are decreasing with increasing specimen height.

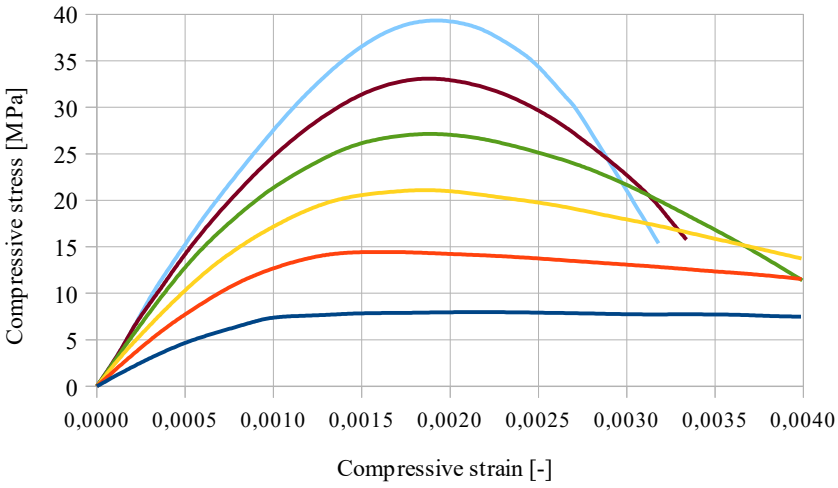

10. Figure - Typical set of uniaxial stress-strain compression curves

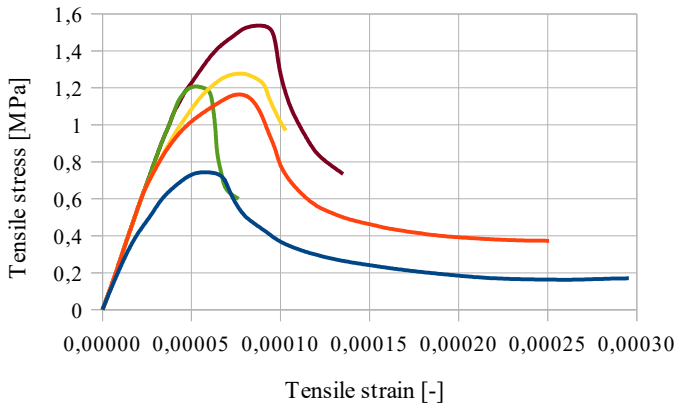

11. Figure - Typical set of uniaxial stress-strain tension curves

In the tension zone (Fig. 11) the elastic behaviour lasts almost up to the f_t tension strength. The modulus of elasticity is usually taken to be the same as in the compression zone. The non-linear zone before reaching f_t is very small therefore it is usually neglected during the formulation of a material model. Near the tension strength the growth of microcracks start, and a very fast propagation of the crack can be observed along the interface of the aggregate and the mortar. This causes the very brittle behaviour of concrete in the tension zone, and that is why the descending part of the stress strain curve is difficult to follow.

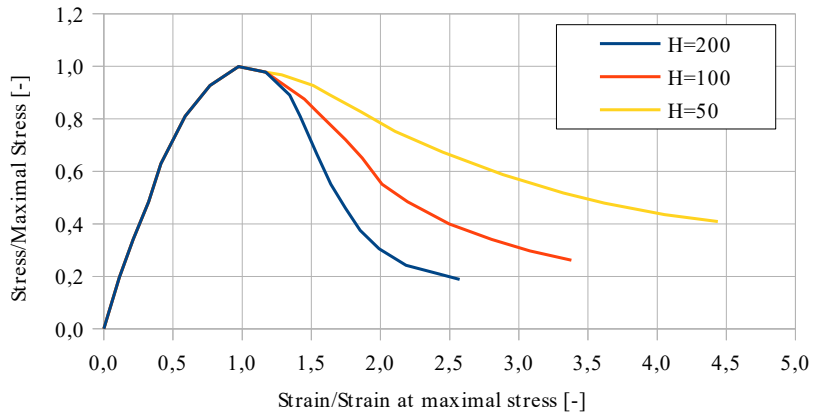

12. Figure - Influence of specimen height (in [mm]) on uniaxial stress-strain curve

To form and adequate material model - beside the uniaxial behaviour - multiaxial measurements are also necessary. The most well known biaxial measurements are done by Kupfer [14], who defined a biaxial failure curve for concrete shown in Fig. 13. To this day this measurement is considered to be one of the most reliable regarding the tested material and boundary conditions of the tests Ref. [3].

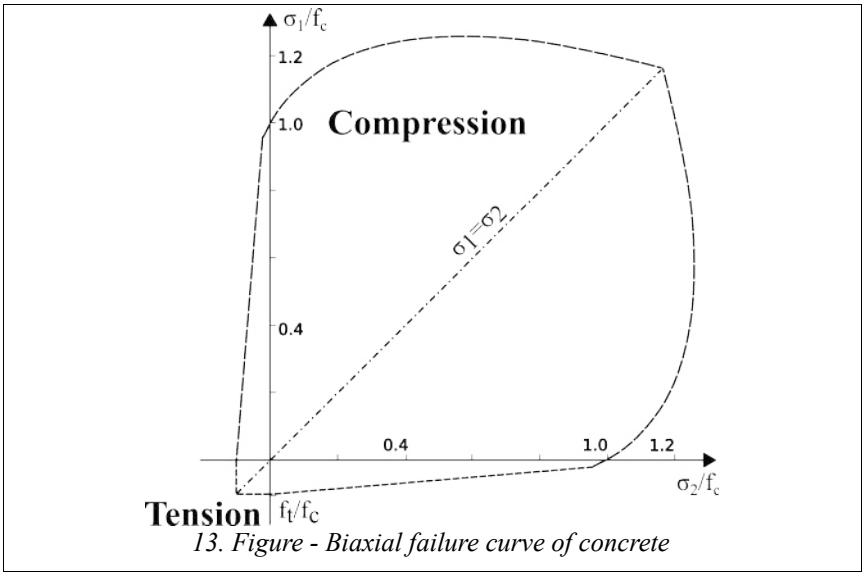

13. Figure - Biaxial failure curve of concrete

The corresponding equations for the curves in the tension, tension-compression, and compression zones are respectively:

$$\sigma_1 = f_t \tag{4.1}$$

$$\frac{\sigma_1}{f_t} + 0.8\frac{\sigma_2}{f_c} = 1 \tag{4.2}$$

$$\left(\frac{\sigma_1}{f_c} + \frac{\sigma_2}{f_c}\right)^2 - \frac{\sigma_1}{f_c} - 3.65\frac{\sigma_2}{f_c} = 1 \tag{4.3}$$

This work showed that in the tension zone the strength of the concrete is not significantly affected by the ratio of the σ_1 and σ_2 tensile stresses.

In the tension-compression zone compressive stress at failure decreases as the tensile stress increases.

In case of biaxial compression Fig. 13 shows very well that the strength of concrete can increase up to 16-20% depending on the σ_1/σ_2 ratio and the concrete class Ref. [14]. This phenomena is attributed to the confinement of the microcracks and the Poisson's ratio Ref. [3]. Combining the presented failure curve in Fig. 13 with the uniaxial stress-strain behaviour in Figs. 10 and 11 the material model for concrete can be developed.

4.1.2 Plasticity in concrete

Concrete is a composite material consists of aggregate and matrix of mortar, which makes its physical behaviour very complex and raises the need for a more complex constitutive law compared to the one presented for steel in Chapter 3. Although being a composite material, the initial state of concrete is assumed to be isotropic and homogeneous in FE scale, hence material matrix can be given by (1.7). Starting from this assumption the material behaviour is captured using a plastic model which falls into the category of phenomenal models. As it was mentioned in Chapter 3 plasticity was originally developed for metals, but from macroscopic point of view concrete shows some similarities regardless of its completely different microstructure. For example the stress-strain law of concrete is also non-linear with a large irreversible strain upon unloading, and concrete subjected to confinement pressure can show ductile behaviour similarly as metals. The irreversible strains in case of concrete are arising due to microcracking instead of crystalline changes, nonetheless plastic theory is capable to treat this effect on macroscopic level.

To cover the curves showed in Section 4.1.1 the plastic model must contain some basic assumptions:

1. An initial yield surface which defines the stress level at which plastic deformation begins. In FEM-Design this is taken to be 40% of the uniaxial compression strength shown in Fig. 14.

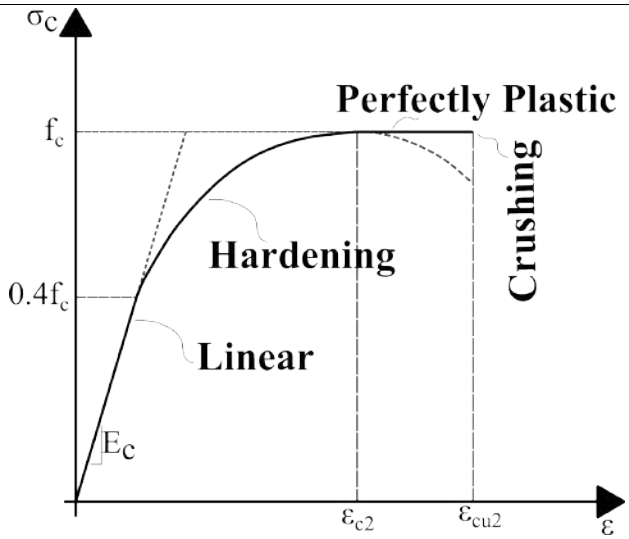

14. Figure - Uniaxial stress-strain law model for compressed concrete

2. A hardening rule which defines the change of the loading surface and material properties

during plastic flow. For this FEM-Design uses the compression zone parabola given by Eurocode EN 1992.1.1 shown in Fig. 15, and defined as:

$$\sigma_c = f_c\left[1-\left(1-\frac{\epsilon_c}{\epsilon_{c2}}\right)^n\right] \tag{4.4}$$

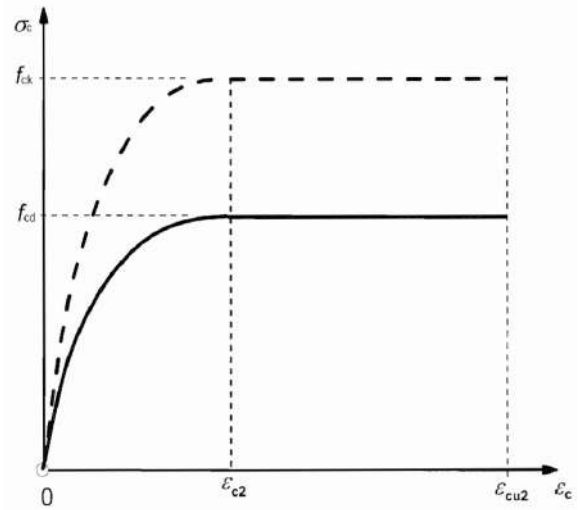

15. Figure - Parabola-rectangle diagram for concrete under compression according to the Eurocode

Where ε_{c2} is the top of the parabola, n is the exponent defined in the EC. This stress-strain curve is used in the 'Hardening' zone shown in Fig. 14, which starts by reaching 40% of the compression strength and lasts up to the compression strength f_c. Note, that throughout Chapter 4 we consequently use f_c to denote the compression strength and do not distinguish between design and characteristic values as it is done in Fig. 15. The real value of the compression strength is always determined in FEM-Design based on the actual settings of the user in accordance with the Eurocode. (In Chapter 5 you can find detailed description about the used parameters for the material model inputs in case of the different limit states). Based on (4.4) the uniaxial stress-strain curve can be expressed and using the discretization given in Section 1.3 the hardening parameters can be estimated for the isotropic strain hardening model, which will be applied for the calculation of compressed concrete.

3. A plastic flow rule is also necessary. It was already stated in Section 1.2 that FEM-Design uses an associated flow rule. In the literature there are also non-associated flow models available for concrete, but from practical point of view FEM-Design uses the normality rule (1.3). Using this assumption concrete can be handled accurately and calculations can be done in an economic way Refs. [3][13]. The potential function for associated flow can be derived based on (1.3) using the equivalent stresses which are defined in the next point.

4. The ultimate strength condition (i.e. failure condition) is set based on the uniaxial tensile and compression strengths and the failure envelope which is developed based on Fig. 13. The crucial point for the development of a numerical model is to find the best compromise between numerical stability and accuracy. In FEM-Design this is done by

the following piecewise flow field:

$$f(\boldsymbol{\sigma}) = \sigma_1 - f_t = 0 \tag{4.5}$$

$$f(\boldsymbol{\sigma}) = 1 - \frac{\sigma_1}{f_c} - \frac{\sigma_2}{f_t} = 0 \tag{4.6}$$

$$f(\boldsymbol{\sigma}) = \alpha I_1 + \sqrt{(3\beta J_2)} - \sigma_0(\varepsilon_{eq}^p) = 0 \tag{4.7}$$

Where σ_1 and σ_2 are the first and second principal stresses respectively to Fig. 16, I_1 is the first scalar invariant, J_2 is the second deviatoric invariant already defined in Section 3.2, and α, β are material constants (α=0.1398, β=1.299). From the three equations above, (4.5) formulates the Rankin failure theory in the tension zone, (4.6) approximates (4.2) - the Kupfer tension-compression zone - by using straight lines, and (4.7) describes the failure curve in the compression zone based on a generalized Prager rule Ref. [10]. In (4.7) $\sigma_0 = f_c$ at failure, otherwise it can be given based on (4.4) applying (1.10) and (1.11) from Section 1.3. As (4.7) is dependent on the I_1 mean normal stress the failure curve is able to capture the plastic volume dilatation near failure under pressure conditions Ref. [3]. Using these the failure envelope used in FEM-Design give the curve shown in Fig. 16. Hardening is also visualized in Fig. 16 by expanding the red initial yield surface.

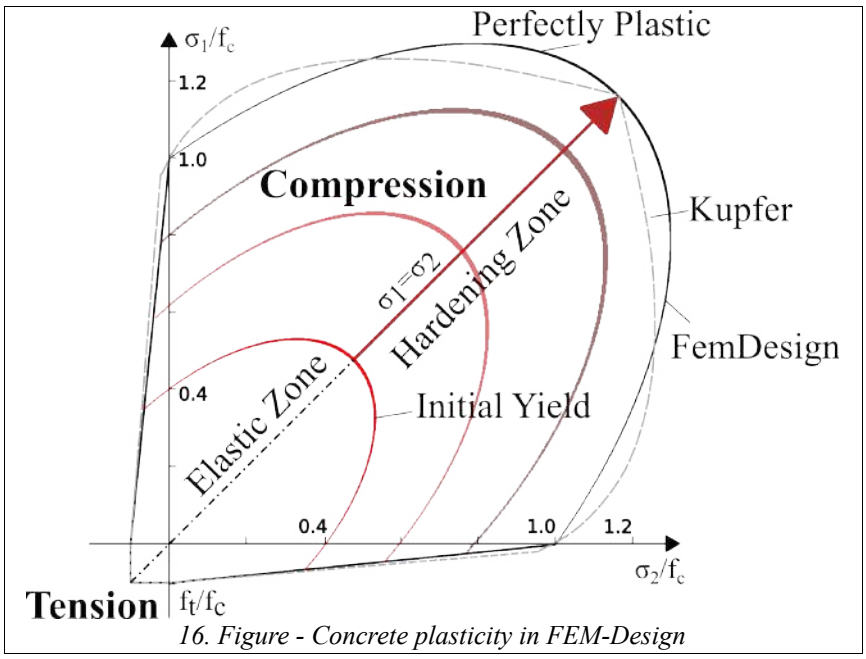

16. Figure - Concrete plasticity in FEM-Design

These points are serving as the very fundament of the plastic model for concrete material in FEM-Design. But as plasticity was originally developed for metals, further considerable extensions of the model are necessary which are discussed in the next sections.

4.1.3 Crushing condition in concrete

Reaching the failure curve shown in Fig. 16 the material model becomes perfectly plastic as suggested by the Eurocode in Fig. 15. This is in accordance with the experimental observations discussed in Section 4.1.1, that the descending part in the compression zone is not a pure material property therefore it is not modelled by the material model in FEM-Design. Instead the

crushing limit of the compressed concrete is implemented and monitored for each material point. The crushing type fracture of concrete is a strain controlled phenomenon, which means that the uniaxial compression limit ε_{cu2} is compared to an equivalent strain, if at least one in-plane principal strain is in compression state ($\varepsilon_2 < 0$). This means, that damage model is applied both in the compression and tension-compression zones. FEM-Design offers several options based on the literature to calculate the equivalent strain ε_{eq}:

- Crisfield rule Ref. [9]:

$$\varepsilon_{eq} = \frac{2}{\sqrt{(3)}} \sqrt{(\varepsilon_1^2 + \varepsilon_1 \varepsilon_2 + \varepsilon_2^2)} \tag{4.8}$$

- Cervera rule Ref. [4]:

$$\varepsilon_{eq} = \sqrt{(\varepsilon_1^2 - \varepsilon_1 \varepsilon_2 + \varepsilon_2^2)} \tag{4.9}$$

- Hinton rule Ref. [1]:

$$\varepsilon_{eq} = 0.1775(\varepsilon_1 + \varepsilon_2) + \sqrt{((0.1775(\varepsilon_1 + \varepsilon_2))^2 + 1.355(\varepsilon_1^2 - \varepsilon_1 \varepsilon_2 + \varepsilon_2^2))} \tag{4.10}$$

- Prager rule:

$$\varepsilon_{eq} = \alpha(\varepsilon_1 + \varepsilon_2) + \sqrt{(\beta(\varepsilon_1^2 - \varepsilon_1 \varepsilon_2 + \varepsilon_2^2))} \tag{4.11}$$

Similarly as in Section 3.3 ε_{eq} is evaluated layer-by-layer and compared to ε_{cu2} to handle complex deformation situations. In the tension-compression zone the ε_1 tension strain is neglected during the calculation of the equivalent strain, if the concrete is cracked Ref. [3]. Reaching the crushing strain limit we consider the material point fully damaged, thus losing all its characteristic strength and rigidity:

$$\boldsymbol{D}^{ep} = \mathbf{0} \tag{4.12}$$

and its contribution to the vector of stresses will be zero as well assuming an immediate stress release.

4.1.4 Cracking effect in concrete

4.1.4.1 Cracking model

Cracking is a complex phenomenon which mainly drives the tensile failure of concrete, and it is a major factor of the non-linear behaviour of concrete. According to Rankin's failure theory (4.5) failure occurs when the maximal stress in any direction exceeds the f_t tensile strength (tension cut-off). This theory represents tensile failure with reasonable accuracy. Reaching f_t cracking is assumed and the crack model is activated. This means that cracks start to form perpendicular to the principal direction along the stresses which reach the tensile strengths as shown in Fig. 17. This means that it is possible to have one or two cracks in a material point depending on the stress state. Cracks are assumed to remain in-plane and always perpendicular to each other.

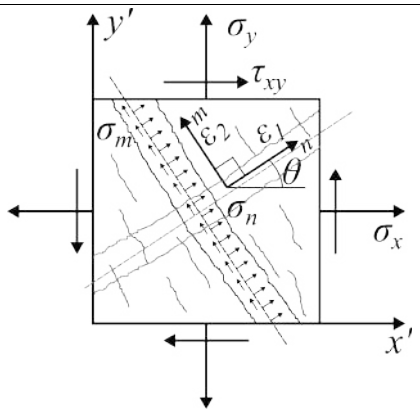

17. Figure - Cracks in the integration point of the LPSM element

FEM-Design implements a rotating crack model, which means that from the point of crack initiation the crack direction is determined by the evolution of the ε_1 and ε_2 principal strains Ref. [1]. This is in accordance with the experimental observations that first microcracks arise and after the increase of loading these microcracks become more and more aligned and start melting together, so formulating visible cracks in the structure Ref. [15]. Compared to the fixed crack models rotating crack models avoid the generation of fictitious shear stresses Ref. [15].

Important to note that cracking failure, similarly as plasticity, is handled layer-by-layer, thus the through thickness variation of the crack depth can be captured as well.

During cracking the plastic condition formulated by (4.5) needs to be modified to follow the crack direction, thus stresses and strains are equilibrated as:

$$\begin{bmatrix} \sigma_n \\ \sigma_m \\ 0 \end{bmatrix} = E \begin{bmatrix} \varepsilon_1 - \varepsilon_n^p - \varepsilon_n^{cr} \\ \varepsilon_2 - \varepsilon_m^p - \varepsilon_m^{cr} \\ 0 \end{bmatrix} \tag{4.13}$$

where $\varepsilon^{cr}{}_n$, $\varepsilon^{cr}{}_m$ are the crack strains normal to the crack surface which are necessary to satisfy the prescribed stresses normal to the crack surfaces. They are calculated based on the basic rules of plasticity given in Section 1.2 harmonized with the crack condition. The usage of the crack strains results in a smeared crack model, which has the advantage compared to a discrete crack model, that discontinuities caused by the cracks are distributed over the area of the integration points, allowing an efficient handling of the material degradation caused by cracking, and being capable to capture the structural behaviour of the system very well.

As soon as the crack surfaces are formulated the material stiffness along the crack normals is considered to be zero. Moreover the Poisson's ratio of the material point is set to zero, thus σ_n and σ_m become independent as (4.13) shows, and the crack surface is assumed to be shear free. Hence, in case if only one crack appears both in the tension and tension-compression zones σ_m is treated either according to elastic or plastic theories corresponding to the stress state of the material point discussed earlier. This means that after a crack calculation the plastic strains may be also updated in a subsequent step.

In case of plain concrete σ_n, σ_m are dropped to zero immediately as the crack surfaces are formulated. This is a usual assumption as concrete is very brittle against tensile loads. This perfectly brittle behaviour is a good assumption as cracking is a factor of primary concern in the deformation analysis and it's influence on the collapse load is usually minor. However in case of

reinforced concrete macroscopic characteristic changes in the post-critical zone ($\varepsilon>\varepsilon_t$). This is discussed in the next section.

4.1.4.2 Tension stiffening effect in case of cracking

If the concrete has reinforcement steel due to the bond between reinforcement and concrete, cracked concrete is able to carry a certain amount of tensile load, which contributes to the overall stiffness of the structure. This means that stress release is not complete at the formulation of the cracks, but after a sudden stress release a gradual decrease in the stress can be observed as Fig. 18 shows. The gradual decrease is linked to the formulation of secondary cracks which are releasing the bond between steel and concrete. This effect is known as the tension stiffening effect of reinforced cracked concrete. This is a complex microscopic phenomena, but it can be taken into account in a smeared crack model on macroscopic level, by considering that the crack stresses σ_n, σ_m are driven based on the ε_1 and ε_2 total strains as Fig. 18 shows. On crack model level this means a rotation and asymmetric constriction of the initial Rankin type failure surface during crack propagation. As the stresses are strain driven during cracking we can consider the FEM-Design crack model as maximum strain failure theory associated with a damage model of the material, which is formulated by the elimination of the material stiffness along the tensile direction by calculating an appropriate material stiffness matrix based on (1.9).

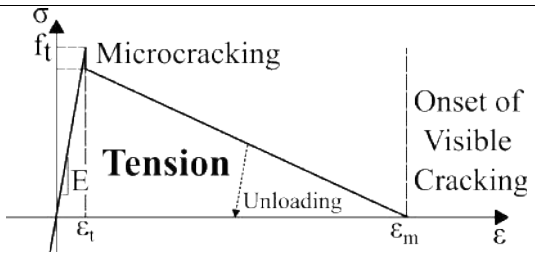

18. Figure - Degradation of concrete material due to cracking in case of tension stiffening

Fig. 18 also shows the elastic unloading which may happen due to rearrangement of the stresses in structural level. This elastic unloading happens linearly using the original elastic modulus of the material point.

The exact shape of the tension stiffening curve can be determined based on experiments. Appropriate theories fitted onto the experimental observations are available as different options in FEM-Design:

- Neglecting the initial stress release at the crack initiation the gradual release of the stress can be easily approximated by a linear curve:

$$\sigma_n = \frac{f_t}{(k_{TS}-1)}\left(k_{TS}-\frac{\varepsilon_1}{\varepsilon_t}\right) \tag{4.14}$$

  where k_{TS} is a free parameter with the ε_m tension cut-off can be set as shown in Fig. 19.

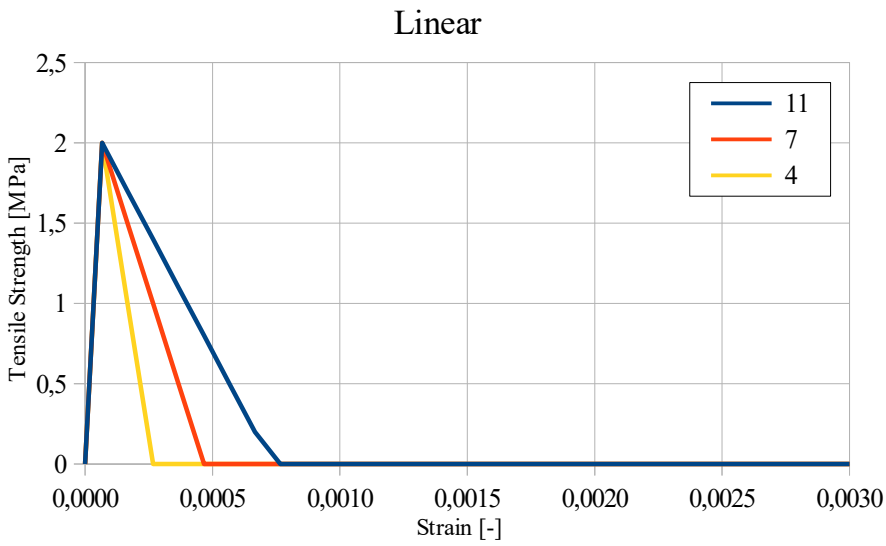

19. Figure - Tension stiffening based on linear rule with adjustable tension cut-off strain

- Hinton and Figueiras defined the curve shown in Fig. 18 based on experiments Refs. [1] [3]:

$$\sigma_n = k_{TS} f_t \left(1 - \frac{\varepsilon_1}{\varepsilon_m}\right) \tag{4.15}$$

where k_{TS} is used to set the initial stress release as shown in Fig. 20 and ε_m=0.002.

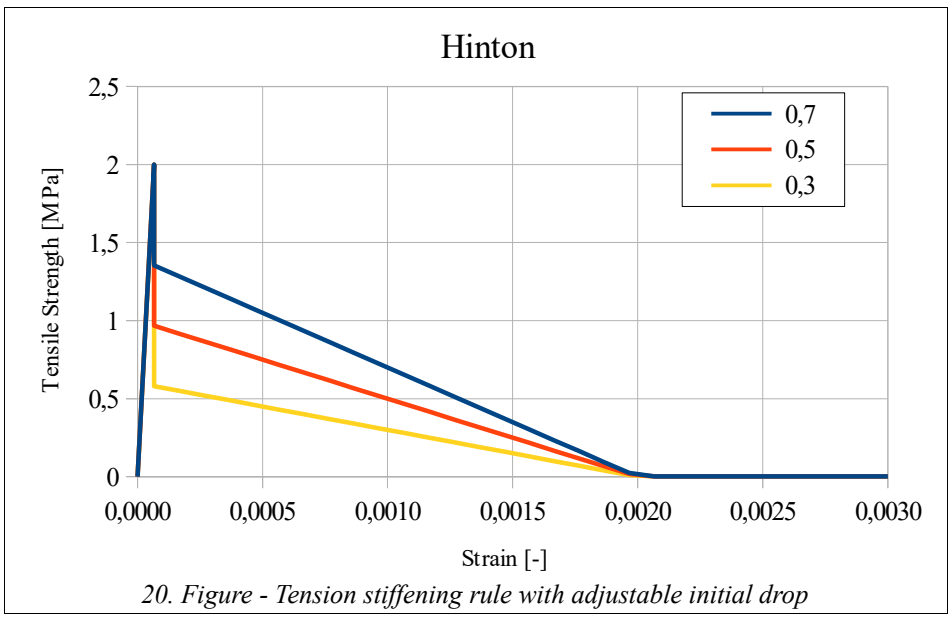

20. Figure - Tension stiffening rule with adjustable initial drop

- Vecchio defined a decaying curve to simulate the increased shear transfer and dowel effects in case of sheared panels Ref. [16]:

$$\sigma_n = \frac{f_t}{\left(1+\sqrt{k_{TS}\varepsilon_1}\right)} \tag{4.16}$$

where k_{TS} controls both the initial stress release and the remaining tensile strength of the concrete as shown in Fig. 21. For comparison of the Hinton and Vecchio rules against measurements the reader should check Section 6.1.10.

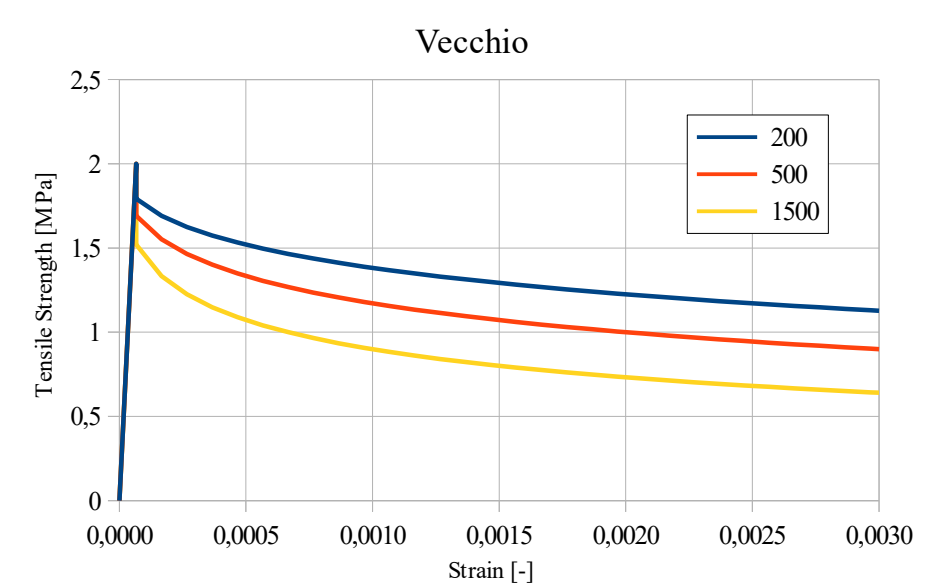

21. Figure - Decreasing tension stiffening rule with remaining tensile strength

- In the work of Cervera tension-stiffening is connected to the fracture energy release rate of concrete Ref. [4]:

$$\sigma_n = f_t e^{\left(\frac{-(\varepsilon_1-\varepsilon_t)}{\alpha}\right)}$$
$$\alpha = \frac{\left(G_f - \frac{1}{2} f_t \varepsilon_t l_c\right)}{f_t l_c} \tag{4.17}$$

where G_f is the facture energy of concrete which is adjustable by the user in kN/m unit and l_c is the characteristic length set based on Ref. [17], l_c=0.2 m. The effect of G_f is shown in Fig. 22.

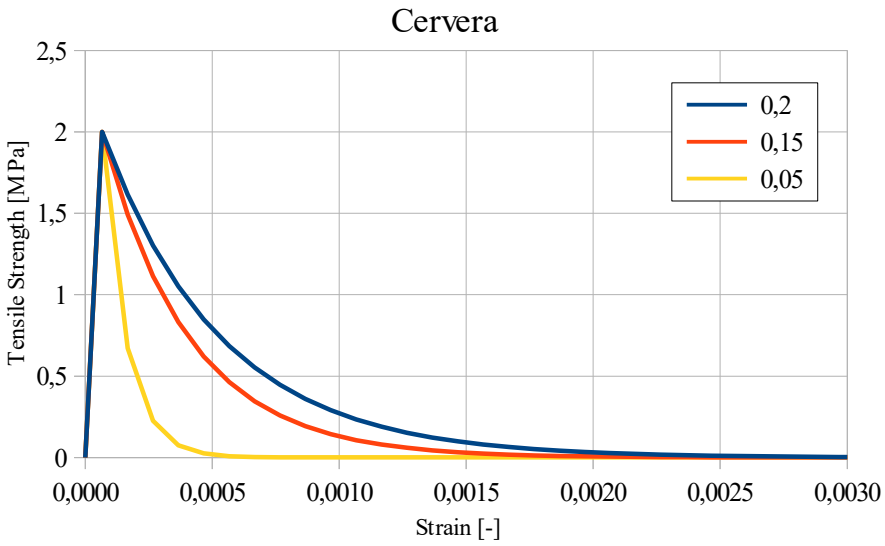

22. Figure - Fracture energy based tension stiffening rule
G_f parameter can be adjusted in [kN/m] *unit*

4.1.4.3 Reduced compression strength effect in case of lateral cracking

Tensile strains in the crack direction effectively reduce the compressive strength in the transverse directions. For this effect the Eurocode defines in case of the strut and tie model a strength reduction factor for compressed cracked concrete, see Ref. [18] as well:

$$\sigma_{Rd,max} = 0.6\,\nu'\,f_{cd} \tag{4.18}$$

where ν' is the effectiveness factor.

In FEM-Design this factor is calculated dynamically during the simulation based on the actual state of a material point. The factor shrinks the failure envelope in Fig. 16 proportionally. This means that all parameters of the concrete regarding compression will be recalculated as Fig. 23 shows.

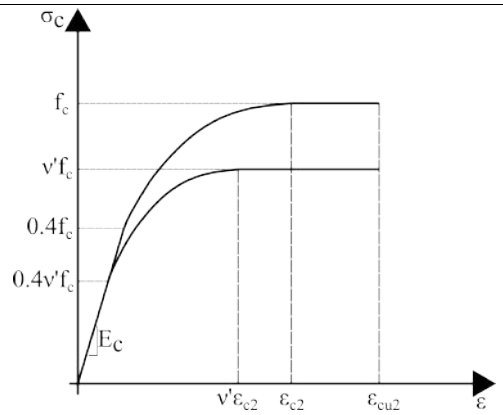

23. Figure - Degradation compression properties of concrete material due to cracking

The value of the effectiveness factor is driven by the tension strain normal to the crack surface. The exact relationship can be chosen in FEM-Design (curves are shown in Fig. 24):

- Vecchio defined the effectiveness factor based on ε_1 and ε_{c2} Ref. [16]:

$$\nu' = \frac{1}{\left(0.8 + 0.34\,\varepsilon_1/\varepsilon_{c2}\right)} \tag{4.19}$$

- In case of the Distributed Stress Field model Vecchio extended the above relationship with the ε_2 compressive strain Ref. [19]:

$$\nu' = \frac{1}{\left(1 + 0.35\left(-\varepsilon_1/\varepsilon_2 - 0.28\right)^{0.8}\right)} \tag{4.20}$$

This formula is plotted in Fig. 24 using a fixed $\varepsilon_2 = 0.001$ strain value.

- Cervera defined a linear rule Ref. [4]:

$$\nu' = 1 - k_2\varepsilon_1/0.005 \tag{4.21}$$

where k_2 is a free parameter and set to 0.55 in Fig. 24.

- Based on the modified FIB Model Code 2010 recommendation and Ref. [18] the effectiveness factor can be given in a piecewise manner:

$$\begin{aligned} \nu' &= 1; && \varepsilon_1 \le \frac{10}{17}\varepsilon_{c2} \\ \nu' &= A\varepsilon_1^2 + B\varepsilon_1 + C; && \frac{10}{17}\varepsilon_{c2} < \varepsilon_1 \le \frac{2}{325}\varepsilon_{c2} \\ \nu' &= \frac{1.0}{\left(1.2 + 55.0\varepsilon_1\right)}; && \frac{2}{325}\varepsilon_{c2} < \varepsilon_1 \end{aligned} \tag{4.22}$$

where A,B and C are constants obtained by fitting a parabola.

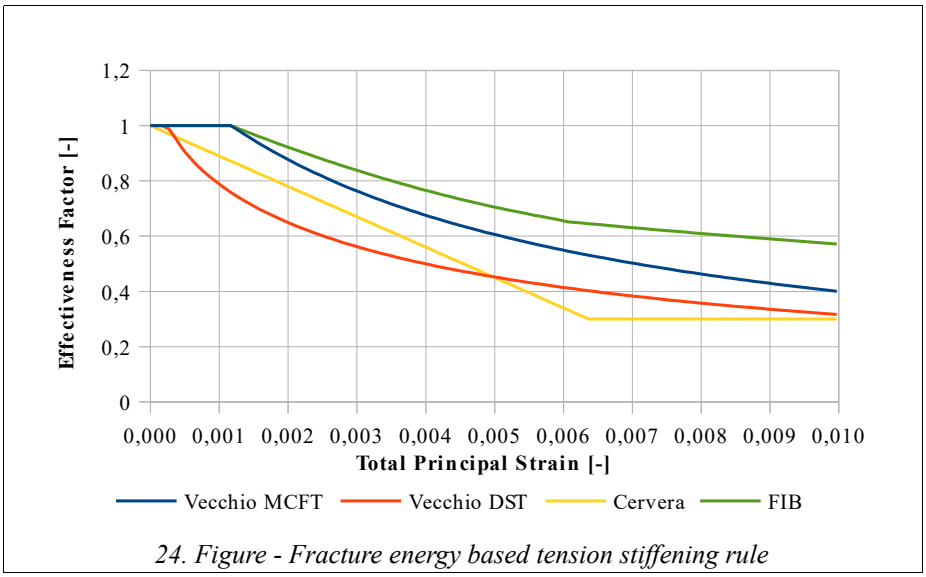

24. Figure - Fracture energy based tension stiffening rule

In case of each option ν'=0.3 is the minimum value. This can be seen in case of the Cervera curve in Fig. 24.

4.1.4.4 Reduced transverse shear stiffness in case of cracking

However transverse shear is not involved in the plasticity model, cracking can have an effect on the transverse shear. Similarly, as in case of the tension stiffening effect the existence of the reinforcement and aggregate interlock (Fig. 25) cause shear transfer even in case of cracked concrete, which can be gradually decreased as the total strains along the crack increase.

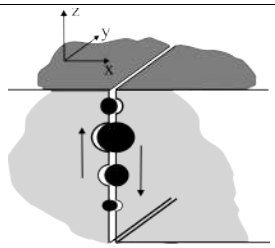

25. Figure - Remaining transverse shear transfer due to aggregate interlock

As transverse shear is calculated in an elastic way, this can be done by reducing the transverse shear modulus of the material point. FEM-Design offers a linear rule for this kind of stiffness reduction:

$$G_{13}=G_{23}=\beta_s G$$
$$\beta_s=\frac{\varepsilon_1-2\,\varepsilon_m}{\varepsilon_t-2\,\varepsilon_m} \tag{4.23}$$

where β_s is the reduction factor as Fig. 26 shows, ε_t is the strain at crack initiation and ε_m=0.002.

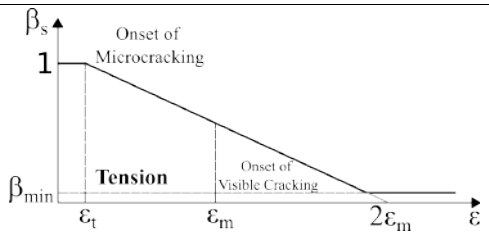

26. Figure - Transverse-shear reduction rule for cracked concrete

Just as in case of the effectiveness factor a small amount of transverse shear moduli is kept to maintain numerical stability of the calculation with β_{min}, see Fig. 26 as well.

4.2 Reinforcement steel

4.2.1 General reinforcement steel behaviour

Reinforced concrete is a composite which in addition of concrete consists of steel reinforcement. The reinforcement is comparatively thin, hence it is assumed that it is capable of transmitting axial forces only. Other properties of reinforcement steel is the same as structural steel, therefore data given in Section 3.1 is also valid here. As the reinforcement can bear axial forces only, a uniaxial material model is sufficient.

Using this simplification a very economic model can be developed without losing the accuracy. To consider steel in the LPSM element the reinforcements are added as separate layers into the model. To show this Fig. 4 can be extended with steel layers. This can be seen in Fig. 27 which shows a reinforced concrete shell accomplished by the LPSM element.

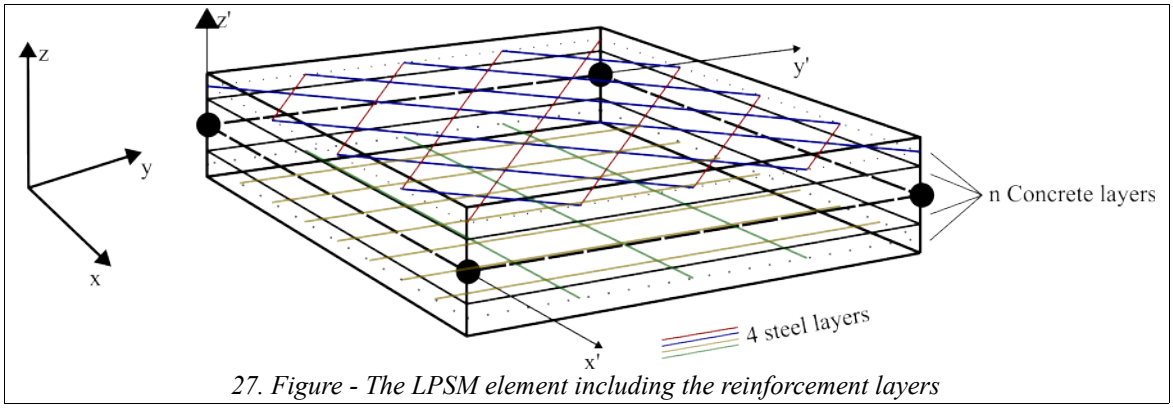

27. Figure - The LPSM element including the reinforcement layers

The model can have 4 arbitrary located reinforcement layers. The parameters of each reinforcement, like the reinforcement ratio and steel material properties can be determined individually. The change of the amount of the reinforcement inside the element can also be handled as the input reinforcement ratio is given for the corner nodes, thus inside the element at the integration points interpolation is used to obtain the correct amount of reinforcement.

Important property is the bond-slip relation between concrete and steel. In FEM-Design it is assumed that there is a perfect bond, thus the reinforced concrete can be modelled as one composite shell element instead of using interface elements between steel and concrete which would increase the calculation cost significantly.

The assumption of the perfect bond and the uniaxial load bearing of the reinforcements causes that local effects like dowel and pull-out actions cannot be taken directly into consideration, but the model mentioned in Section 4.1.4 are used to describe the interaction on macroscopic level. As a result local effects cannot be evaluated but on structural level the behaviour is accurate.

4.2.2 Plasticity and yielding in reinforcement steel

For sake of simplicity the uniaxial perfectly plastic steel model is repeated here in Fig. 28. For the uniaxial steel layers in each equilibrium iteration an elastic trial stress can be calculated using the total steel strains:

$$\boldsymbol{\varepsilon}_k = \boldsymbol{\varepsilon}_0 + \boldsymbol{\kappa}\, z_{s,k} \tag{4.24}$$

where $z_{s,k}$ is the effective height of the k^{th} steel layer measured from the reference plane (mid-plane) of the shell. From this the strain in the reinforcement can be obtained as:

$$\varepsilon_s = \varepsilon_{x,k}\cos^2(\Theta_{s,k}) + \varepsilon_{y,k}\sin^2(\Theta_{s,k}) + \gamma_{xy,k}\cos(\Theta_{s,k})\sin(\Theta_{s,k}) \tag{4.25}$$

where the $\Theta_{s,k}$ angle is the angle of the steel layer in the local coordinate system. Using the plastic strain of the reinforcement the trial stress in the reinforcement is given as:

$$\sigma_s = E_s(\varepsilon_s - \varepsilon_s^p) \tag{4.26}$$

where subscript *s* denotes that values, are relating to the reinforcement. All of the quantities above are calculated in the steel directions one-by-one. This trial stress can be checked against the material rule shown in Fig. 28 and in case of need the return mapping, given in Section 1.4, can be used to fulfil the material law.

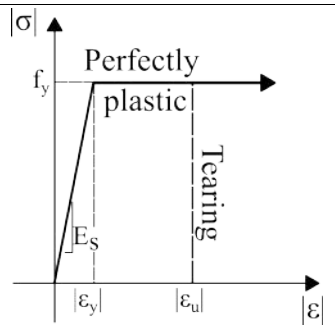

28. Figure – Linear Elastic-Perfectly Plastic material law of steel

After successful stress return the uniaxial stress has to be converted back to the element local coordinate system:

$$\boldsymbol{\sigma}_{s,k} = \begin{bmatrix} \sigma_s\cos^2(\Theta_{s,k}) \\ \sigma_s\sin^2(\Theta_{s,k}) \\ \sigma_s\cos(\Theta_{s,k})\sin(\Theta_{s,k}) \end{bmatrix} \tag{4.27}$$

and the contribution to the stress resultants can be obtained by using the specific area of the reinforcement layer:

$$\begin{bmatrix} \boldsymbol{m}_{s,k} \\ \boldsymbol{n}_{s,k} \end{bmatrix} = \begin{bmatrix} \boldsymbol{\sigma}_{s,k}\, a_{s,k}\, z_{s,k} \\ \boldsymbol{\sigma}_{s,k}\, a_{s,k} \end{bmatrix} \tag{4.28}$$

where $a_{s,k}$ is the specific area of the reinforcement.

Based on the result of the plastic return mapping the E_{Ts} tangent modulus of the steel can be also obtained which is related to the steel direction therefore it has to be rotated into the element local system to obtain the material matrix:

$$\boldsymbol{D}^{ep}_{s,k} = \underline{T}^{-1}_{(3x3)} \begin{bmatrix} E_{Ts} & 0 & 0 \\ 0 & 0 & 0 \\ 0 & 0 & 0 \end{bmatrix} \underline{T}^{-T}_{(3x3)} \tag{4.29}$$

where $\boldsymbol{T}$ is an appropriate transformation matrix using the angle of the steel.

$\boldsymbol{D}^{ep}_{s,k}$ can be used to calculate the contribution to the element stiffness according to (2.13) and Section 2.3.

4.2.3 Failure mode in reinforcing steel due to ultimate strain

Just as in case of structural steel shell fracture strain limit can be monitored in the reinforcement layers. Calculation of equivalent strain is not necessary as ε_s in (4.25) can be directly compared to ε_u.

In case of fracture just as in Section 3.3, it is assumed that the steel layers completely lose their structural stiffness and the stress release is complete and immediate.

5 Remarks and some recommendations in the light of finite element calculations

5.1 Material model options in case of Structural Steel

Material model of plastic structural steel shells are configurable in FEM-Design as follows:

- Plasticity options are available for any steel *'Plane Plate'* or *'Plane Wall'* by clicking the *'Plastic Analysis Data...'* button as Fig. 29 shows

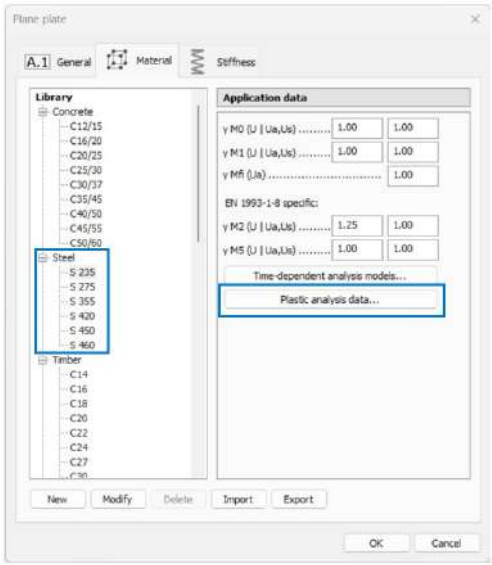

29. Figure - Configuring plasticity for structural steel shells

- Plasticity can be enabled or disabled for any element distinctly for SLS and ULS calculations. For this the *'Elasto-Plastic behaviour'* has to be adjusted which is shown in Fig. 30.

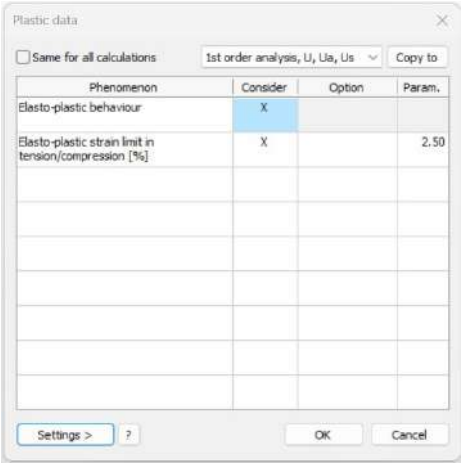

30. Figure - Plasticity options for structural steel shells

- If plasticity is enabled it can be controlled whether the ε_u is monitored as written in Section 3.3 or not. This controls whether a material point is able to flow without any limits along the straight plateau in Fig. 31 until the FE solver is able to find an equilibrium configuration on structural level, which means no plastic mechanism is formulated yet. If strain limit is enabled, reaching the limit value the material point is "turned off".
- ε_u is adjustable in the '*Param.*' column given in %.

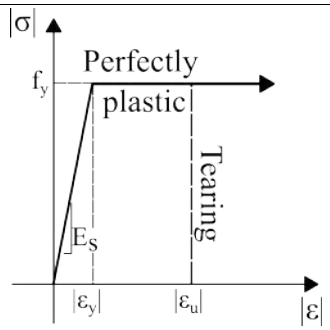

31. Figure - Elastic-Perfectly Plastic material law of steel

In FEM-Design plastic shell calculations the considered material model input by structural steel in the different limit states can be seen in Fig. 32. Fig. 32 left side shows the uniaxial material model for structural steel with the Eurocode notations in case of ultimate limit state. Fig. 32 right side shows the uniaxial material model for structural steel with Eurocode notations in case of serviceability limit states. In the proper f_y yield strength of structural steel material model the nominal thickness of the shell is considered according to EN 1993-1-1 Table 3.1. The behaviour is symmetric in tension and compression.

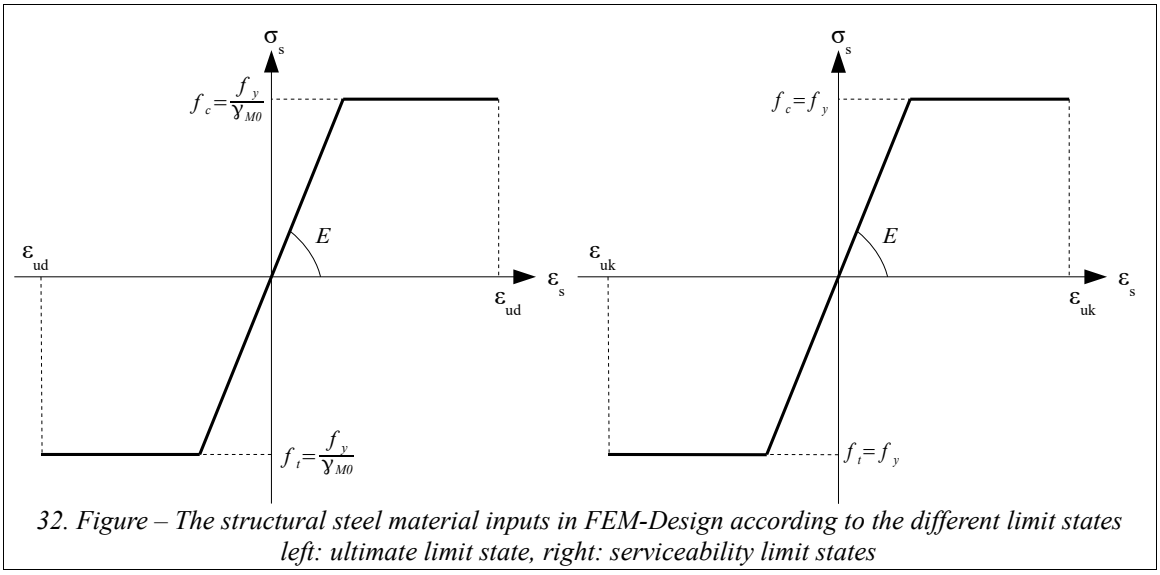

32. Figure – The structural steel material inputs in FEM-Design according to the different limit states left: ultimate limit state, right: serviceability limit states

5.2 Material model options in case of Reinforced Concrete

Similarly, as in case of Structural Steel plasticity model for Concrete is also adjustable element by *'Plane Plate'* or *'Plane Wall'* element using the *'Plastic Analysis Data...'* button as Fig. 33 shows. This get the user to all of the concrete plasticity options for the user as Fig. 34 shows.

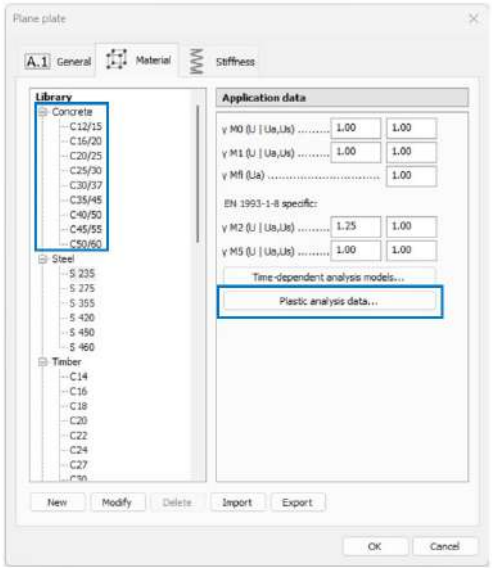

33. Figure - Configuring plasticity for concrete shells

Turning on the *'Elasto-Plastic behaviour'* several options become available, with the user is able to control the material model, which uniaxial representation is shown in Fig. 35.

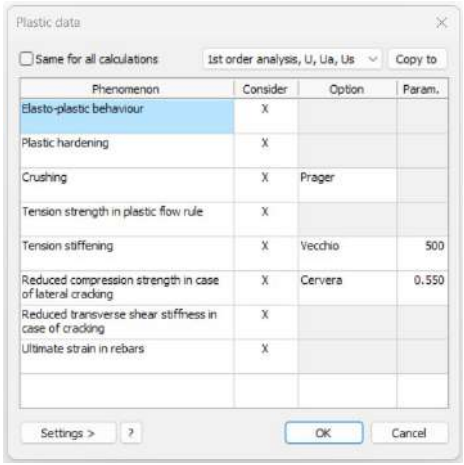

34. Figure - Plasticity options for concrete shells

Material options are influencing the stress-strain law as follows:

- Turning on *'Plastic hardening'* causes that in the compression zone the stress strain law will follow the solid curve in the compression zone in Fig. 35. In this case all of the calculations are according to Section 1.3. If hardening is not used than the dashed-dotted line is followed in the compression zone. Hardening has mainly an effect on the final deformations of the structure and very minor effect on the ultimate load, therefore if only the load bearing capacity is important than turning this option off calculation can be made slightly faster. In case of plain concrete without any reinforcement, hardening is turned off during the analysis automatically to improve numerical stability.

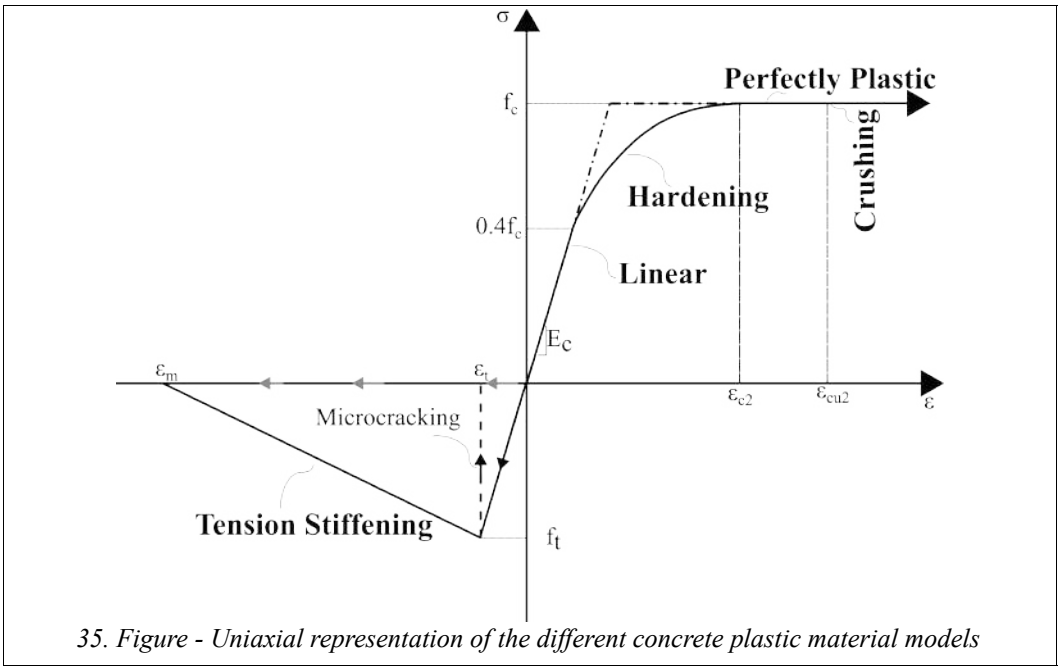

35. Figure - Uniaxial representation of the different concrete plastic material models

- The *'Crushing'* option controls the damage model presented in Section 4.1.3. Enabling this causing the damage of the material point by reaching ε_{cu2}, otherwise perfectly plastic flow can continue until the evolution of a plastic mechanism, which causes the collapse of the structure. This option has a strong influence on the compression failure of

concrete, therefore it is a very important parameter to capture the ultimate load of the structure. The model for the equivalent strain can be selected in the *'Option'* column based on Section 4.1.3 and Eq. (4.8)-(4.11).

- Turning off the '*Tension strength in plastic flow rule*' option will cause that the concrete material point in the tension zone will follow the gray arrows using a perfectly plastic behaviour and no tension strength at all. Using this option the user can remain on the safe side of the load bearing capacity of the structure, but for an accurate deformation calculation it is strongly advised to consider the tension strength of concrete. Moreover the consideration of the tension strength improves the numerical stability of the calculation.
- If the *'Tension stiffening'* rule is not considered after reaching f_t the stress strain law will follow the black arrows. At the onset of Microcracks concrete loses all of its strength and rigidity. From this point stress in the material point releases fully and material model will follow the gray arrows assuming a perfectly plastic flow. This model is adequate for plain concrete and it is forced during the calculation if no reinforcement is applied for the element. However in case of reinforced concrete the consideration of a proper tension stiffening rule is strongly advised because it improves the deformation results of the FE model and increases numerical stability. The tension stiffening models presented in Section 4.1.4.2 can be selected in the *'Option'* column and the rules can be adjusted using the *'Param'* column based on Fig. 19-22. If a tension stiffening rule is selected material law will follow the solid black line in Fig. 35. To select an appropriate tension stiffening rule the reader should check the verification examples in Section 6.1. The rule of thumb for the selection of the tension stiffening rule is that Vecchio rule fits for shear dominant load cases of panels whereas the other rules are serving good in case of other loading situations. In the latter case the user should apply the rule for which the most reliable parameters are available. The default parameters for the different options here were selected according to the indicated references in Section 4.1.4.2. As it was mentioned the tensions stiffening rule mostly has an effect on the final deformations and less influence on the load bearing capacity of the structure.
- The *'Reduced compression strength in case of lateral cracking'* is available for controlling the material model as written in Sections 4.1.4.3. The option is available to make the cracking model more accurate, thus allowing the user to have better results both in SLS and ULS calculations. In *Reduced compression strength in case of lateral cracking'* option, the name of the selectable methods in FEM-Design 3D structure corresponds the name of the rules in Fig. 24 in the following way:
  - Vecchio 1 means Vecchio MCFT according to Eq. (4.19).
  - Vecchio 2 means Vecchio DST according to Eq. (4.20).
  - Cervera means Cervera according to Eq. (4.21).
  - Model Code 2010 means FIB according to Eq. (4.22).
- The *'Reduced transverse shear in case of lateral cracking'* (see Fig. 26) option is available to make the cracking model more accurate, thus allowing the user to have better results both in SLS and ULS calculations, see Section 4.1.4.4.
- *'Ultimate strain in rebars'* is an option related to reinforcement steel. For the reinforcement basic parameters can be set on the *'Concrete'* design tab of FEM-Design as

Fig. 36 shows. The reinforcement set here will be transferred into the plastic finite element calculation converting the steel layers into equivalent steel based on the settings done in the *'Calculation parameters'* dialogue. The yield stress, specific area and modulus of elasticity will be transferred to the plastic shell calculation based on these settings. The only thing which is adjustable in the plasticity dialogue, shown in Fig. 34, is the *'Ultimate strain in rebars'*. With this option the user is able to control the steel material model on a similar manner as in case of structural steel in Section 5.1, by enabling the damage model for the reinforcement layers if the strain in the reinforcement reaches the preset value of ε_u.Considering the fracture of steel allows the user a more accurate load bearing capacity in FE calculation.

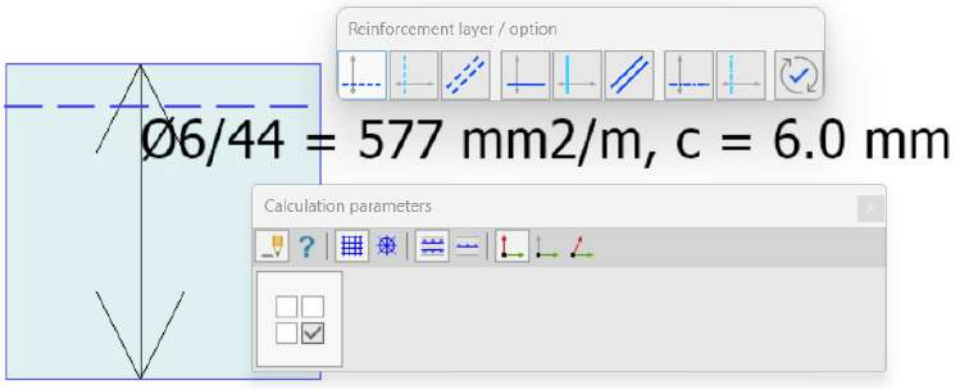

36. Figure - Reinforcement steel setup for plastic shell

In FEM-Design plastic shell calculations the considered material model input by concrete in the different limit states can be seen in Fig. 37. Fig. 37 left side shows the uniaxial material model for concrete with the Eurocode notations in case of ultimate limit state. Fig. 37 right side shows the uniaxial material model for concrete with Eurocode notations in case of serviceability limit states. In the proper material models of concrete the creep coefficients and partial factors are considered according to EN 1992-1-1, see Fig. 37.

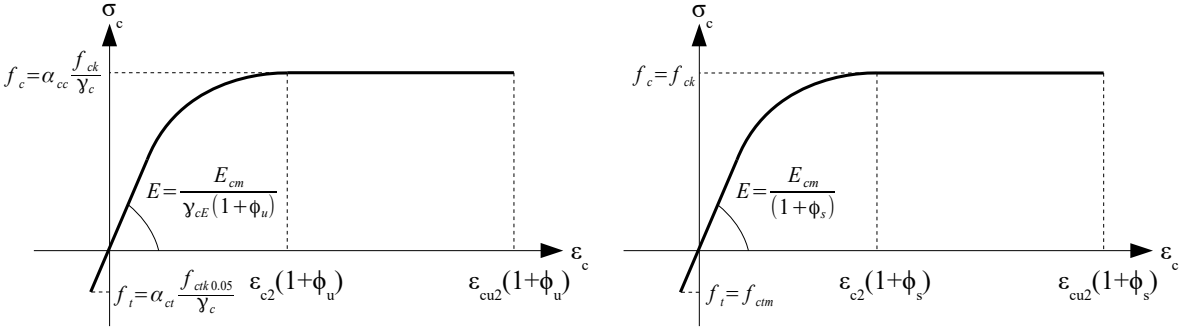

37. Figure - The concrete material inputs in FEM-Design according to the different limit states left: ultimate limit state, right: serviceability limit states

In FEM-Design plastic shell calculations the considered material model input by reinforcement

steel in the different limit states can be seen in Fig. 38. Fig. 38 left side shows the uniaxial material model for reinforcement steel with the Eurocode notations in case of ultimate limit state. Fig. 38 right side shows the uniaxial material model for reinforcement steel with Eurocode notations in case of serviceability limit states. In the proper material models of reinforcement steel the partial factors are considered according to EN 1992-1-1, see Fig. 38.

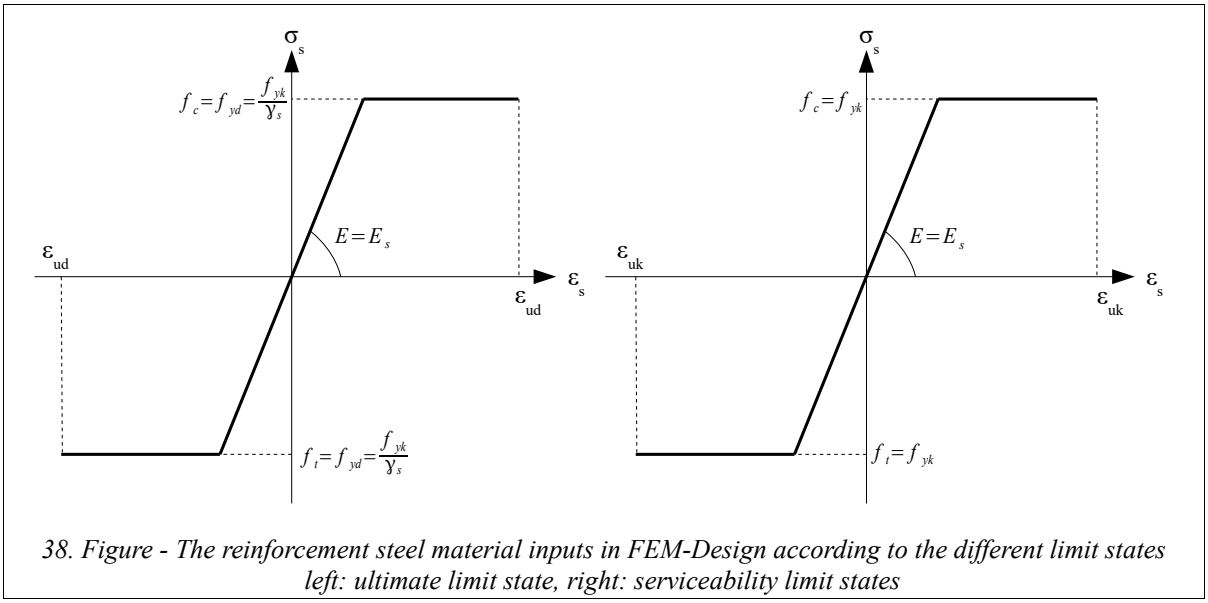

38. Figure - The reinforcement steel material inputs in FEM-Design according to the different limit states left: ultimate limit state, right: serviceability limit states

5.3 Through thickness resolution of the LPSM elements

As it was written in Section 2.1 the LPSM elements can have arbitrary number of layers. This can be globally controlled by the user to allow to find a good compromise between accuracy and calculation cost of the simulation.

Fig. 39 shows the *'Calculation option'* dialogue of the load combination calculation. Here the number of layers in an LPSM element can be adjusted by specifying a number in the *'Number of layers in elasto-plastic shells'* option.

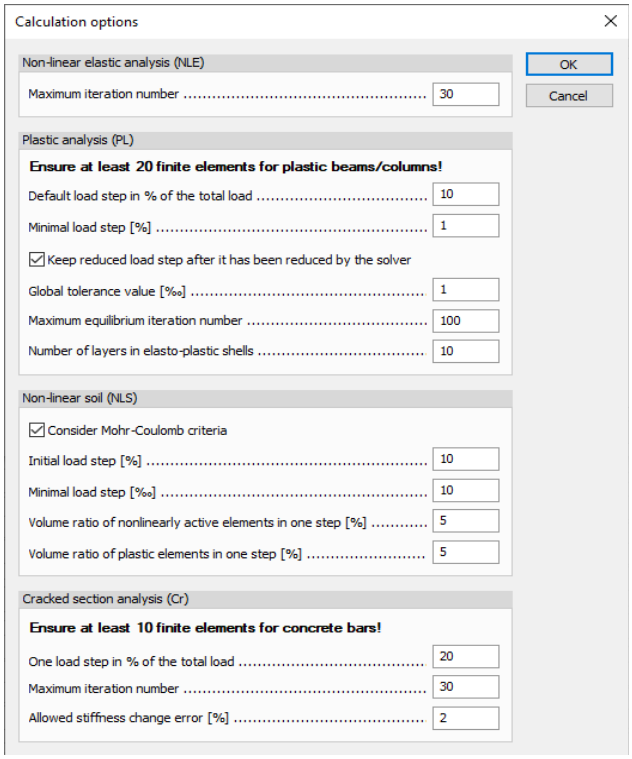

39. Figure - Reinforcement steel setup for plastic shell

The default value is 10 which normally gives accurate results. In special cases when the model can suffer membrane loading only the user may set this number to 1 to achieve faster calculation, but in this case the user has to be sure that the plastic elements are completely bending free.

5.4 Convergence parameters of the calculation

In the *'Calculation options'* dialogue in Fig. 39 several parameters can be adjusted to influence the convergence of a plastic calculation:

- The *'Default Load step...'* sets the initial amount of the total load which will be applied on the structure during a load increment. With a good choice of this parameter the calculation speed can be dramatically improved. Too small load steps may cause a lot of unnecessary iterations in the elastic domain of the structure. On the contrary too many may cause a lot of failed iterations when the load step has to be adjusted and the current iteration has to be repeated.
- The *'Minimal Load step'* defines the smallest amount of the total load with the solver is allowed to try to accomplish a load increment iteration.
- The *'Keep reduced loadstep...'* checkbox controls the solver behaviour in case of an iteration is successful after a failed one. If the checkbox is active then the solver will keep the load increment of the last successful iteration. This is the advised option in case of an LPSM calculation. If it is turned out the solver will try the next iteration using the default load step. This latter mode is good if the structure has switch like non-linearities, like an uplifting connector etc. In this case after the status change of the element the structure may keep its elastic, thus the bigger loadstep can be convergent.

- With the *'Global tolerance'* value the allowed value of the residual force discussed in Section 1.1 can be controlled. Increasing the tolerance may cause faster convergence with the price of a less accurate simulation result.
- The *'Maximum number of iterations'* set the internal equilibrium iterations can be controlled with the solver tries to fulfil the *'Global tolerance'* criteria. In case of a complex plastic shell structure this value is advised to set to a relative high value. In case if the ultimate load has to be captured very accurately the increase of this number is advised e.g. to a value of 200, and in parallel the *'Global tolerance'* should be kept on a low value like one thousandths to avoid the accumulation of unbalanced forces during the equilibrium iterations.

6 Reinforced concrete application of the plastic shell theory

6.1 Verification examples

6.1.1 Normally RC beam under pure bending compared with analytical calculation

In this example we compare the FEM-Design calculation result with “analytical” solution based on Ref. [20] according to general strength of material calculation regarding reinforced concrete. This example in Ref. [20] shows the pure bending moment (M) vs. curvature (κ) diagrams of a rectangle cross-section (300x450 mm) in normally reinforced case (A_s=1257 mm^2, 4ϕ20 on the tensioned side). The normally reinforced condition means that the failure occurs in the section with the crushing of the concrete at the extreme fibre while the reinforcement is in yielding condition. In Ref. [20] linear elastic perfectly plastic behaviour was assumed for the reinforcement (in tension) and for the concrete (in compression). In tension the concrete material was considered linear elastic until the extreme fibre reached the tension strength, but after tensile cracking the tension stiffening was neglected thus Ref. [20] shows the M-κ curve for this loading and reinforcement condition.

Fig. 40 shows the FEM-Design model with the mesh, fixed boundary condition and the line constant moment at the end of a cantilever. With these settings the cantilever is mostly in pure bending condition.

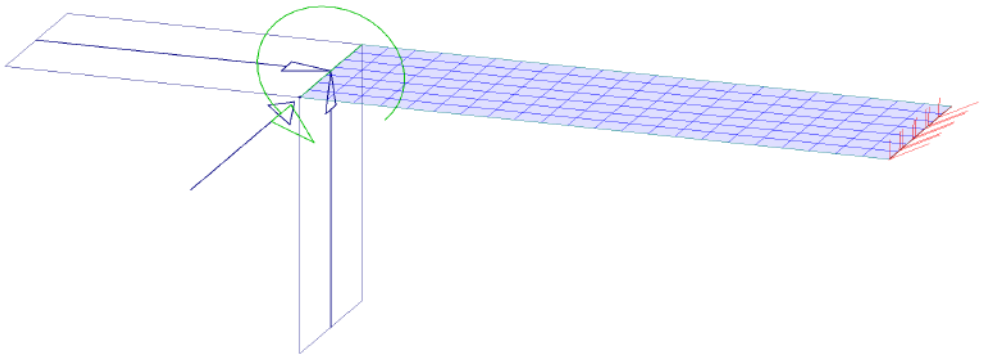

40. Figure - The FEM-Design model with the mesh and the applied constant moment

The FEM-Design plastic data settings can be seen in Fig. 41 in case of tension stiffening and

concrete hardening considerations.

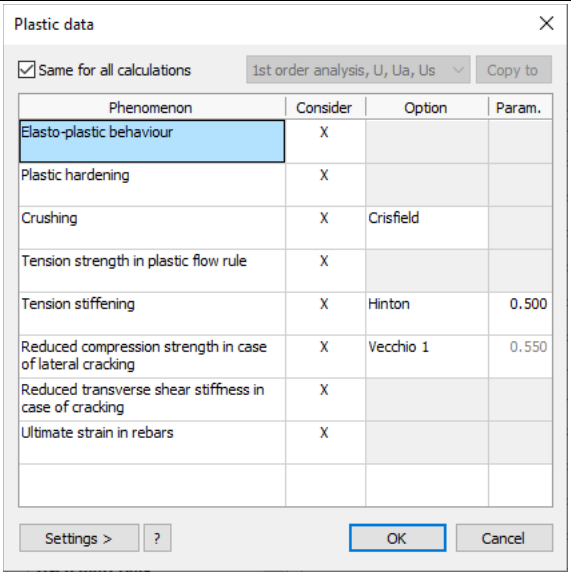

41. Figure - FEM-Design plastic data set

Fig. 42 shows the moment-curvature diagrams about the benchmark result and the FEM-Design results. To follow the "analytical" result more precisely, during the non-linear plastic shell calculation 1% load step was adjusted with 10 concrete shell core layers and one bottom reinforcement layer. In FEM-Design six different cases were considered:

- Tension stiffening (option: Hinton, parameter: 0.5) without concrete hardening
- Tension stiffening (option: Hinton, parameter: 0.5) with concrete hardening
- Without tension stiffening, without concrete hardening
- Without tension stiffening, with concrete hardening
- Without tension strength, without concrete hardening
- Without tension strength, with concrete hardening

Due to the normally reinforced section the failure occurs with concrete crushing while reinforcement reaches yield stress.

The benchmark result gives the following ultimate moment, see Fig 42.

$M_{Rd} = 200\,\text{kN}$

FEM-Design ultimate bending moments are as follows with the six different data sets above:

$M_{Rd\,FD1} = 204\,\text{kN}$; $M_{Rd\,FD2} = 201\,\text{kN}$; $M_{Rd\,FD3} = 201\,\text{kN}$;

$M_{Rd\,FD4} = 189\,\text{kN}$; $M_{Rd\,FD5} = 198\,\text{kN}$; $M_{Rd\,FD5} = 189\,\text{kN}$.

According to Fig. 42 we can say that the strains and the ultimate moment capacities are in good agreement with the "analytical" result. Note that in the benchmark result the linear elastic

perfectly plastic material model was considered in concrete, therefore the FEM-Design results in case of hardening of concrete show a bit softer behaviour with a bit smaller ultimate moment capacities. In every analysed case the non-linear solutions stopped with the concrete crushing while the reinforcements were in yielding condition which means that the finite element model gave back the normally reinforced situation.

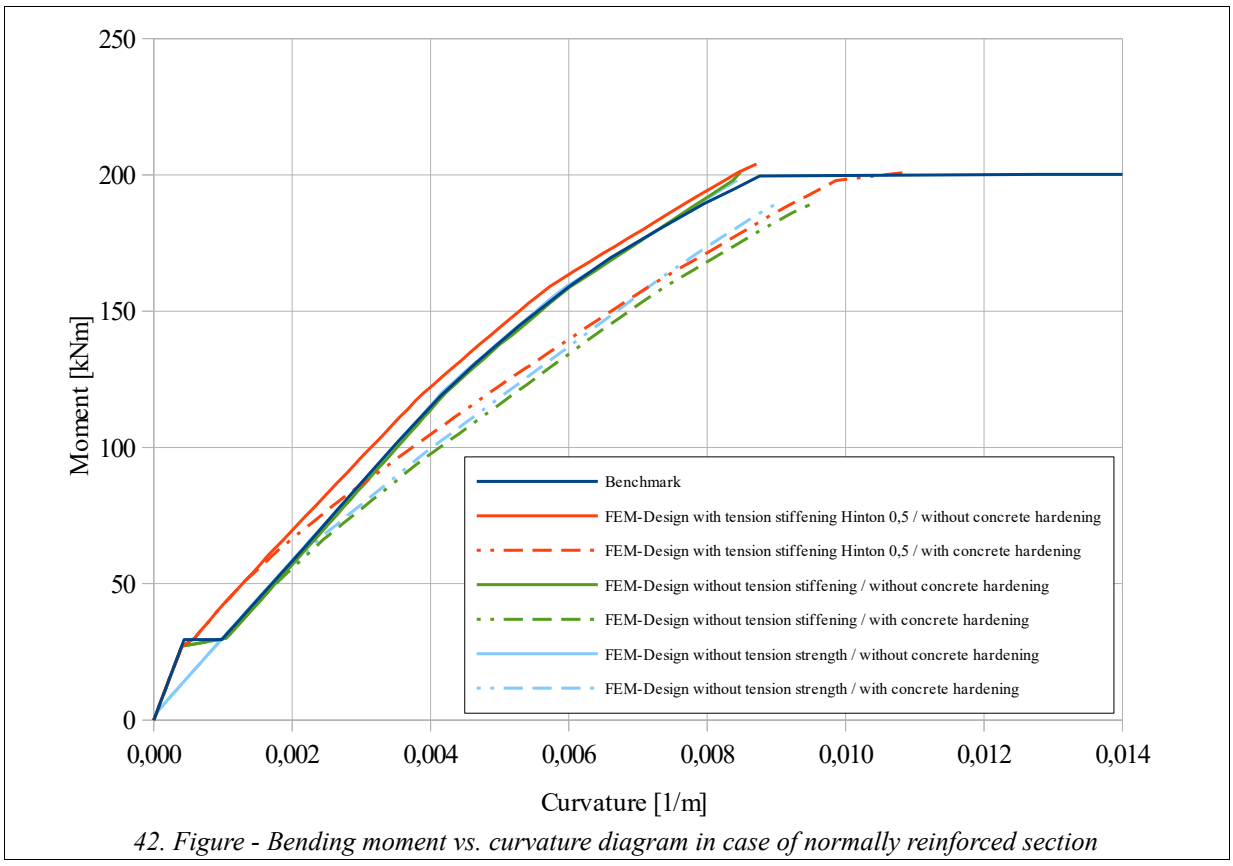

42. Figure - Bending moment vs. curvature diagram in case of normally reinforced section

6.1.2 Weakly RC beam under pure bending compared with analytical calculation

In this example we compare the FEM-Design calculation result with "analytical" solution based on Ref. [20] according to general strength of material calculation regarding reinforced concrete. This example in Ref [20] shows the pure bending moment (M) vs. curvature (κ) diagrams of a rectangle cross-section (300x450 mm) in weakly reinforced case (A_s=226 mm^2, 2ϕ12 on the tensioned side). The weakly reinforced condition means that the failure occurs in the section with the reinforcement fracture while the concrete is far from its crushing strain (approximately elastic). This is the same reference which was in the previous example, thus all assumptions in the material models are the same as in the previous example.

The FEM-Design model geometry and loading condition were the same compared with the previous example. Only the applied reinforcement was different (A_s=226 mm^2, 2ϕ12).

Fig. 40 shows the FEM-Design model with the mesh, fixed boundary condition and the line constant moment at the end of the cantilever. With these settings the cantilever is mostly in pure bending condition.

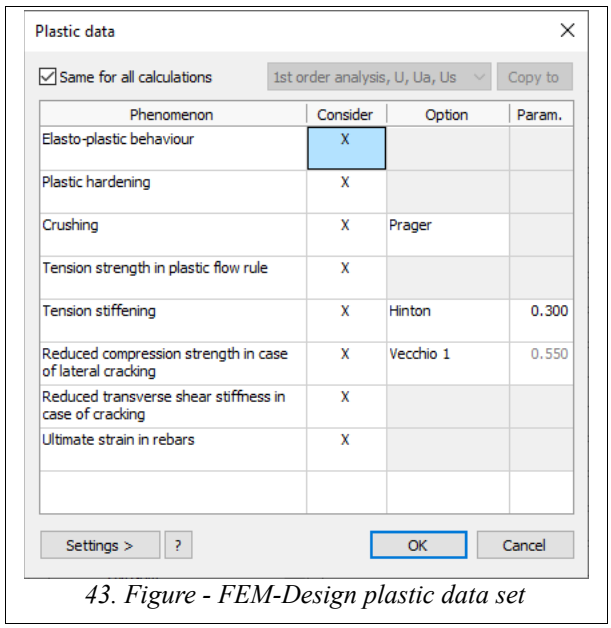

43. Figure - FEM-Design plastic data set

The FEM-Design plastic data settings can be seen in Fig. 43 in case of tension stiffening and concrete hardening considerations.

Fig. 44 shows the moment-curvature diagrams about the benchmark result and the FEM-Design results. To follow the "analytical" result more precisely, during the non-linear plastic shell calculation 1% load step was adjusted with 10 concrete shell core layers and one bottom reinforcement layer. In FEM-Design six different cases were considered:

- Tension stiffening (option: Hinton, parameter: 0.3) without concrete hardening
- Tension stiffening (option: Hinton, parameter: 0.3) with concrete hardening

- Without tension stiffening, without concrete hardening
- Without tension stiffening, with concrete hardening
- Without tension strength, without concrete hardening
- Without tension strength, with concrete hardening

Due to the weakly reinforced section the failure occurs with reinforcement fracture.

The benchmark result gives the following ultimate moment see Fig. 44:

$M_{Rd} = 43\,\text{kN}$

FEM-Design ultimate bending moments are as follows with the six different data sets above:

$M_{Rd\,FD1} = 45\,\text{kN}$; $M_{Rd\,FD2} = 44\,\text{kN}$; $M_{Rd\,FD3} = 42\,\text{kN}$;

$M_{Rd\,FD4} = 41\,\text{kN}$; $M_{Rd\,FD5} = 45\,\text{kN}$; $M_{Rd\,FD5} = 44\,\text{kN}$.

According to Fig. 44 we can say that the strains and the ultimate moment capacities are in good agreement with the “analytical” result. Note that in the benchmark result the section is weakly reinforced, therefore the FEM-Design results in case of hardening of concrete don't show considerable differences compared with non-hardening cases because the concrete was in linear elastic condition at failure. In every analysed case the non-linear solutions stopped with the reinforcement fracture while the concrete was almost linear elastic which means that the finite element model gave back the weakly reinforced situation.

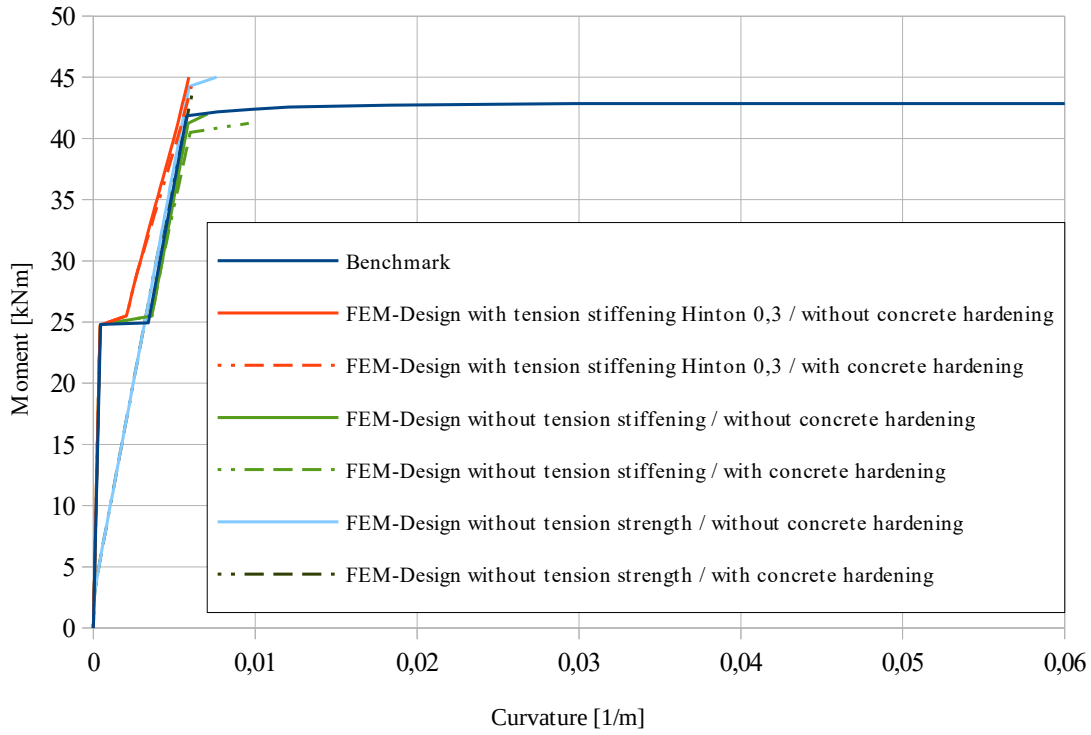

44. Figure - Bending moment vs. curvature diagram in case of weakly reinforced section

6.1.3 Over RC beam under pure bending compared with analytical calculation

In this example we compare the FEM-Design calculation result with "analytical" solution based on Ref. [20] according to general strength of material calculation regarding reinforced concrete. This example in Ref [20] shows the pure bending moment (M) vs. curvature (κ) diagrams of a rectangle cross-section (300x450 mm) in over reinforced case (A_s=1885 mm^2, 6ϕ20 on the tensioned side). The over reinforced condition means that the failure occurs in the section with the concrete crushing while the reinforcement is in elastic condition. This is the same reference which was in the previous example, thus all assumptions in the material models are the same as in the previous example.

The FEM-Design model geometry and loading condition were the same compared with the previous example. Only the applied reinforcement was different (A_s=1885 mm^2, 6ϕ20).

Fig. 40 shows the FEM-Design model with the mesh, fixed boundary condition and the line constant moment at the end of the cantilever. With these settings the cantilever is mostly in pure bending condition.

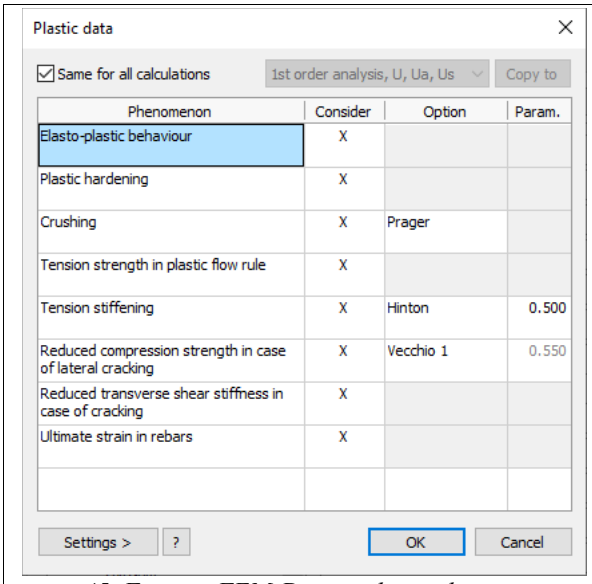

45. Figure - FEM-Design plastic data set

The FEM-Design plastic data settings can be seen in Fig. 45 in case of tension stiffening and concrete hardening considerations.

Fig. 46 shows the moment-curvature diagrams about the benchmark result and the FEM-Design results. To follow the "analytical" result more precisely, during the non-linear plastic shell calculation 1% load step was adjusted with 10 concrete shell core layers and one bottom reinforcement layer. In FEM-Design six different cases were considered:

- Tension stiffening (option: Hinton, parameter: 0.5) without concrete hardening
- Tension stiffening (option: Hinton, parameter: 0.5) with concrete hardening
- Without tension stiffening, without concrete hardening
- Without tension stiffening, with concrete hardening
- Without tension strength, without concrete hardening
- Without tension strength, with concrete hardening

Due to the over reinforced section the failure occurs with concrete crushing.

The benchmark result gives the following ultimate moment:

$M_{Rd} = 263\,\mathrm{kN}$

FEM-Design ultimate bending moments are as follows with the six different data sets above:

$M_{Rd\,FD1} = 252\,\mathrm{kN}$; $M_{Rd\,FD2} = 228\,\mathrm{kN}$; $M_{Rd\,FD3} = 255\,\mathrm{kN}$;

$M_{Rd\,FD4} = 228\,\mathrm{kN}$; $M_{Rd\,FD5} = 252\,\mathrm{kN}$; $M_{Rd\,FD5} = 243\,\mathrm{kN}$.

According to Fig. 46 we can say that the strains and the ultimate moment capacities are in good agreement with the "analytical" result. Note that in the benchmark result the linear elastic

perfectly plastic material model was considered in concrete, therefore the FEM-Design results in case of hardening of concrete show a bit softer behaviour with a bit smaller ultimate moment capacities. In every analysed case the non-linear solutions stopped by concrete crushing while the reinforcements were in linear elastic condition which means that the finite element model gave back the over reinforced situation.

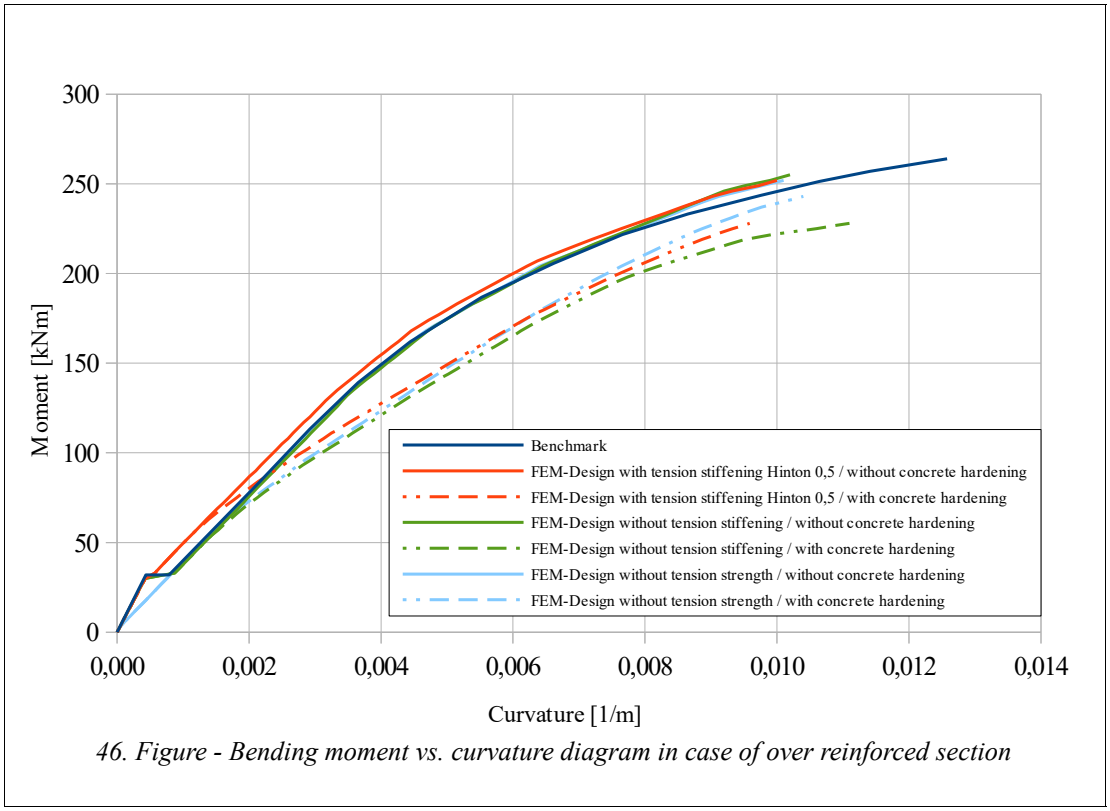

46. Figure - Bending moment vs. curvature diagram in case of over reinforced section

6.1.4 Simply supported RC beams compared with experimental data

Section and material properties	Beam A	Beam B
Height [mm]	h=561.34	h=556.26
Width [mm]	b=307.34	b=228.60
Effective depth [mm]	d=466.09	d=461.01
Effective depth [mm]	d'=50.8	d'=50.8
Reinf. bottom [mm^2]	A_s=3910	A_s=3257
Reinf. top [mm^2]	$A_{s'}$=257	$A_{s'}$=257
Span length [m]	L=6.4	L=6.4
Concrete Young's mod. [GPa]	E_c=29.80	E_c=31.97
Poisson's ratio [-]	ν=0.15	ν=0.15
Ultimate comp. strength [MPa]	f_c=35.0	f_c=38.7
Ultimate tens. strength [MPa]	f_t=4.3	f_t=4.2
Ultimate yield strain [-]	ε_{c2}=0.0020	ε_{c2}=0.0020
Ultimate comp. strain [-]	ε_{c3}=0.0030	ε_{c3}=0.0025
Reinf. steel Young's mod. bottom [GPa]	E_s=205.3	E_s=205.3
Yield stress bottom [MPa]	f_y=552	f_y=552
Reinf. steel Young's mod. top [GPa]	$E_{s'}$=201.2	$E_{s'}$=201.2
Yield stress top [MPa]	$f_{y'}$=345.2	$f_{y'}$=345.2

In this verification example two simply supported RC beams will be analysed. The experimental test layouts and results were taken from Refs. [21] and [3]. In FEM-Design the structures were modelled with shell elements and line loads. The static structural system and the applied load can be seen in Fig. 47 with the different analysed cross-sections. The geometrical and material data are in the table above.

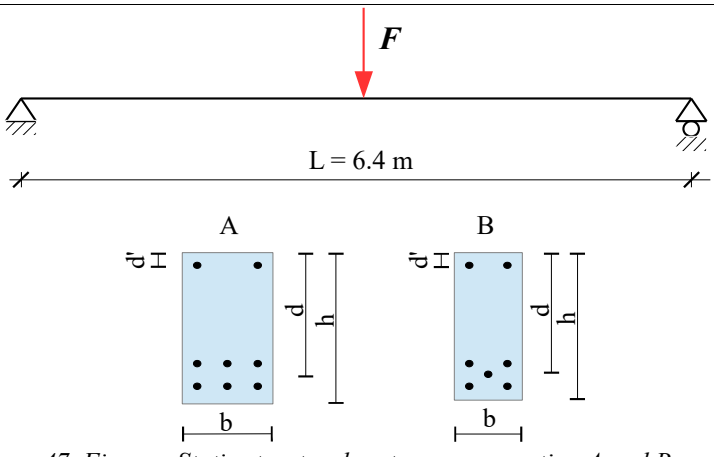

47. Figure - Static structural system, cross-section A and B

The FEM-design model with the finite element mesh and the applied line load can be seen in the following figure (Fig. 48):

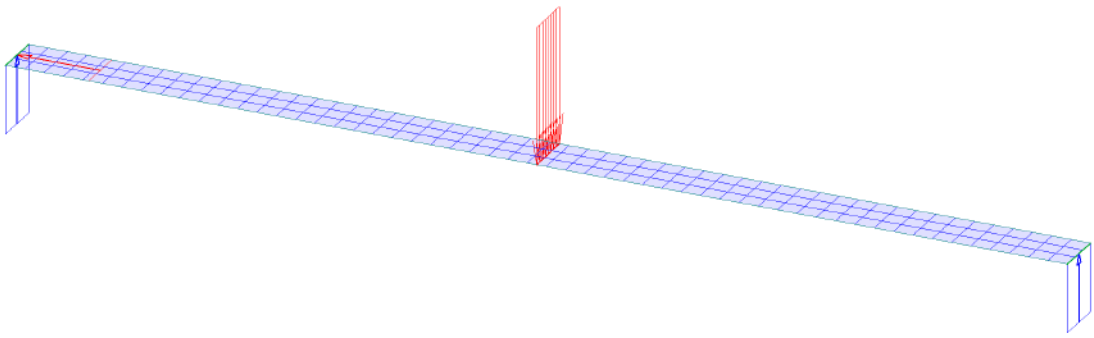

48. Figure - FEM-Design model with the applied mesh

In FEM-design plastic shell analysis the applied layer number was n_{lay} = 10. The adjusted plastic shell data were the following (Fig. 49):

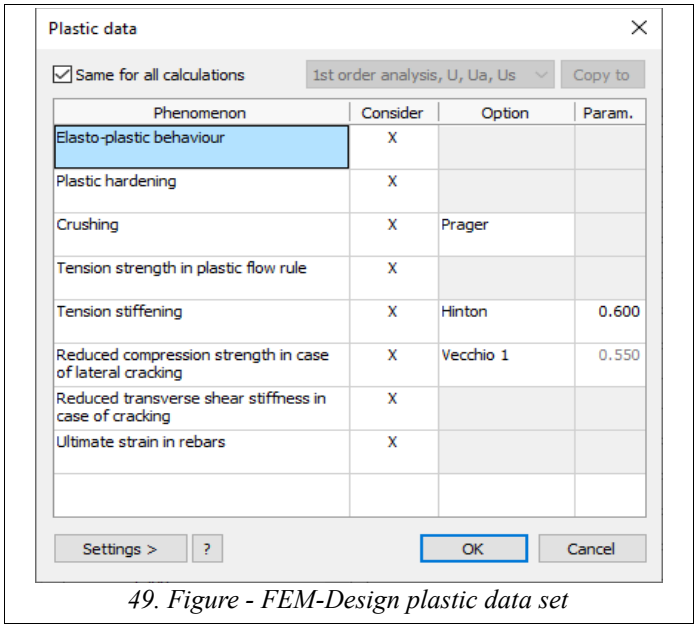

49. Figure - FEM-Design plastic data set

The following load displacement diagram shows the result of the test experiment (beam A) with the applied load and mid-span deflections. In the same diagram the FEM-Design result is also available.

According to the test results, the failure occurred on the compressed side of the beam at mid-span with concrete crushing while the tension reinforcement bars on the bottom side remained elastic and the compression reinforcement on the top side became plastic.

The FEM-Design result gives the same failure behaviour and the load vs. mid-span deflection curve is in good agreement with the experimental results (see Fig. 50). The ultimate load-bearing capacity and the mid-span deflection before failure are almost match each other comparing the numerical FEM-Design calculation with the experimental test result (see Fig. 51 as well).

The ultimate loads, mid-span deflections and ultimate bending moments at mid-span are as

follows:

$F_{test}=468.1\,\text{kN}$, $d_{test}=0.0355\,\text{m}$, $M_{Rd\,test}=749\,\text{kNm}$

$F_{FD}=465\,\text{kN}$, $d_{FD}=0.03338\,\text{m}$, $M_{Rd\,FD}=734\,\text{kNm}$

The differences between the results are less than 5 %.

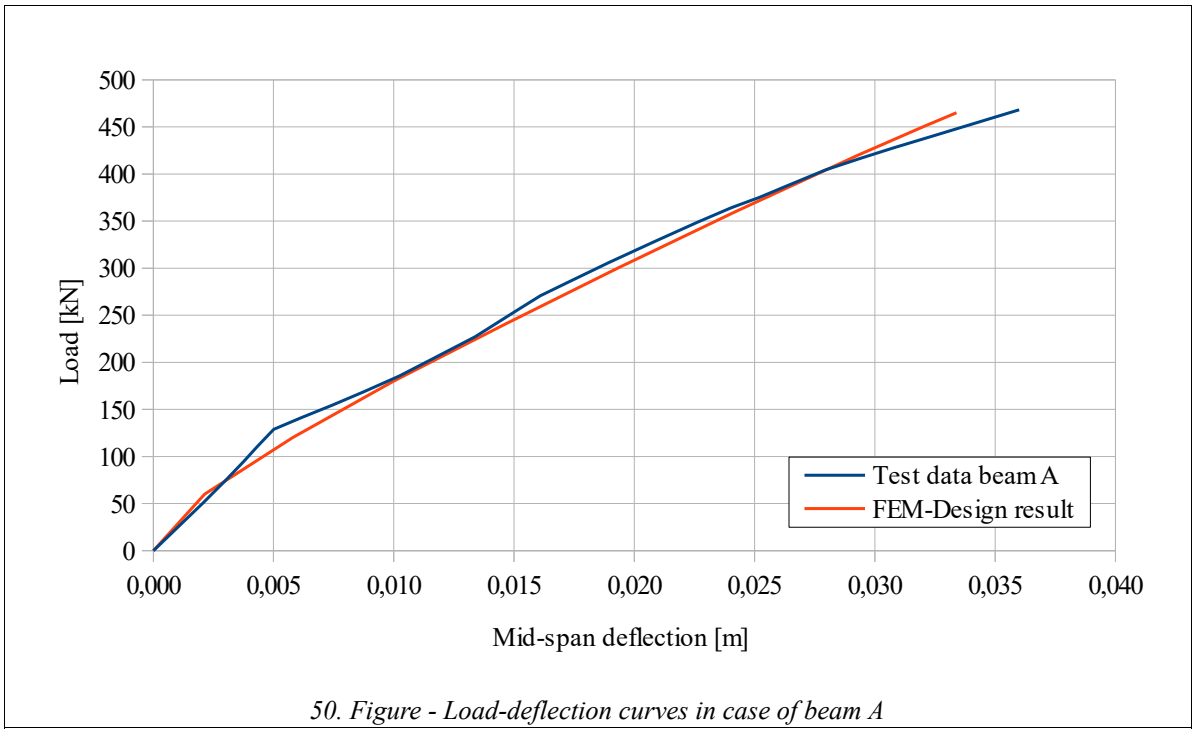

50. Figure - Load-deflection curves in case of beam A

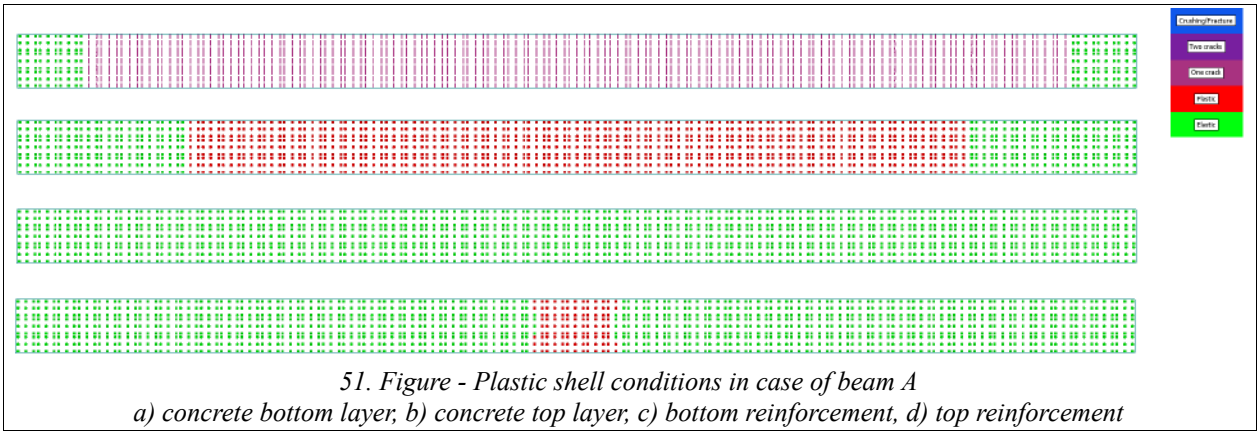

51. Figure - Plastic shell conditions in case of beam A
a) concrete bottom layer, b) concrete top layer, c) bottom reinforcement, d) top reinforcement

The following load displacement diagram shows the result of the test experiment (beam B, Fig. 52) according to the applied load and mid-span deflections. In the same diagram the FEM-Design result is also available.

According to the test results, the failure occurred on the compressed side of the beam at mid-span with concrete crushing while the reinforcement bars on the bottom and top sides remained elastic (see Fig. 53).

The FEM-Design result gives the same failure behaviour and the load vs. mid-span deflection curve is in good agreement with the experimental results (see Fig 52). The ultimate load-bearing capacity and the mid-span deflection before failure are almost matching to each other comparing the numerical FEM-Design calculation with the experimental test result.

The ultimate loads, mid-span deflections and ultimate bending moments at mid-span are as follows:

$F_{test}=353.4\,\text{kN}$, $d_{test}=0.033\,\text{m}$, $M_{Rd\,test}=565\,\text{kNm}$

$F_{FD}=344\,\text{kN}$, $d_{FD}=0.029912\,\text{m}$, $M_{Rd\,FD}=550\,\text{kNm}$

The difference between the results are less than 10 %.

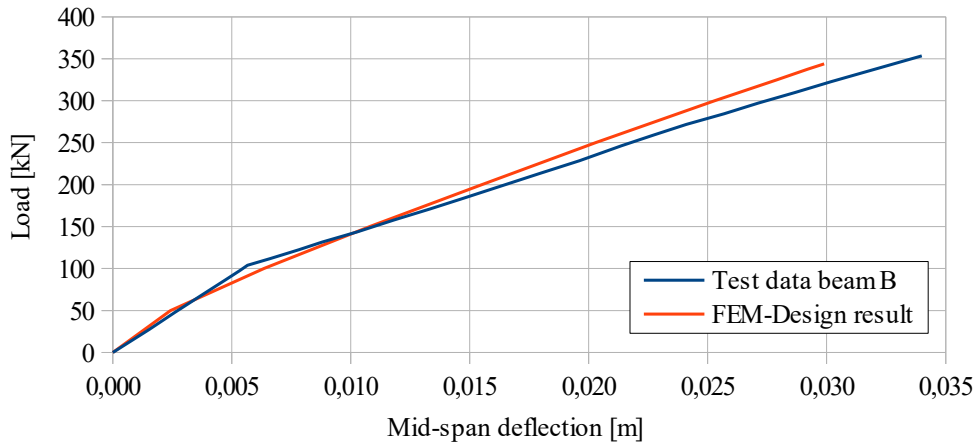

52. Figure - Load-deflection curves in case of beam B

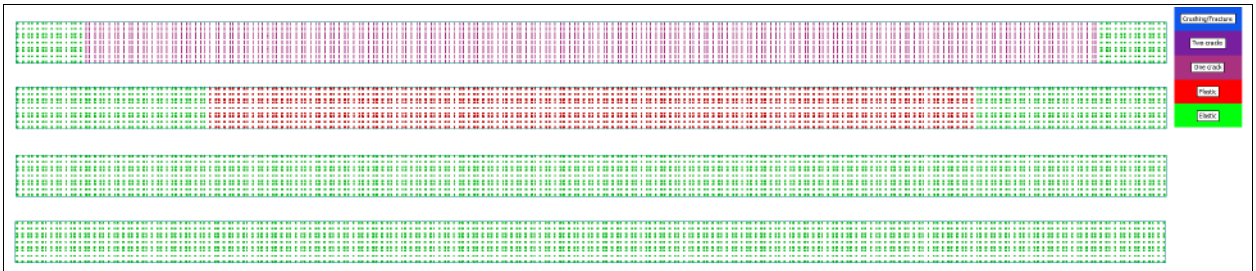

53. Figure - Plastic shell conditions in case of beam B
a) concrete bottom layer, b) concrete top layer, c) bottom reinforcement, d) top reinforcement

6.1.5 Clamped-clamped beam with uniform distributed load

Section and material properties	
Height [mm]	h=200
Width [mm]	b=100
Effective depth [mm]	d=170
Effective depth [mm]	d'=30
Reinf. bottom [mm^2/m]	a_s=2262 (ϕ12/50)
Reinf. top [mm^2/m]	$a_{s'}$=2262 (ϕ12/50)
Span length [m]	L=5
Concrete Young's mod. [GPa]	E_c=34
Poisson's ratio [-]	ν=0.0
Ultimate comp. strength [MPa]	f_c=35
Ultimate yield strain [-]	ε_{c2}=0.002
Ultimate comp. strain [-]	ε_{cu}=0.0035
Reinf. steel Young's mod. bottom [GPa]	E_s=210
Yield stress bottom [MPa]	f_y=500
Ultimate strain of reinforcements [-]	ε_{su}=0.05

In this example a beam with clamped supports subjected to uniformly distributed load will be analysed. The longitudinal elongation in the beam is free, see Fig. 54.

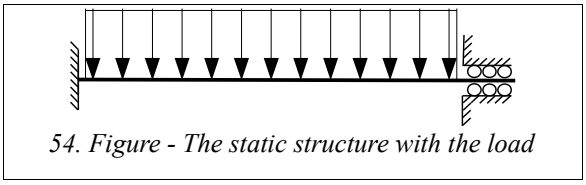

54. Figure - The static structure with the load

The geometry and material properties of the beam with rectangle cross-section can be seen in the above table. The reinforcement is symmetric and applied in the longitudinal direction. In this example Ref. [22] was considered as a benchmark for this case. According to the mentioned reference the ultimate intensity of the distributed load is around:

$$p_u = 106\ \mathrm{kN/m} \quad ,$$

which is the ultimate load according to the plastic-hinge theory.

Fig. 55 shows the FEM-Design model with the applied load and mesh.

In FEM-Design four different calculations were performed using the settings according to Fig. 56. In FEM-Design 10 concrete layers were considered as the concrete core in the laminated plastic shell model, plus two reinforcement layers (bottom, top).

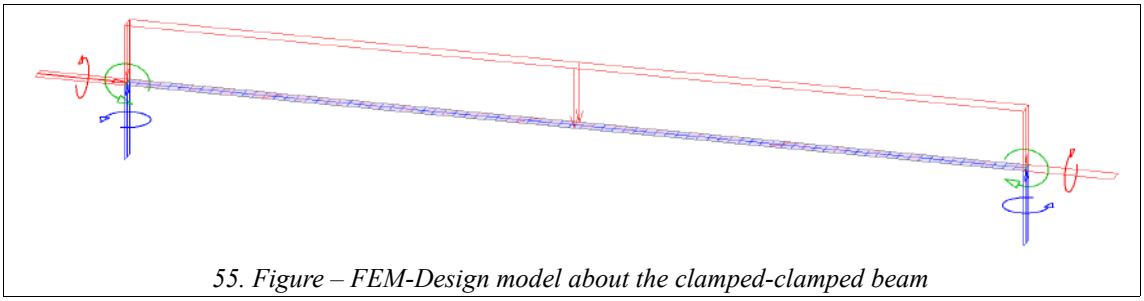

55. Figure – FEM-Design model about the clamped-clamped beam

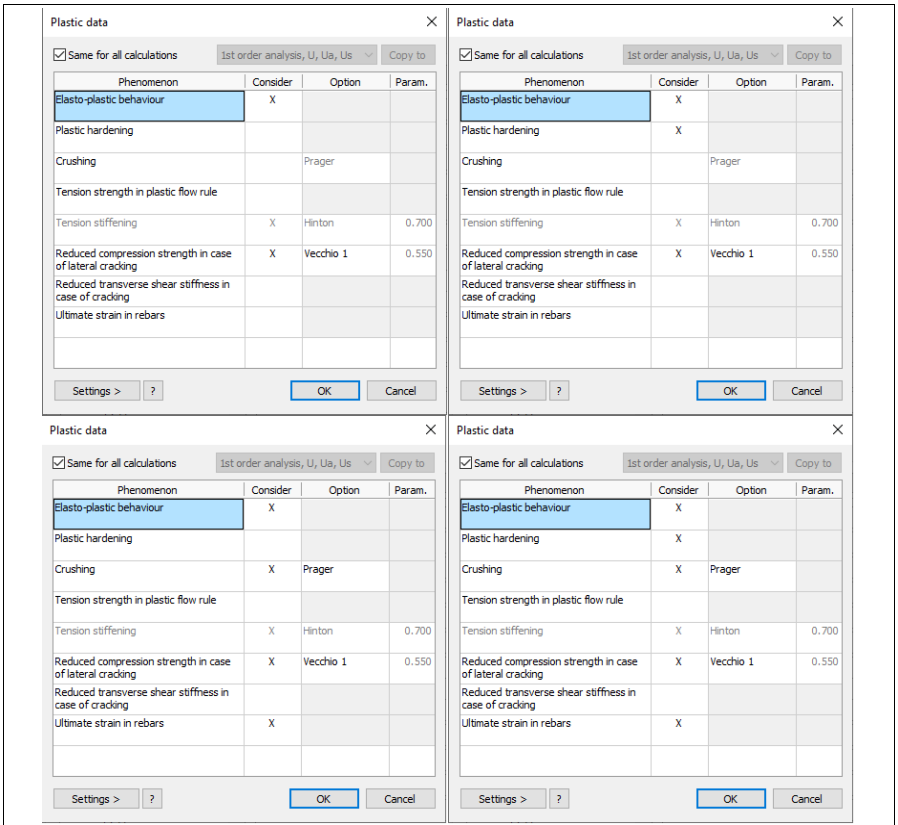

56. Figure – FEM-Design plastic settings about the four different cases

In Fig. 57 the load-mid deflection curves can be seen. In Ref [22] the solution was preformed using limit analysis theory in which the strain check is just a post processing. The black asterisk in Fig. 57 shows the post-processing strain limit checks in reinforcement steel according to different methods (nodal/averaged). Here you can see also the FEM-Design results. If no strain limit was considered the ultimate load according to FEM-Design was:

$$p_{u\,FD} = 110\,\mathrm{kN/m}$$

If the strain limits were considered (concrete crushing and ultimate strain in rebar) the ultimate load level was:

$$p_{u\,FD\,with\,strain\,limits} = 92\,\mathrm{kN/m}$$

Note that in FEM-Design the concrete crushing was the relevant failure mode. In Ref. [22] only the reinforcement strain limit was considered, see the black asterisks in Fig. 57.

Thus, we can say that the FEM-Design result is very close to the theoretical plastic-hinge

solution regardless the strain limits. If the strain limit is considered, the FEM-Design result is close to the benchmark result but a bit lower, but do not forget that in the benchmark only the reinforcement steel strain limit was considered.

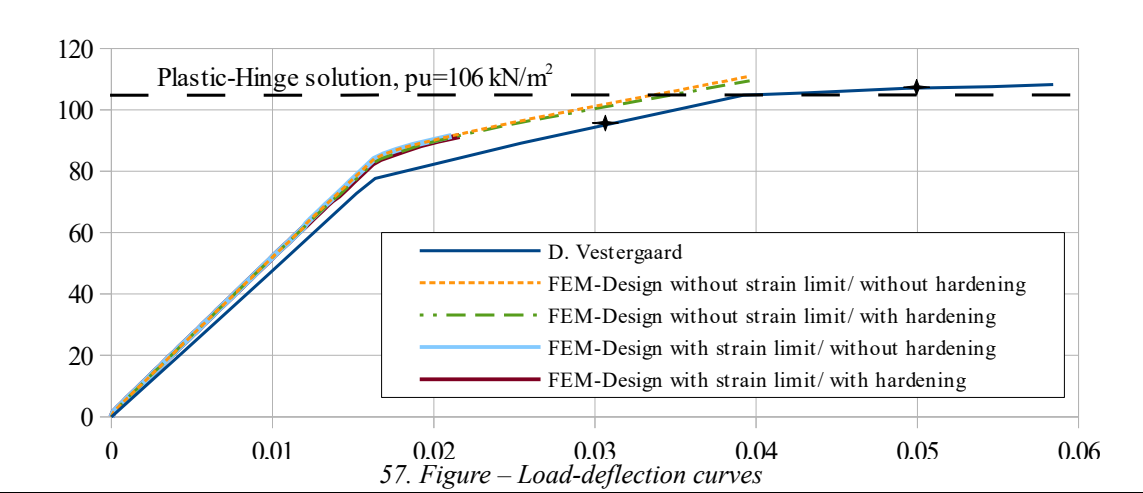

57. Figure – Load-deflection curves

In case of concrete hardening and strain limits consideration in FEM-Design calculation Fig. 58 shows the bottom/top concrete, bottom/top reinforcement plastic conditions and the bending moment diagram at ultimate load level.

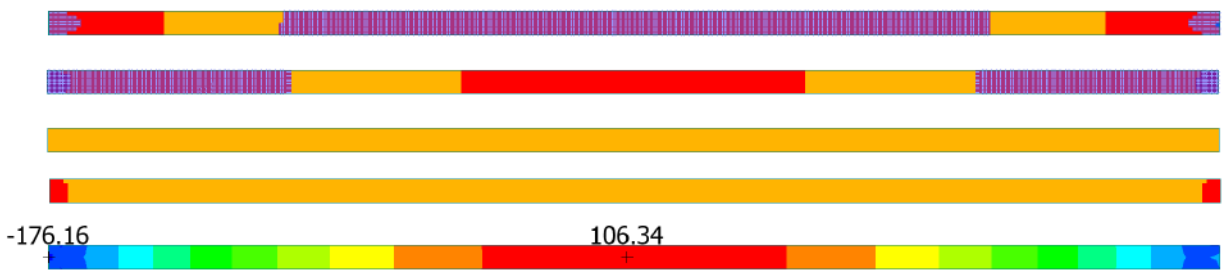

58. Figure - Bottom concrete layer plastic conditions
Top concrete layer plastic conditions
Bottom reinforcement plastic conditions
Top reinforcement plastic conditions
Bending moment diagram [kNm/m]
Colour palette schema for plastic conditions:
Elastic (yellow), Plastic (red),One crack (light purple), Two cracks (dark purple), Crushing/Fracture (blue)

According to Fig. 58 it can be concluded that the ultimate bending moment of the section is around 176 kNm/m, because the clamped ends reached that limit. The mid-section due to the strain limits doesn't reach this ultimate bending moment (see Fig. 58 as well). If the strain limits were neglected in FEM-Design the mid-section bending moment was closer to this ultimate bending moment as well (see Fig. 59).

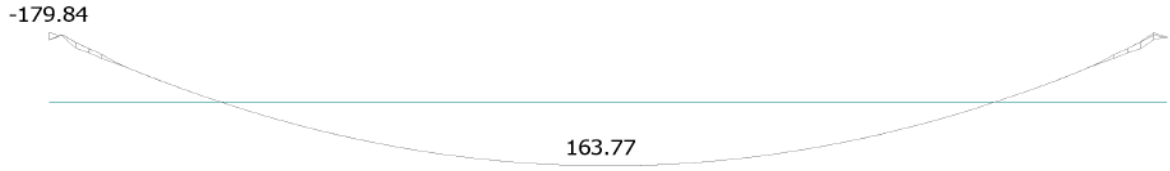

59. Figure - Bending moment diagram [kNm/m] without strain limits

6.1.6 Two span RC beam compared with experimental data

Section and material properties	
Height [mm]	h=80
Width [mm]	b=60
Effective depth [mm]	d=73
Effective depth [mm]	d'=7
Reinf. bottom [mm^2]	A_s=50.26
Reinf. top [mm^2]	$A_{s'}$=50.26
Span length [m]	L=0.84
Concrete Young's mod. [GPa]	E_c=16.66
Poisson's ratio [-]	ν=0.0
Ultimate comp. strength [MPa]	f_c=32.0
Ultimate tens. strength [MPa]	f_t=3.2
Ultimate yield strain [-]	ε_{c2}=0.0027
Ultimate comp. strain [-]	ε_{cu}=0.004
Reinf. steel Young's mod. bottom [GPa]	E_s=196
Yield stress bottom [MPa]	f_y=574
Reinf. steel Young's mod. top [GPa]	$E_{s'}$=196
Yield stress top [MPa]	$f_{y'}$=574

The statically indeterminate structure was experimentally tested by Ref. [23] and reported in Ref. [24] and [2]. In contrast with the previous example this beam exhibits a large non-linear response with extensive cracking and yielding of concrete before collapse occurs. Fig. 60 and the table above shows the static structural system and the section data of the experimental layout.

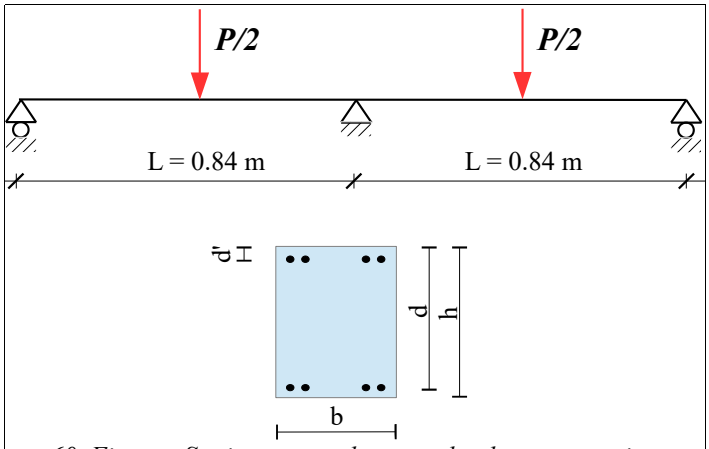

60. Figure - Static structural system, loads, cross-section

In FEM-Design the beam was modelled with shell element according to Fig. 61. The plastic shell calculation data can be seen in Fig. 62. The applied layer number was n_{lay} = 10.

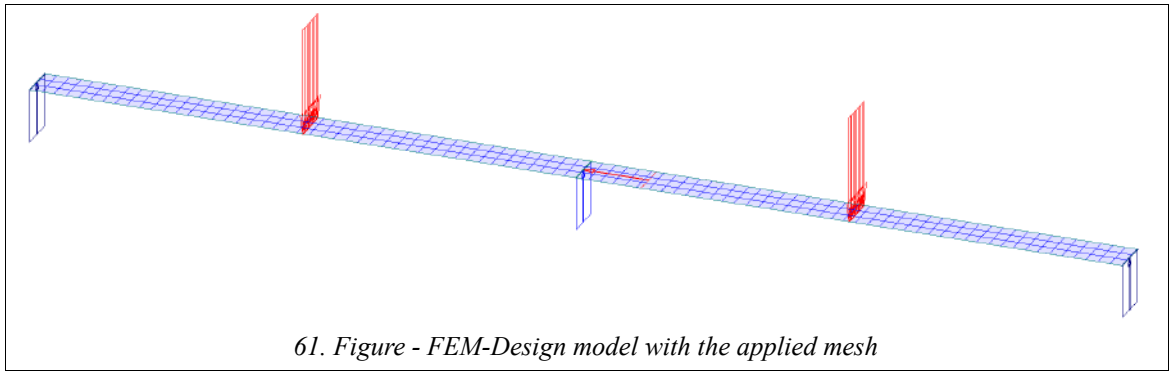

61. Figure - FEM-Design model with the applied mesh

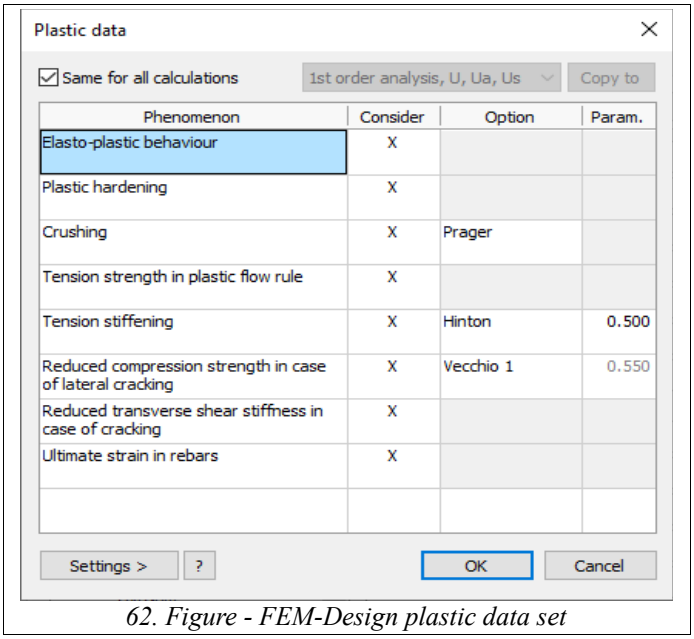

62. Figure - FEM-Design plastic data set

The following load displacement diagram shows the result of the test experiment (two span

beam). FEM-Design result is also available in the same figure.

FEM-Design load-displacement curve is in good agreement with the experimental results (see Fig. 63). The ultimate load-bearing capacity is a bit lower compared to the test result.

In the following calculations we assume the first "yielding" load level, where the middle support section reach the ultimate moment capacity of the RC section. After that according to the plastic-hinge theory the final ultimate load-bearing capacity will be calculated.

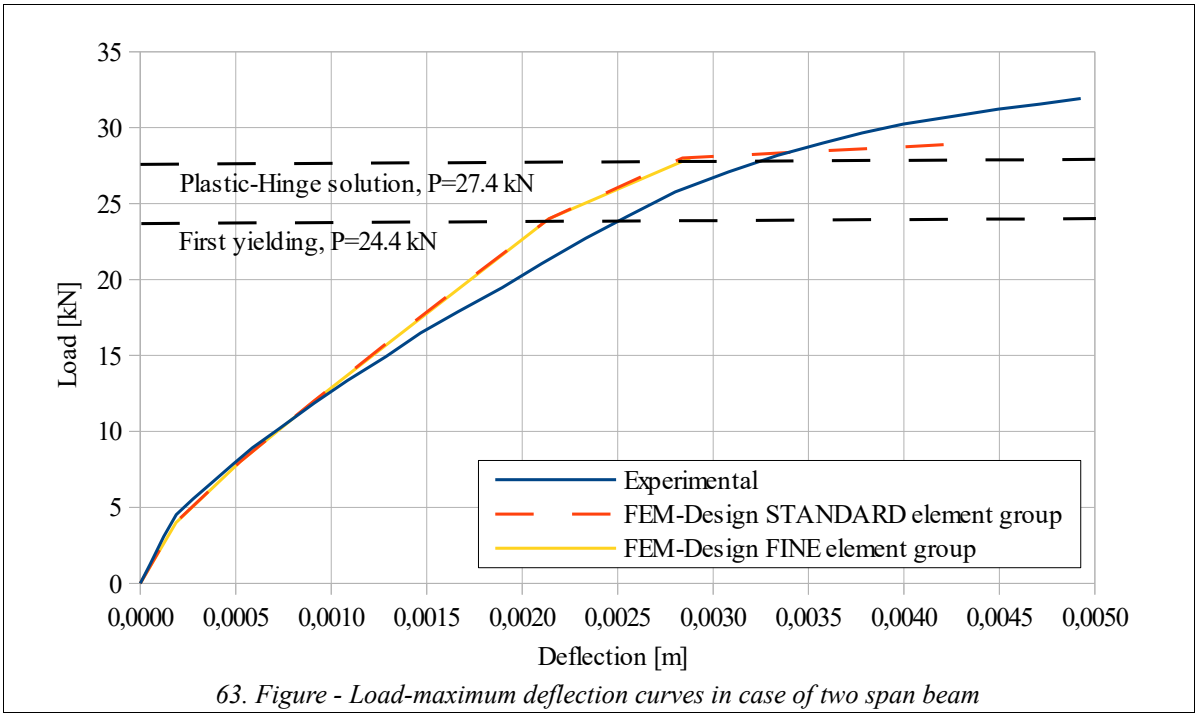

63. Figure - Load-maximum deflection curves in case of two span beam

According to the test result the ultimate load-bearing capacity was:

$P_{test} = 31.9\,\text{kN}$.

According to the given input data the RC section ultimate moment capacity can be assumed according to general strength of material approximations as:

$M_{Rd\,analytical} = 1.92\,\text{kNm}$.

The first "yield" where one section reaches this theoretical moment capacity occurs on the following load level based on the analytical ultimate moment capacity value:

$$P_{first\ yield\ analytical} = \frac{32}{3}\frac{M_{Rd\,analytical}}{L} = \frac{32}{3}\frac{1.92}{0.84} = 24.4\,\text{kN}$$

According to the plastic hinge solution if the ultimate moment capacity of the section is given:

$$P_{plastic\ hinge\ analytical} = 12\frac{M_{Rd\,analytical}}{L} = 12\frac{1.92}{0.84} = 27.4\,\text{kN}$$

The numerical results based on FEM-Design are as follows:

$P_{FD_{fine}} = 28\,\text{kN}$, $M^{+}_{Rd\,FD_{fine}} = 1.91\,\text{kNm}$, $M^{-}_{Rd\,FD_{fine}} = 1.98\,\text{kNm}$

$P_{FD_{standard}} = 29\,\text{kN}$, $M^{+}_{Rd\,FD_{standard}} = 1.94\,\text{kNm}$, $M^{-}_{Rd\,FD_{standard}} = 1.95\,\text{kNm}$

In FEM-Design the standard and the fine element group were also used for the two different analysis. The ultimate load-bearing capacity is a bit lower compared with the test result, but the ultimate positive and negative moment at the final converged load level are in good agreement with the analytical moment capacity. In this case the theoretical plastic hinge calculation result almost match the numerical FEM-Design result, but this is not true in all cases, it depends on the structure and applied loads as well in general.

According to the test results, collapse occurs by concrete crushing at mid-span and mid-supported sections after excessive deformation of the tensile reinforcement.

Fig. 64 shows the non-linear conditions of the RC beam based on the FEM-Design plastic shell analysis. In the bottom concrete layer above the mid-support the concrete is in plastic condition as expected and also in the top concrete layer under the applied loads as well. At the ultimate load level the reinforcements are in plastic (yielding) condition. In the bottom reinforcement at mid-span and in the top reinforcement at the mid-support (see Fig. 64).

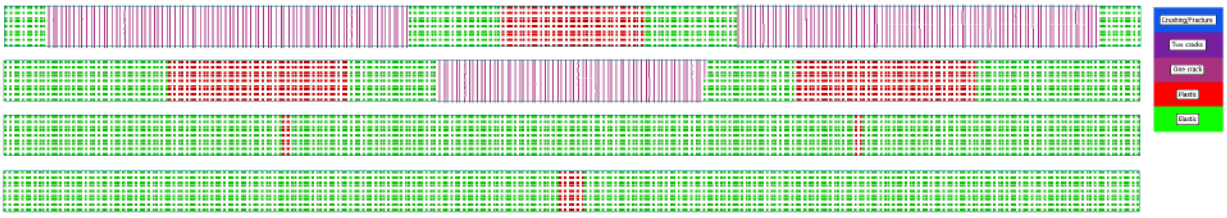

64. Figure - Plastic shell conditions in case of two span beam
a) concrete bottom layer, b) concrete top layer, c) bottom reinforcement, d) top reinforcement

6.1.7 Corner supported square slab with different reinforcement ratios compared with experimental data

Section and material properties	
Thickness [mm]	h=65
Slab length [mm]	L=1170
Effective depth [mm]	d=56
Effective depth [mm]	d'=9
S1 Reinf. bottom x direction [mm^2/m]	a_s=397
S1 Reinf. top x direction [mm^2/m]	$a_{s'}$=193
S2 Reinf. bottom x direction [mm^2/m]	a_s=519
S2 Reinf. top x direction [mm^2/m]	$a_{s'}$=253
S3 Reinf. bottom x direction [mm^2/m]	a_s=582
S3 Reinf. top x direction [mm^2/m]	$a_{s'}$=283
S1 reinforcement in y direction	ρ_x/ρ_y = 1.00
S2 reinforcement in y direction	ρ_x/ρ_y = 1.89
S3 reinforcement in y direction	ρ_x/ρ_y = 2.75
Concrete Young's mod. [GPa]	E_c=16.40
Poisson's ratio [-]	ν=0.15
Ultimate comp. strength [MPa]	f_c=43.0
Ultimate tens. strength [MPa]	f_t=3.0
Ultimate comp. strain [-]	ε_{cu}=0.0035
Reinf. steel Young's mod. [GPa]	E_s=201
Yield stress [MPa]	f_y=600
Ultimate strain [-]	ε_{su}=0.025

In this example a corner supported square slab with a point load at the centre will be analysed. In the three different (S1, S2, S3) cases the reinforcements are different (see. Fig. 65 and 66 and the table above). The example was taken from Ref. [25] and [3]. In the first reference the experimental data can be find. In the other reference a numerical calculation result can be found. FEM-Design results will be compared both experimental, numerical and analytical (yield line) results as well. The input table contains all of the necessary information about the geometry, material properties and reinforcements based on the references.
Fig. 67 shows the FEM-Design model with the applied mesh (average mesh size = 0.07m) and loads. The load was considered as distributed load on a 100/100mm square surface at the centre of the slab. In FEM-Design all of the plastic reinforced concrete shell options (except concrete hardening) were considered, see Fig. 68.

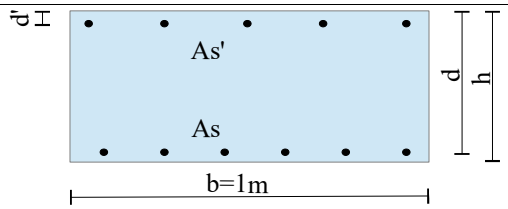

65. Figure - Schematic drawing about the reinforcements in x or y directions, the effective depth assumed equal in both directions

First, the pure ultimate moment capacities of the slabs will be calculated to assume the ultimate loads based on yield line theory. During the hand calculation of the ultimate moment capacities rectangle concrete and linear elastic perfectly plastic reinforcement steel material model will be used.

Due to the symmetric reinforcement in case of Sl slab the x and y directional moment capacities are the same, which one will be the basic input to the yield line theory calculation. In S2 and S3 slabs, the weaker ultimate moment capacities will be in the y direction.

S1 slab:

If the reinforcement is in elastic condition the stress in the compressed side can be assumed as:

$$\sigma_s = \frac{E_s \cdot \varepsilon_{cu} \cdot d'}{1.25\, x_c} - E_s \cdot \varepsilon_{cu} = 562.8 \frac{d'}{x_c} - 703.5\,[\mathrm{MPa}]$$

Equilibrium equations are as follows:

$$x_c \cdot f_c - (562.8 \frac{d'}{x_c} - 703.5) a_{s'} = f_s \cdot a_s \quad ;$$

$$m_{Rd} = \left(562.8 \frac{d'}{x_c} - 703.5\right) a_{s'} \cdot (d' - \frac{x_c}{2}) + f_s a_s (d - \frac{x_c}{2})$$

The solution of the above equations:

$m_{Rd} = m_{x'Rd} = m_{y'Rd} = 12.76\,\mathrm{kNm/m}$, $x_c = 6.106\mathrm{mm}$, $\sigma_s = 600\,\mathrm{MPa}$, $\sigma_{s'} = 126\,\mathrm{MPa}$

(top and bottom reinforcements are in tension, because the compressed zone is small)

The ultimate moment capacity according to the yield line theory assuming the same ultimate moment capacities in x and y directions:

$$P_{yield\ line} \cdot e_{disp} = 2\, L\, m_{Rd} \frac{2}{L} e_{disp} \quad ; \quad P_{yield\ line} = 4\, m_{Rd} = 51.04\,\mathrm{kN}$$

With the same calculation assumptions in S2 and S3 slabs the moment capacities and the ultimate load levels according to the yield line theory are as follows:

S2 slabs:

$m_{y'Rd} = 9.13\,\mathrm{kNm/m}$, $x_c = 4.88\mathrm{mm}$, $\sigma_s = 600\,\mathrm{MPa}$, $\sigma_{s'} = 334\,\mathrm{MPa}$

(top and bottom reinforcements are in tension, because the compressed zone is small)

$$P_{yield\ line} e_{disp} = L\, m_{yRd} \frac{4}{L} e_{disp} \quad ; \quad P_{yield\ line} = 4\, m_{yRd} = 36.52\,\text{kN}$$

S3 slabs:

$m_{y'Rd} = 7.207\,\text{kNm/m}$, $x_c = 4.1735\,\text{mm}$, $\sigma_s = 600\,\text{MPa}$, $\sigma_{s'} = 510\,\text{MPa}$
(top and bottom reinforcements are in tension, because the compressed zone is small)

$$P_{yield\ line} e_{disp} = L\, m_{yRd} \frac{4}{L} e_{disp} \quad ; \quad P_{yield\ line} = 4\, m_{yRd} = 28.83\,\text{kN}$$

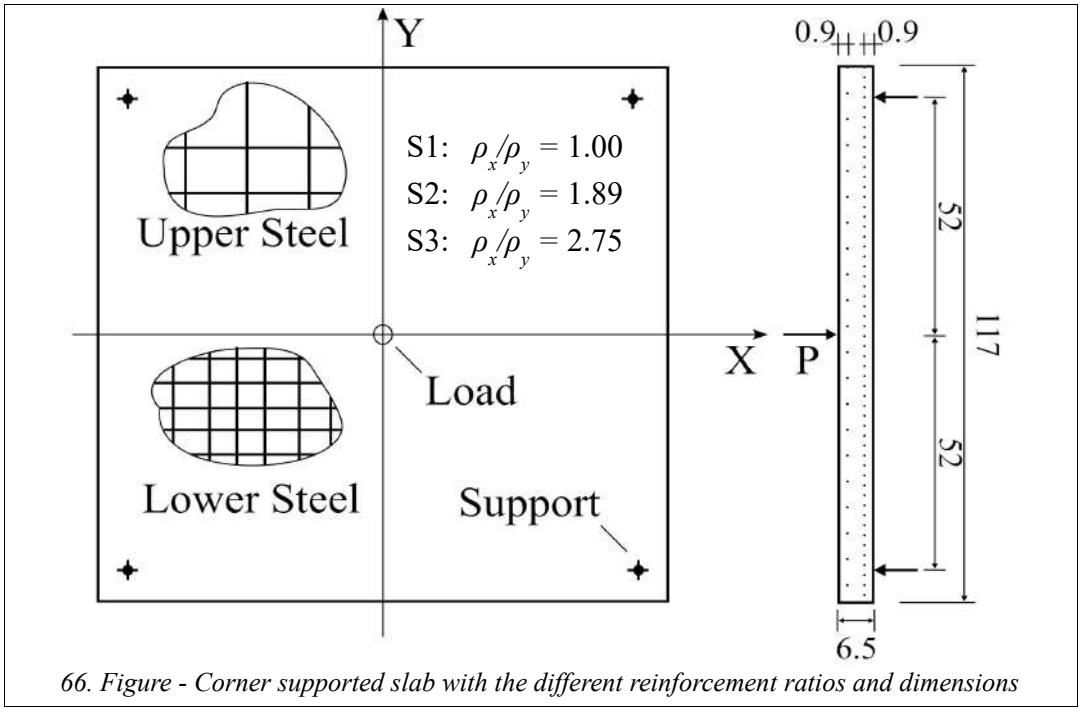

66. Figure - Corner supported slab with the different reinforcement ratios and dimensions

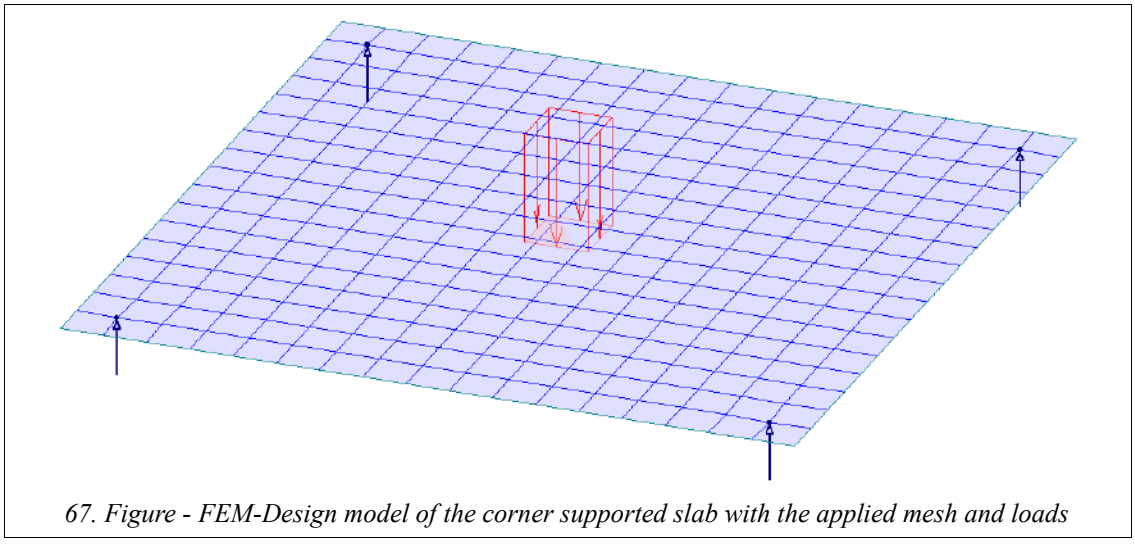

67. Figure - FEM-Design model of the corner supported slab with the applied mesh and loads

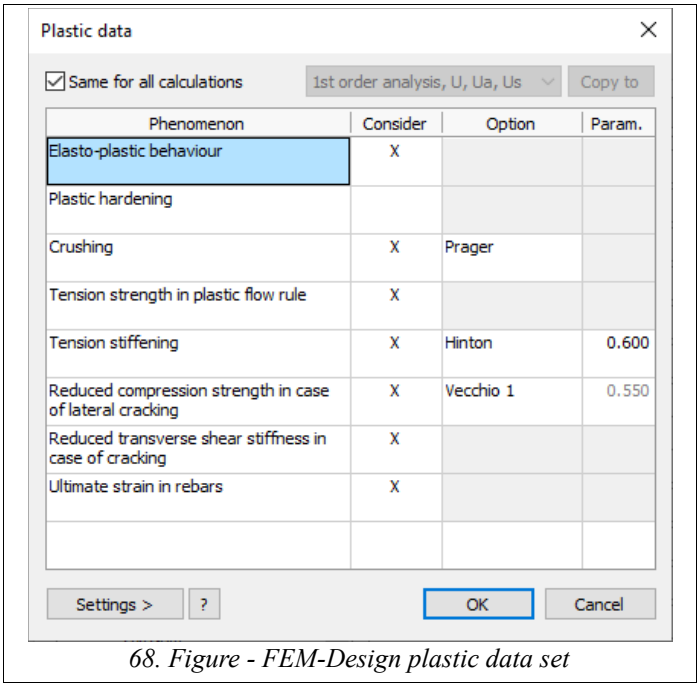

68. Figure - FEM-Design plastic data set

Figure 69 shows the load vs. centre point deflections curves based on experimental and benchmark numerical data. This figure also shows the FEM-Design results and the yield line solutions as well.

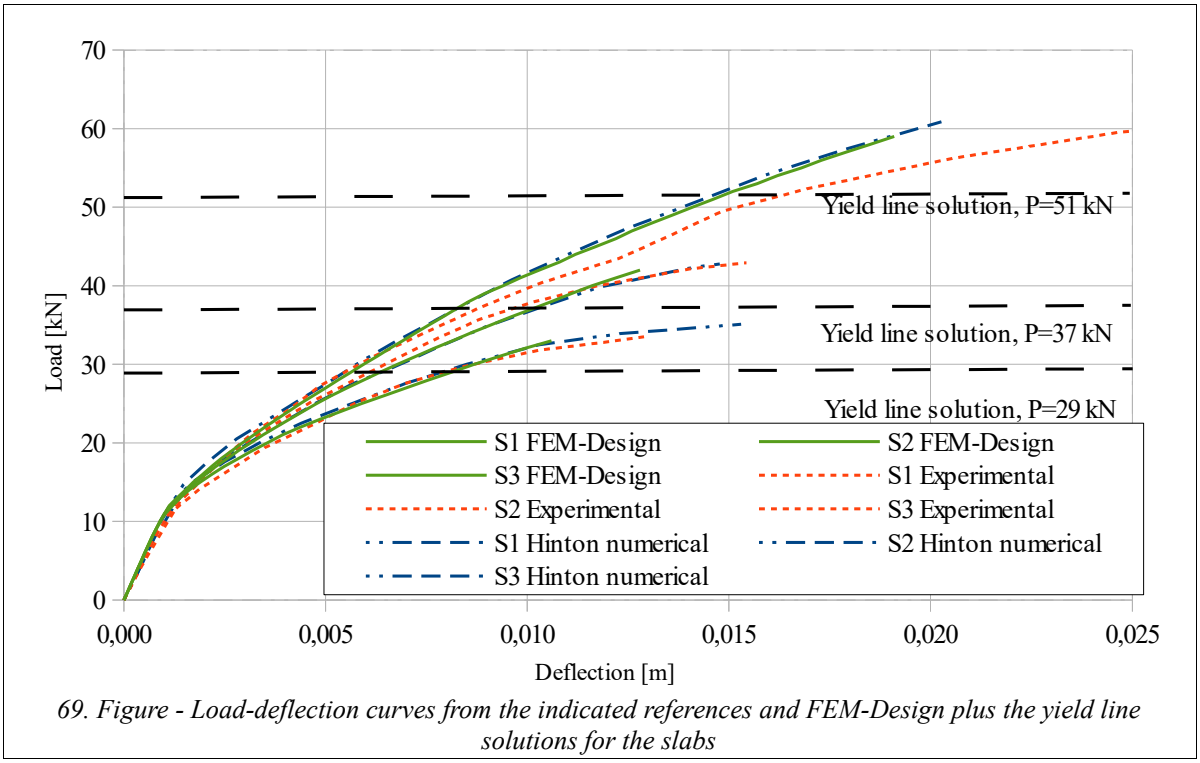

69. Figure - Load-deflection curves from the indicated references and FEM-Design plus the yield line solutions for the slabs

Here you can see the ultimate load levels for the three different slabs (S1,S2,S3) based on the experimental, independent numerical and FEM-Design results. The yield line solutions also indicated here:

Experimental ultimate load levels:

$P_{S1\,test}=61\,\text{kN}$, $P_{S2\,test}=43\,\text{kN}$, $P_{S3\,test}=34\,\text{kN}$

Numerical benchmark ultimate load levels:

$P_{S1\,numerical\,Hinton}=61\,\text{kN}$, $P_{S2\,numerical\,Hinton}=43\,\text{kN}$, $P_{S3\,numerical\,Hinton}=34\,\text{kN}$

Yield line solution ultimate load levels:

$P_{S1\,yield\,line}=51\,\text{kN}$, $P_{S2\,yield\,line}=37\,\text{kN}$, $P_{S3\,yield\,line}=29\,\text{kN}$

FEM-Design ultimate load levels:

$P_{S1\,FD}=59\,\text{kN}$, $P_{S2\,FD}=42\,\text{kN}$, $P_{S3\,FD}=33\,\text{kN}$

We can say that FEM-Design results are in good agreement with the experimental test results and the independent numerical results as well. The yield line solutions here are always below the numerically calculated/experimental ultimate loads. The reason in this case is that the ultimate bending moments by the yield line solutions are only approximations and in the numerical calculations (and on the experimental tests) the biaxial behaviour of the concrete was also considered.

The above comparisons are related only the load levels and the centre point deflections. In the mentioned references e.g. in the experimental tests the deflections along the symmetric axes and based on strain gauges data the bending moments along the symmetric axes at specific load levels were also reported.

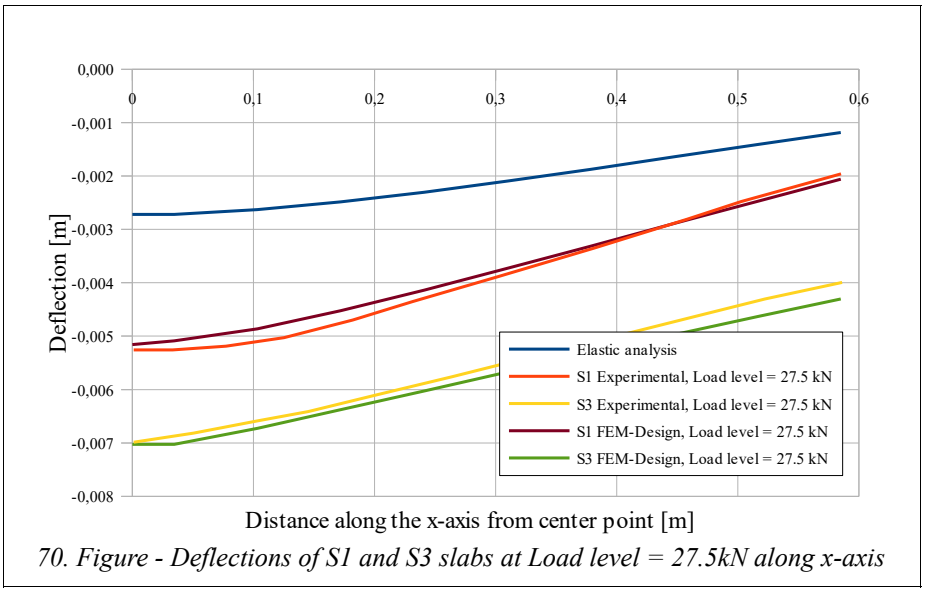

70. Figure - Deflections of S1 and S3 slabs at Load level = 27.5kN along x-axis

Fig. 70 and 71 show the deflections in S1 and S3 slabs along the x and y symmetric axes at 27.5kN load level. These figures also indicate, how the elastic FE calculation result look like based on a pure linear elastic material slab without reinforcement. These results are exactly the same in both cases because they neglect the reinforcement ratios.

We can say that the deflections are in good agreement with the FEM-Design results, and also that the non-linear effect has great effect on the deflections compared with linear elastic case.

It is important to note that in S1 the deflections are almost the same along x and y axis due to the same reinforcements in x and y directions. In case of S3 slab the deflections greater along x axis because the reinforcement in y direction is weaker.

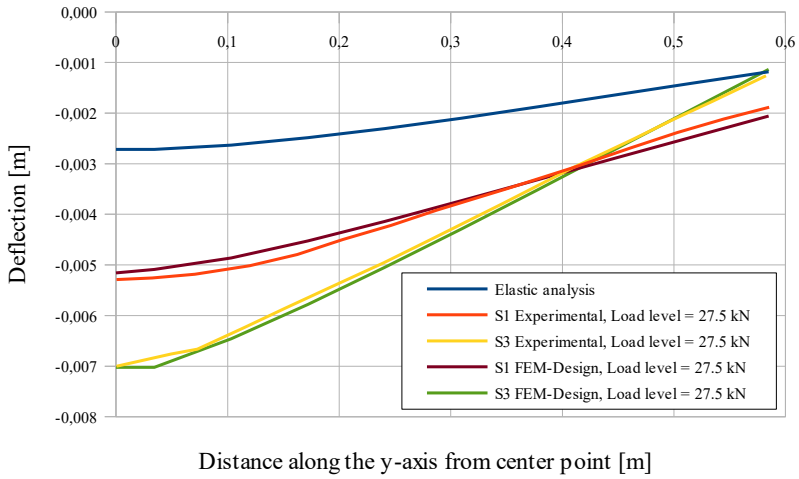

71. Figure - Deflections of S1 and S3 slabs at Load level = 27.5kN along y-axis

Fig. 72-74 show the M_y bending moments along x and y axes in S1 and S3 slabs at specific load levels based on experimental data (strain gauge approximation) and FEM-Design numerical results. We can say that the distribution of the bending moments in FEM-Design are in good agreement with the experimental results. Some discrepancy can be seen but it comes from the FE idealization and the approximation from strain gauge calculation.

Fig. 75 shows the plastic conditions of the bottom and top concrete layers at the integration points in S1 slab from FEM-Design. The top layer is almost fully elastic because the experimental data about the concrete material contained only very small perfectly plastic part prior crushing. Fig. 76 shows the plastic conditions of the reinforcements. The results coincide with the yield line solution assumptions. Fig. 77 shows the section results about m_x and m_y in S1 slab at ultimate load level.

Fig. 78 shows the plastic conditions of the bottom and the y directional reinforcement layer at the integration points in S3 slab from FEM-Design. The plastic results of the reinforcements coincide with the yield line solution assumptions. Fig. 79 shows the section results about m_x and my in S3 slab at ultimate load level. Fig. 80 shows the unbalanced moments in S3 slab at first unstable load level. This result also returned the assumed yield line at failure.

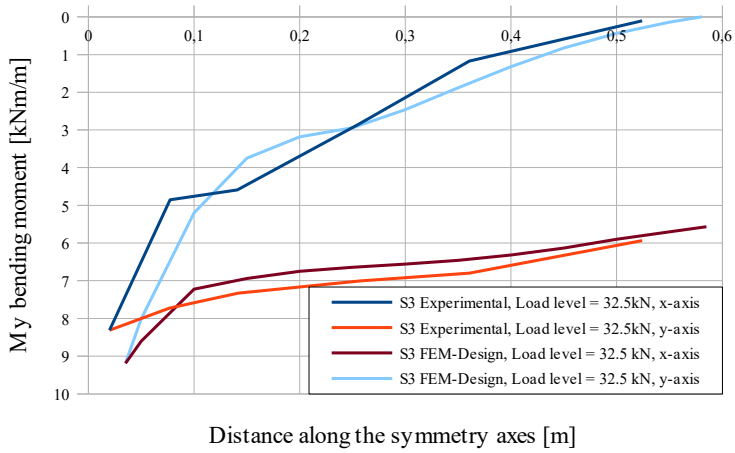

72. Figure - My bending moment in S3 slab at Load level = 32.5kN along x and y axes

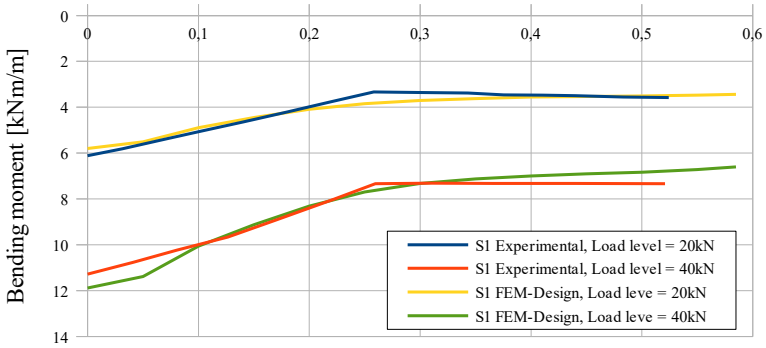

73. Figure - My bending moment in S1 slab at Load level 20 and 40kN along x axis

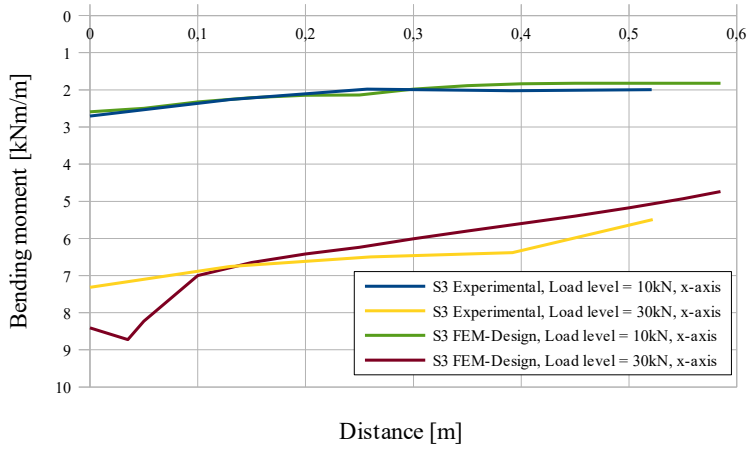

74. Figure - My bending moment in S3 slab at Load level 10 and 30kN along x axis

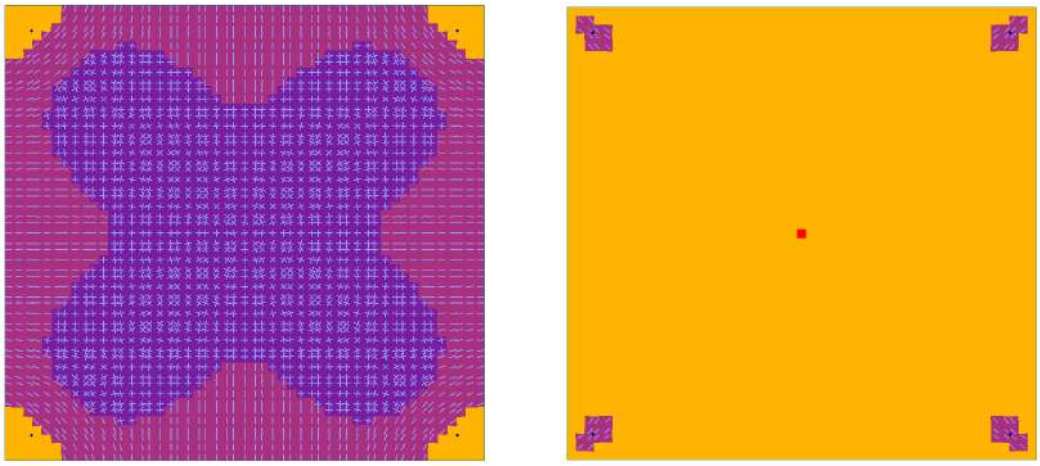

75. Figure - The bottom and top concrete layer plastic conditions in S1 slab at ultimate load level
Elastic (yellow), Plastic (red),One crack (light purple), Two cracks (dark purple), Crushing/Fracture (blue)

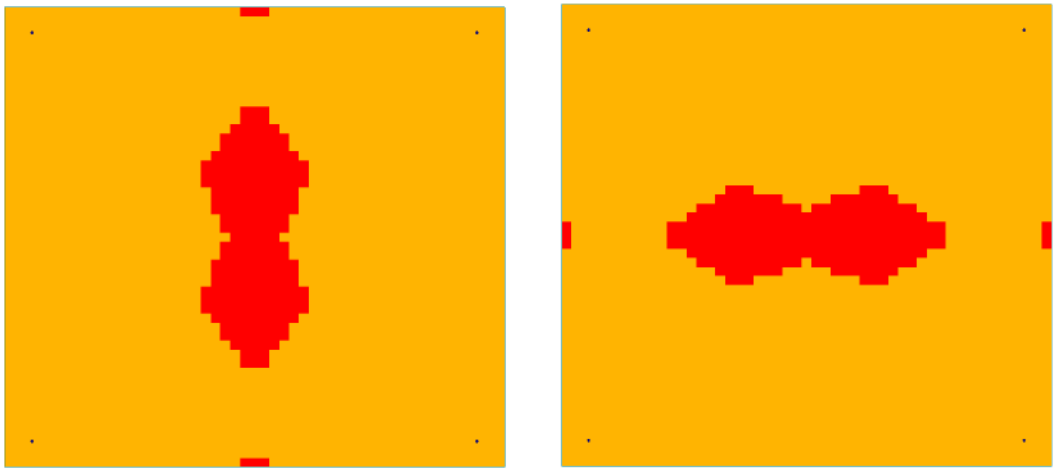

76. Figure - The bottom x and y directional reinforcements plastic conditions in S1 slab at ultimate load level
Elastic (yellow), Plastic (red)

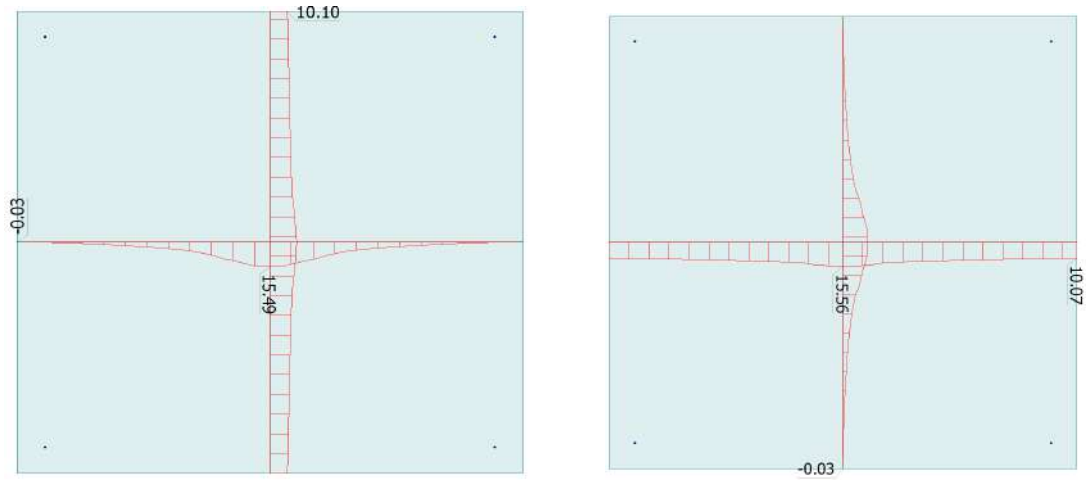

77. Figure - Section results about m_x and my bending moments [kNm/m] in S1 slab at ultimate load level

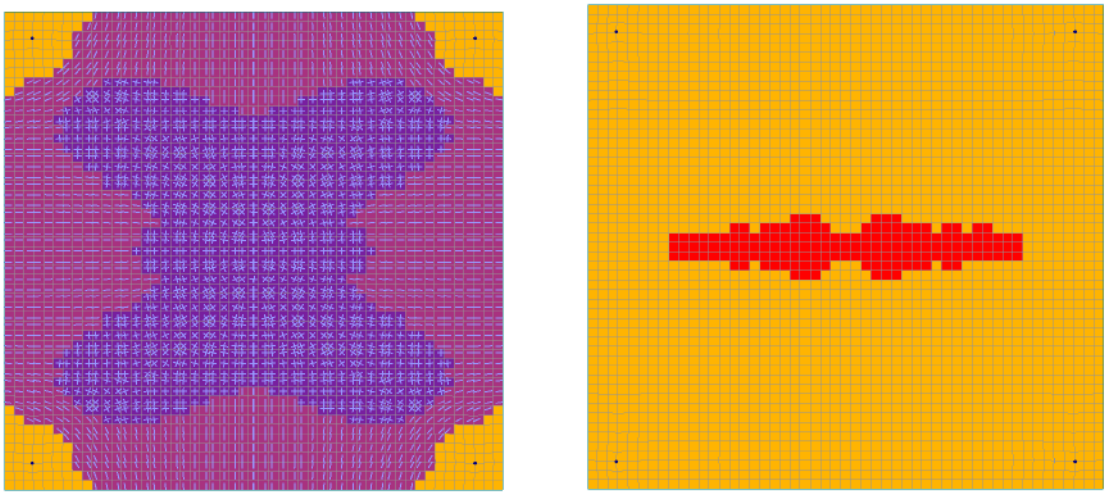

78. Figure - The bottom concrete and y direction reinforcement layer plastic conditions in S3 slab at ultimate load level
Elastic (yellow), Plastic (red),One crack (light purple), Two cracks (dark purple), Crushing/Fracture (blue)

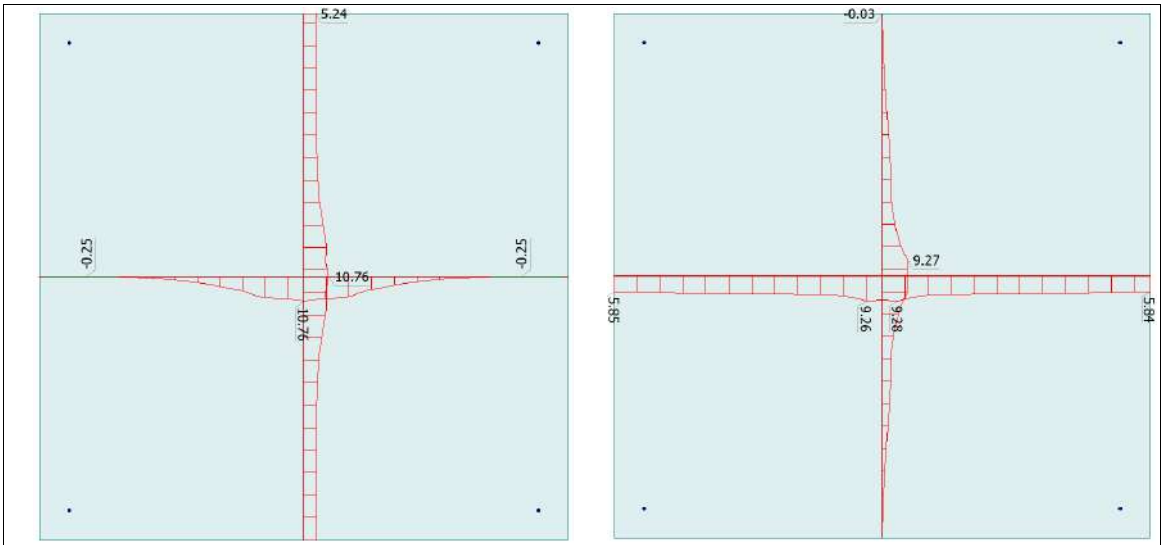

79. Figure - Section results about m_x and my bending moments [kNm/m] in S3 slab at ultimate load level

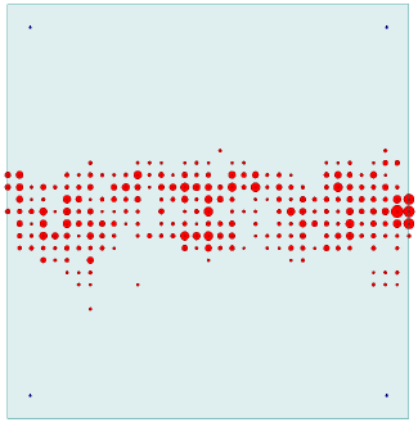

80. Figure - The unbalanced moments in S3 slab at first unstable result after ultimate load

Fig. 81 shows the FEM-Design results with and without the consideration of tension strength (and tension stiffening) in the concrete material model. The ultimate load levels without tension strength are almost equal to the tension stiffening case in all the three slabs.

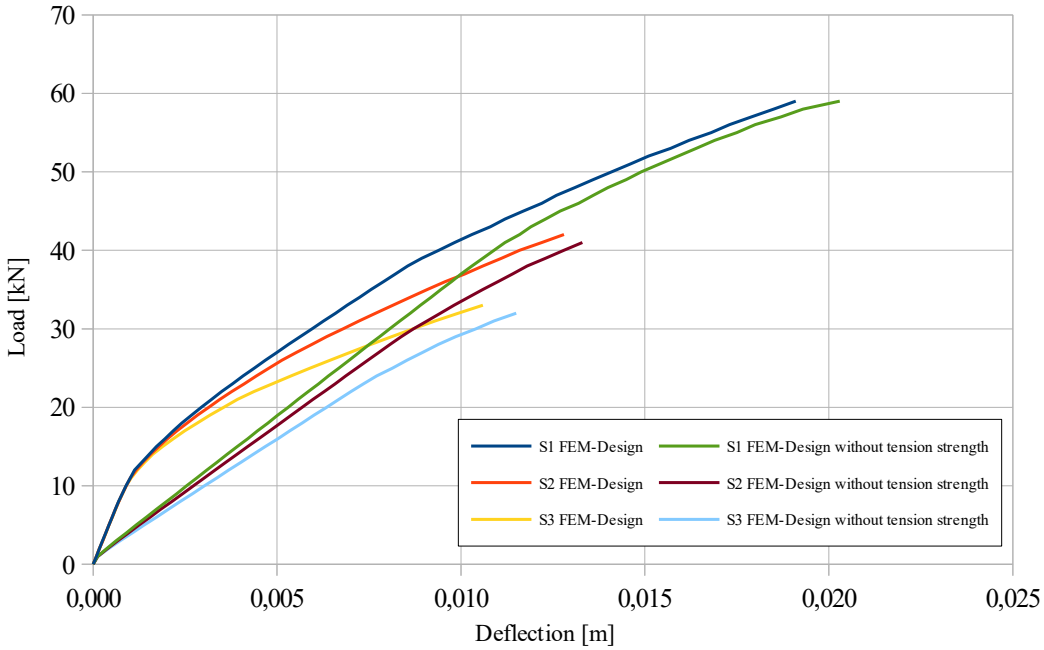

81. Figure - Load-deflection curves based on FEM-Design with tension strength (and tension stiffening) and without tension strength in concrete

Fig. 82 shows the first unstable unbalanced moment result in S1 slab without tension strength in concrete. The pattern of the unbalanced moments coincide with the yield line theory failure pattern.

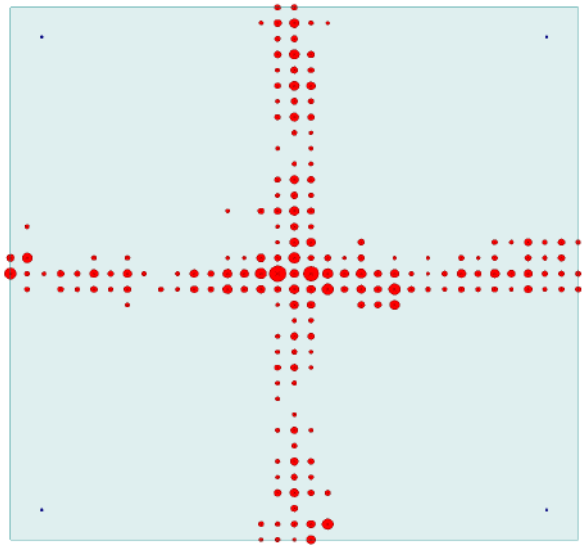

82. Figure - The unbalanced moments in S1 slab at first unstable result after ultimate load

Fig. 83 shows the plastic state of x and y directional reinforcements in S1 slab without tension strength in concrete calculation. The pattern of the yield lines match with the yield line theory failure pattern as well.

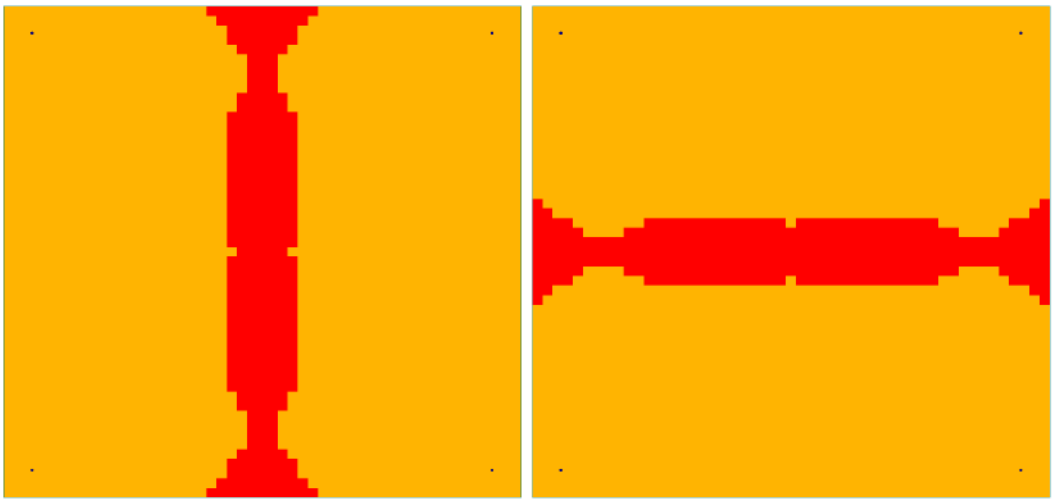

83. Figure - The bottom x and y directional reinforcements plastic conditions in S1 slab at ultimate load level without tension strength in concrete material model calculation
Elastic (yellow), Plastic (red)

6.1.8 Simply supported square plate compared with experimental and analytical data

Section and material properties	
Thickness [mm]	h=51
Slab length [mm]	L=1980 (effective length: 1830)
Effective depth [mm]	d_x=43.8
Effective depth [mm]	d_y=39.04
S1 Reinf. bottom x direction [mm^2/m]	a_{sx}=235
S1 Reinf. bottom y direction [mm^2/m]	a_{sy}=281
S6 Reinf. bottom x direction [mm^2/m]	a_{sxdiag}=201
S6 Reinf. bottom y direction [mm^2/m]	a_{sydiag}=235
S1 Concrete Young's mod. [GPa]	E_c=32.42
S1 Poisson's ratio [-]	ν=0.18
S1 Ultimate comp. strength [MPa]	f_c=35.0
S1 Ultimate tens. strength [MPa]	f_t=3.79
S1 Ultimate comp. strain [-]	ε_{cu}=0.0035
S6 Concrete Young's mod. [GPa]	E_c=32.42
S6 Poisson's ratio [-]	ν=0.18
S6 Ultimate comp. strength [MPa]	f_{cdiag}=35.0
S6 Ultimate tens. strength [MPa]	f_t=3.5
S6 Ultimate comp. strain [-]	ε_{cu}=0.0035
S1 Reinf. steel Young's mod. [GPa]	E_s=206.91
S1 Yield stress [MPa]	f_y=431
S1 Ultimate strain [-]	ε_{su}=0.025
S6 Reinf. steel Young's mod. [GPa]	E_s=206.91
S6 Yield stress [MPa]	f_{ydiag}=459
S6 Ultimate strain [-]	ε_{su}=0.025

In this example a simply supported slab will be analysed. The analysed case comes from Ref. [26] where experimental results were shown. The corners of the slabs can uplift, there were no anchoring to the simply supports at corners. S1 and S6 slabs differ from each other, while in S1 slab parallel reinforcements were applied with edges, in S6 diagonal (45 degree to the edges) reinforcements were applied. The applied loads were 16 surface loads on 5/5cm square patches, see Fig. 84. The material, geometric and other properties can be seen in the table above. Reinforcements were applied on bottom sides in both cases. The-FEM-Design model with the applied mesh and loads can be seen in Fig. 85.

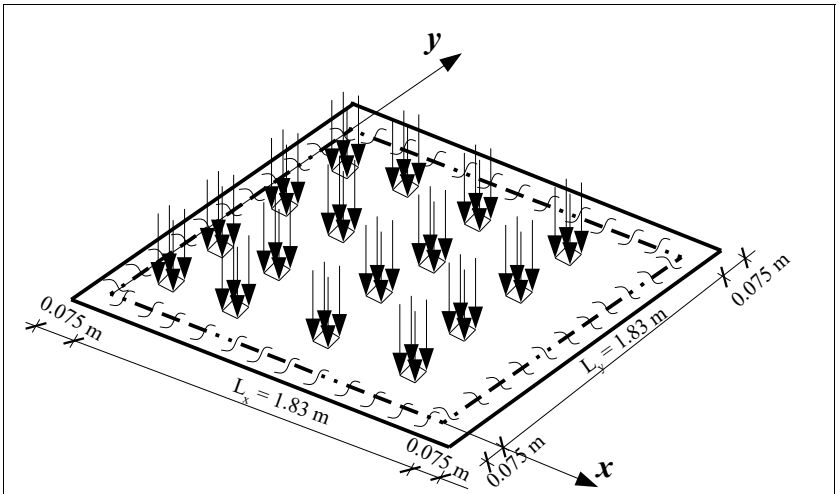

84. Figure - Simply supported square slab with 16 "point" loads

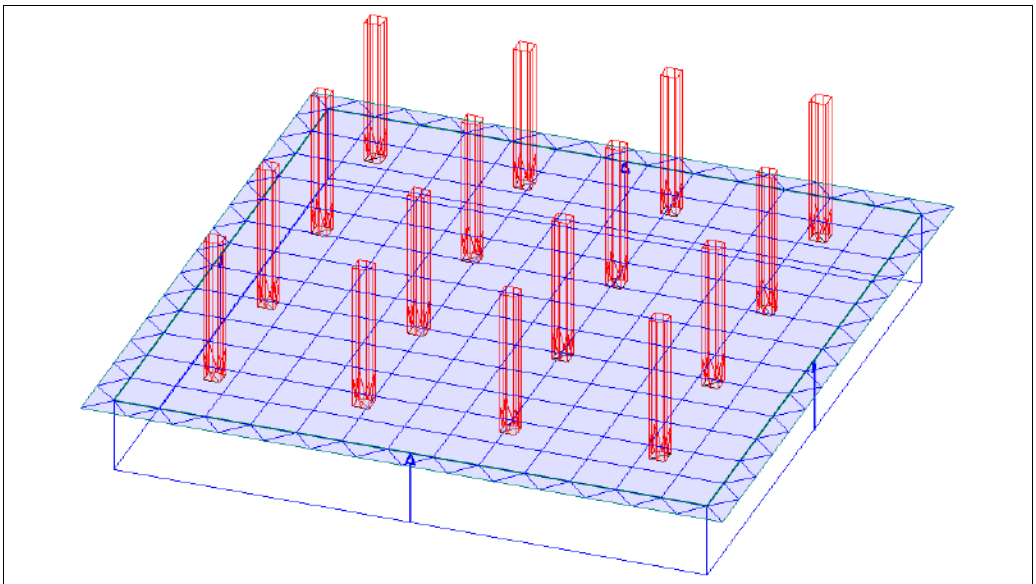

85. Figure - FEM-Design model with the applied loads and default mesh

First of all the ultimate load will be calculated according to the yield line theory, (see Ref. [3]). The ultimate bending moment capacities of the sections are as follows, which will be the basics of the yield line calculation method:

S1 slab:
In x direction:
Equilibrium equations:

$$x_{cx} \cdot f_c = f_y \cdot a_{sx} \quad ; \quad m_{x'Rd} = f_y a_{sx} \left(d_x - \frac{x_{cx}}{2}\right)$$

The solution of the above equations:

$$m_{x'Rd} = 4.29 \text{kNm/m} \quad , \quad x_{cx} = 2.89 \text{mm}$$

In y direction:
Equilibrium equations:

$$x_{cy} \cdot f_c = f_y \cdot a_{sy} \quad ; \quad m_{y'Rd} = f_y a_{sy} \left(d_y - \frac{x_{cy}}{2} \right)$$

The solution of the above equations:

$$m_{y'Rd} = 4.52 \text{kNm/m} \quad , \quad x_{cy} = 3.46 \text{mm}$$

Average ultimate moment capacity:

$$m_{Rd} = \frac{m_{x'Rd} + m_{y'Rd}}{2} = 4.4 \text{kNm/m}$$

For simplicity assume a total uniform distributed load instead of the real 16 “point” loads, the yield line theory gives the following ultimate load-bearing capacity (as resultant force):

$$p_{yield\ line} \cdot e_{disp} \frac{1}{3} L^2 = 2 L m_{Rd} \frac{4}{L} e_{disp} \quad ; \quad p_{yield\ line} L^2 = 24 m_{Rd} = 24 \cdot 4.4 = 105.6 \text{kN}$$

S6 slab:
In x diagonal direction:

- Equilibrium equations:

$$x_{cx} \cdot f_c = f_{ydiag} \cdot a_{sxdiag} \quad ; \quad m_{x'Rd\ diag} = f_{ydiag} a_{sxdiag} \left(d_x - \frac{x_{cx}}{2} \right)$$

- The solution of the above equations:
  $m_{x'Rd\ diag} = 3.92 \text{kNm/m} \quad , \quad x_{cx} = 2.63 \text{mm}$

In y diagonal direction:

- Equilibrium equations:

$$x_{cy} \cdot f_c = f_{ydiag} \cdot a_{sydiag} \quad ; \quad m_{y'Rd\ diag} = f_{ydiag} a_{sydiag} \left(d_y - \frac{x_{cy}}{2} \right)$$

- The solution of the above equations:
  $m_{y'Rd\ diag} = 4.04 \text{kNm/m} \quad , \quad x_{cy} = 3.08 \text{mm}$

Average ultimate moment capacity:

$$m_{Rd\ diag} = \frac{m_{x'Rd\ diag} + m_{y'Rd\ diag}}{2} = 3.98 \text{kNm/m}$$

Assuming a total uniform distributed load instead of the 16 “point” loads the yield line theory gives the following ultimate load-bearing capacity (resultant load):

$$p_{yield\ line} L^2 = 24 m_{Rd\ diag} = 24 \cdot 3.98 = 95.52 \text{ kN}$$

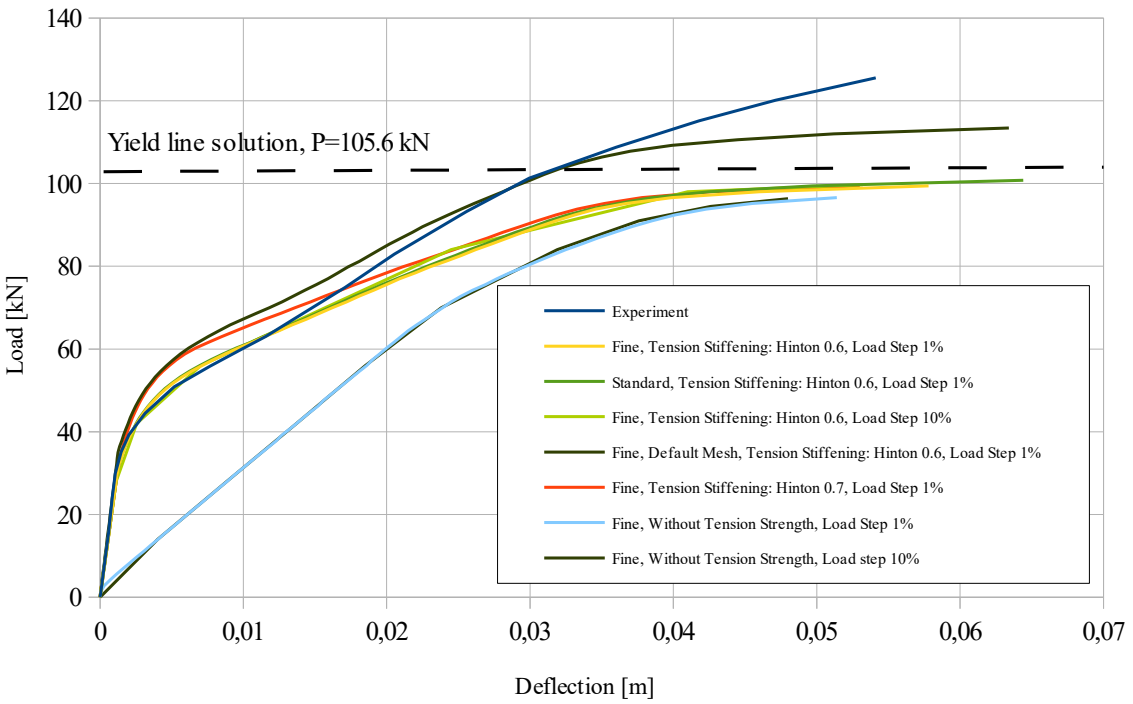

86. Figure - S1 slab results, load vs deflection, experimental and FEM-Design results

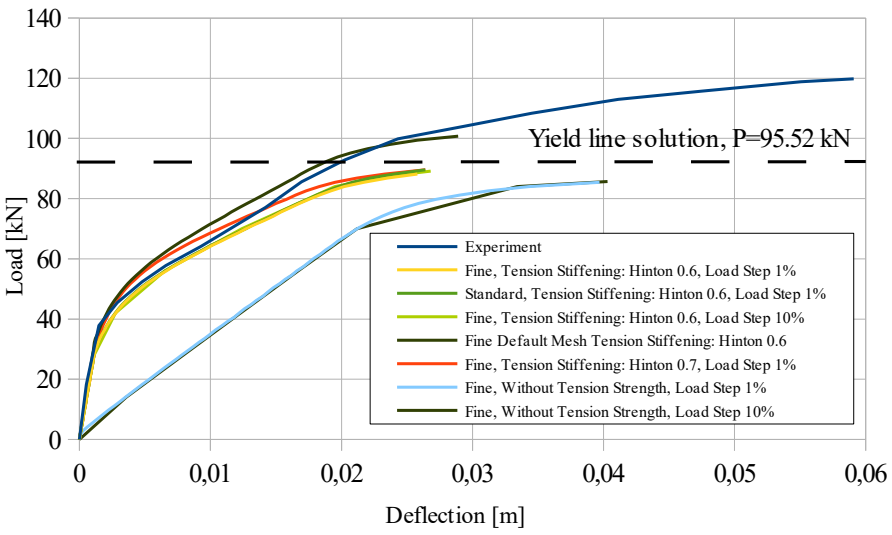

87. Figure - S6 slab results, load vs deflection, experimental and FEM-Design results

In FEM-Design seven different cases were considered in S1 and S6 slabs as well. In every case 10 concrete shell core layers and two bottom reinforcement layers (x' and y') were considered.

- Fine element group, average mesh size: 0.07 m, tension stiffening (option: Hinton, parameter: 0.6) with concrete hardening, Initial load step 1%.
- Standard element group, average mesh size: 0.07 m, tension stiffening (option: Hinton,

parameter: 0.6) with concrete hardening, Initial load step 1%.

- Fine element group, average mesh size: 0.07 m, tension stiffening (option: Hinton, parameter: 0.6) with concrete hardening, Initial load step 10%.
- Fine element group, default average mesh size: 0.14 m, tension stiffening (option: Hinton, parameter: 0.6) with concrete hardening, Initial load step 1%.
- Fine element group, average mesh size: 0.07 m, tension stiffening (option: Hinton, parameter: 0.7) with concrete hardening, Initial load step 1%.
- Fine element group, average mesh size: 0.07 m, without tension strength, with concrete hardening, Initial load step 1%.
- Fine element group, average mesh size: 0.07 m, without tension strength, with concrete hardening, Initial load step 10%.

Based on Fig. 86 and Fig. 87 we can say that S1 and S6 experimental results are very close to the FEM-Design default mesh results, however the denser mesh results show the proper results based on mesh density tests. The 0.07m average mesh size results are very very close to the yield line solution as well. The experimental sustained loads higher than their theoretical collapse load determined by the yield-line theory or with FEM-Design. This is attributable partly to the strain hardening of the reinforcement (which was excluded from the calculated results). Another effect which considerably influences load-carrying capacity is the tensile membrane action which develops at high deflections. At these high deflections, loads are no longer carried to the supports by normal bending action as the penetration of tensile cracks to the top surface illustrates.

It is important to note that without the tension strength consideration (see Fig. 86-87) the ultimate load level only slightly differs from the tension stiffening cases.

It is also important to note that the 1% and 10% initial load step cases provided the same results and approximately the same ultimate load levels as well.

Fig. 88 shows the bottom concrete layer conditions in the integration points of S1 and S6 slabs at ultimate load levels with the first setting case. Almost every points are in cracked condition.

Fig. 89 shows the top concrete layer conditions in the integration points of S1 and S6 slabs at ultimate load levels with the first setting case. Along the main diagonals of the slabs the concrete is in plastic condition which fits with the yield line theory.

Fig. 90 shows the x' and y' reinforcement layer conditions in the integration points of S1 slab at ultimate load levels with the first setting case. Along the main diagonals of the slabs the reinforcements are plastic condition which fits with the yield line theory.

Fig. 91 shows the +45° directional reinforcement and –45° directional reinforcement layer conditions in the integration points of S6 slab at ultimate load levels with the first setting case. Because the reinforcements were applied in the diagonal directions only one diagonal of the reinforcement is in plastic condition separately which fits with the yield line theory.

Fig. 92 shows the unbalanced moments at the first unstable state in the iteration process for S1 and S6 slabs with the first setting case. The pattern of the unbalanced moments follows the diagonals in both cases which fits with the yield line theory.

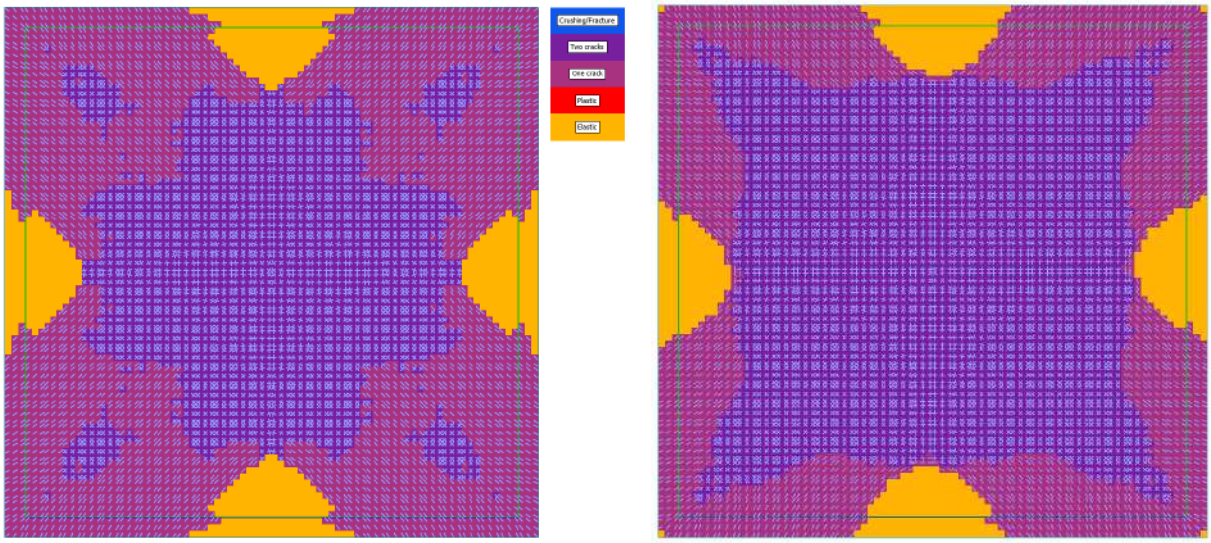

88. Figure - FEM-Design results about the conditions of the integration points
Bottom concrete layer
Left: S1 slab and Right S6 slab
Colour palette schema:
Elastic (yellow), Plastic (red),One crack (light purple), Two cracks (dark purple), Crushing/Fracture (blue)

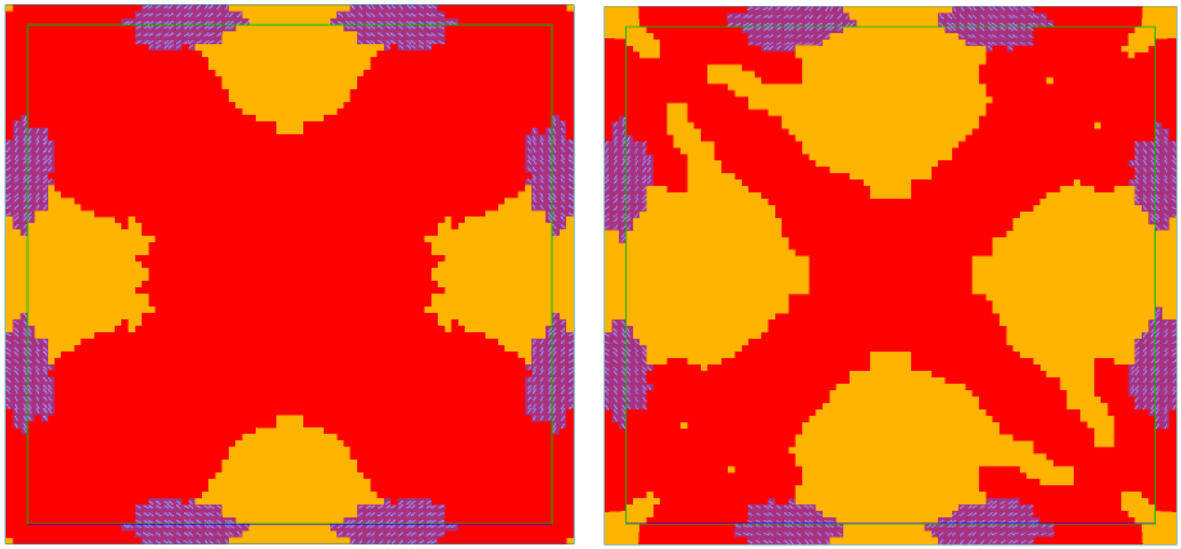

89. Figure - FEM-Design results about the condition of the integration points
Top concrete layer
Left: S1 slab and Right S6 slab
Colour palette schema:
Elastic (yellow), Plastic (red),One crack (light purple), Two cracks (dark purple), Crushing/Fracture (blue)

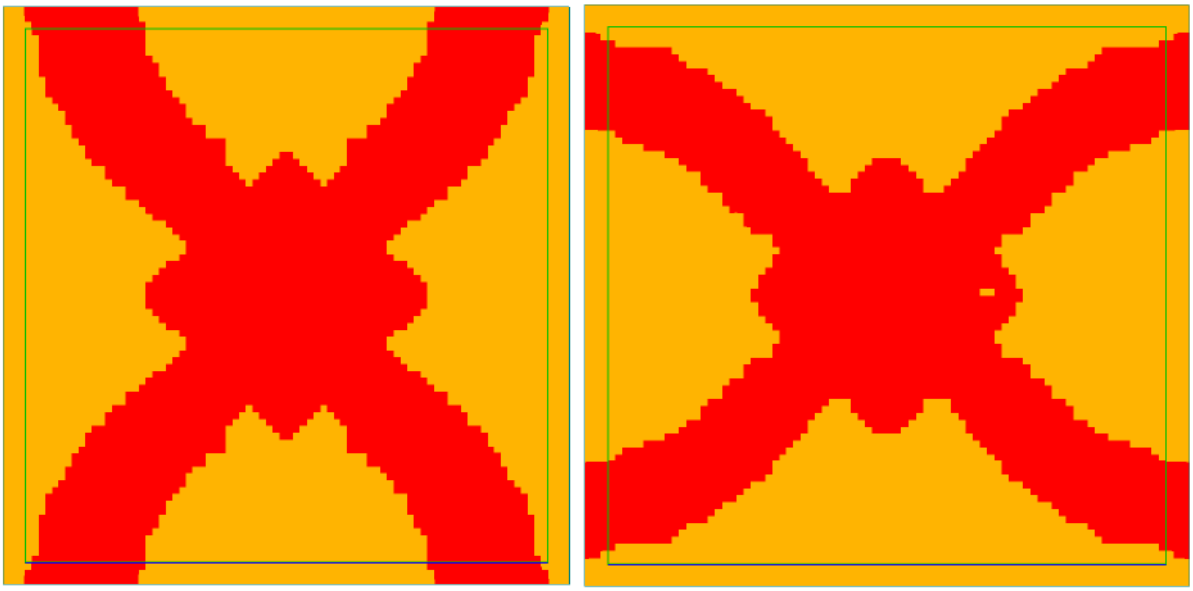

90. Figure - FEM-Design results about the condition of the integration points
Left: S1 slab x' directional reinforcement, Right: S1 slab y' directional reinforcement
Colour palette schema:
Elastic (yellow), Plastic (red)

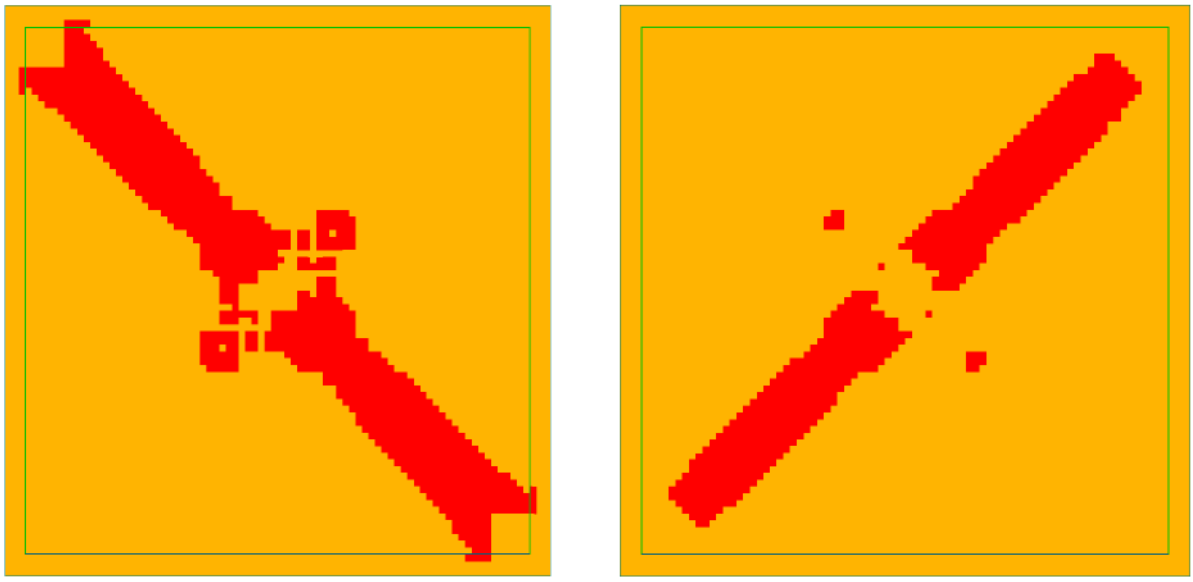

91. Figure - FEM-Design results about the condition of the integration points
Left: S6 slab +45° directional reinforcement, Right: S6 slab –45° directional reinforcement
Colour palette schema:
Elastic (yellow), Plastic (red)

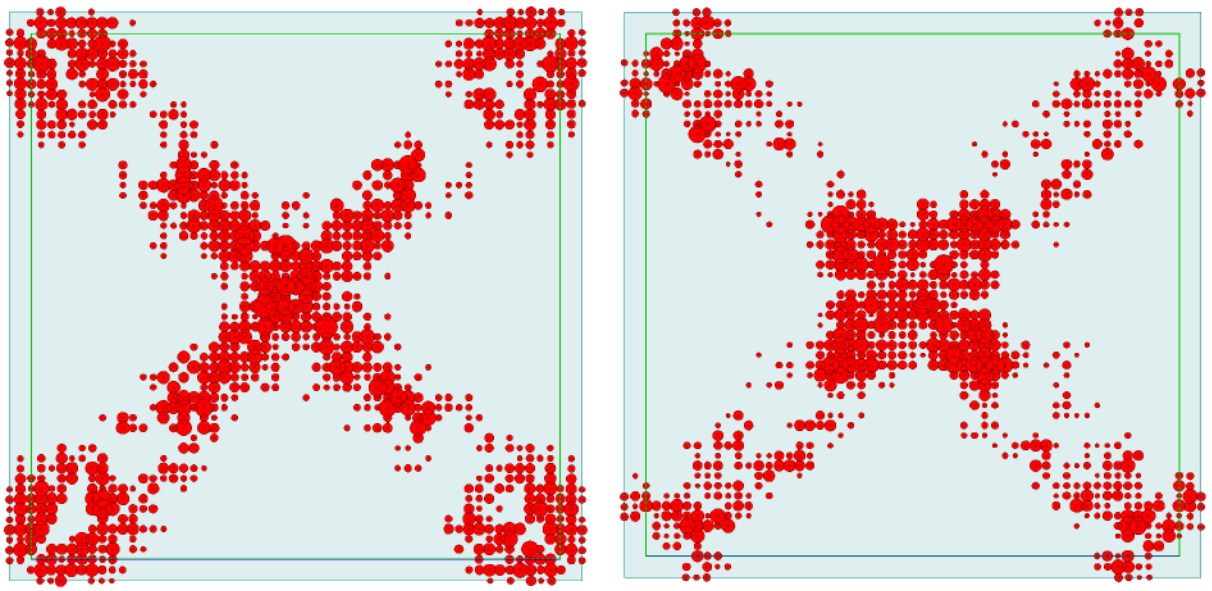

92. Figure - FEM-Design results about the unbalanced moments in first unstable state
Left: S1 slab, Right: S6 slab

6.1.9 Clamped square slab compared with analytical and numerical calculations

Section and material properties	
Thickness [mm]	h=200
Slab length [mm]	L=5000
Effective depth, both in x and y direction [mm]	d=170
Effective depth, both in x and y direction [mm]	d'=30
Reinf. bottom x and y direction [mm^2/m]	a_s=2094 (ϕ20/150)
Reinf. top x and y direction [mm^2/m]	a'_s=2094 (ϕ20/150)
Concrete Young's mod. [GPa]	E_c=34
Poisson's ratio [-]	ν=0.0
Ultimate comp. strength [MPa]	f_c=35.0
Ultimate tens. strength [MPa]	f_t=3.2
Strain at peak stress [-]	ε_{c2}=0.002
Ultimate comp. strain [-]	ε_{cu}=0.0035
Reinf. steel Young's mod. [GPa]	E_s=210
Yield stress [MPa]	f_y=500
Ultimate strain [-]	ε_{su}=0.05

Consider a clamped square slab of reinforced concrete loaded by the uniformly distributed transverse load p as illustrated in Fig. 93. The "exact" ultimate load level according to limit analysis with perfectly plastic m_u ultimate moment capacity in negative and positive directions as well and with complicated yield line was demonstrated in Ref. [27]:

$$p_u = 42.851 \frac{m_u}{L^2}$$

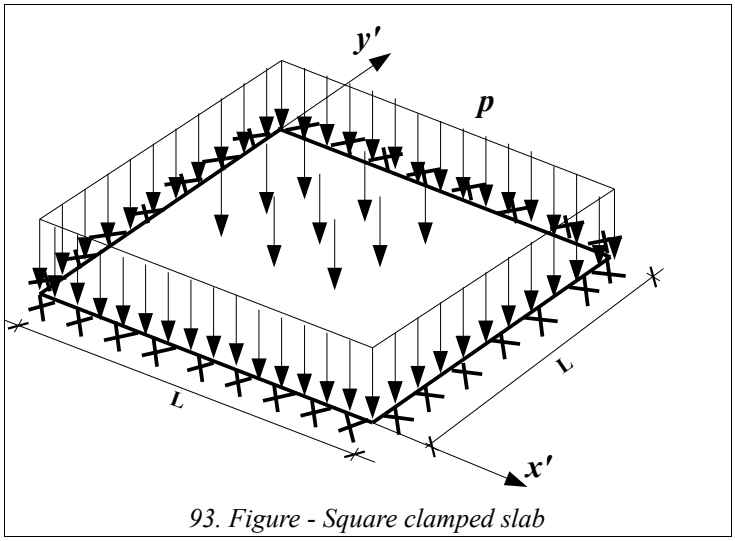

93. Figure - Square clamped slab

Here, in this case it should be noted that based on simpler (commonly used) yield line consideration the ultimate load level is a bit higher:

$$p_u = 48\frac{m_u}{L^2}$$

First of all let's calculate and approximate ultimate bending moment capacity of the reinforced concrete slab cross-section provided in the table above.

If the reinforcement is elastic the stress in the top or bottom reinforcement considering their own effective depth can be calculated with the following approximation:

$$\sigma_s = \frac{E_s \cdot \varepsilon_{cu} \cdot d}{1.25\, x_c} - E_s \cdot \varepsilon_{cu} = 588\frac{d}{x_c} - 735\,[\mathrm{MPa}] \quad .$$

The equilibrium equations, sum of forces and moments are as follows:

$$x_c \cdot f_c - \left(588\frac{d'}{x_c} - 735\right) a_{s'} = f_y \cdot a_s \quad ; \quad m_u = \left(588\frac{d'}{x_c} - 735\right) a_{s'} \cdot \left(d' - \frac{x_c}{2}\right) + f_y a_s \left(d - \frac{x_c}{2}\right)$$

These two equations need to be solved. The compressed zone position: $x_c = 26.21\,\mathrm{mm}$, the stress in bottom reinforcement $\sigma_{s\,bot} = 500\,\mathrm{MPa}$ (tension, yielding), the stress in top reinforcement $\sigma_{s'\,top} = -61.94\,\mathrm{MPa}$ (compression, elastic).

Based on these results the ultimate bending moment capacity by hand calculation:

$m_u = 162\,\mathrm{kNm/m}$.

The ultimate load-bearing capacity of the square clamped slab according to Ref. [27]:

$$p_u = 42.851 \frac{m_u}{L^2} = 278 \text{ kNm/m}$$

In the comparison with FEM-Design this ultimate load level and some numerical limit analysis results will be shown based on Ref. [22]. In FEM-Design a clamped slab was modelled using the input data from the table above. The geometry, mesh and load can be seen in Fig. 94.

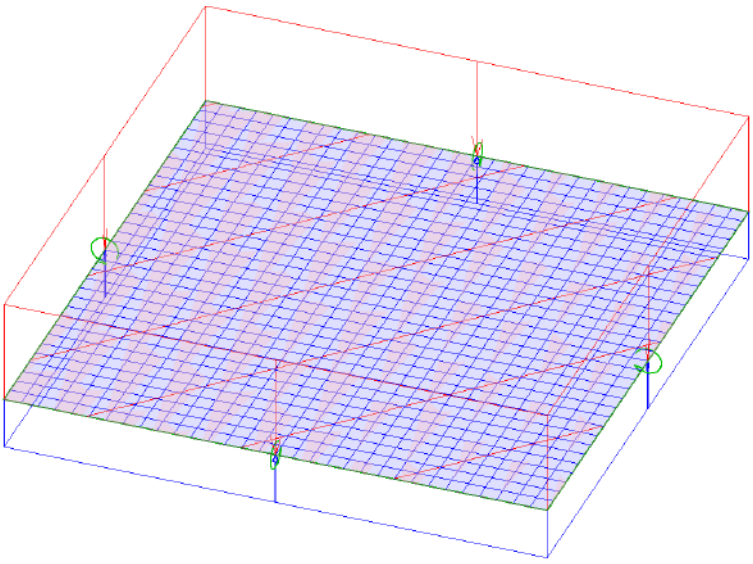

94. Figure – FEM-Design model with the mesh, load and boundary conditions

The FEM-Design elasto-plastic calculation settings are in Fig. 95. Because the limit analysis reference neglected the tension strength of concrete in the calculation, therefore in the FEM-Design calculation the tension strength was also neglected in the concrete material flow rule.

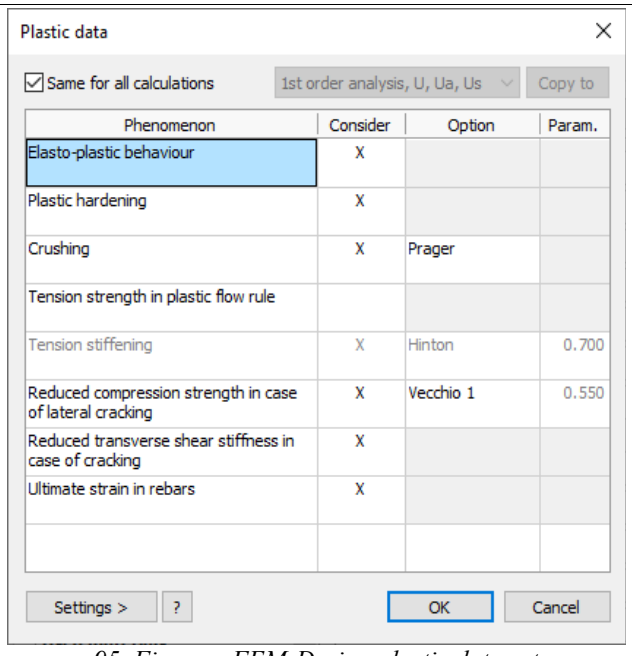

95. Figure – FEM-Design plastic data set

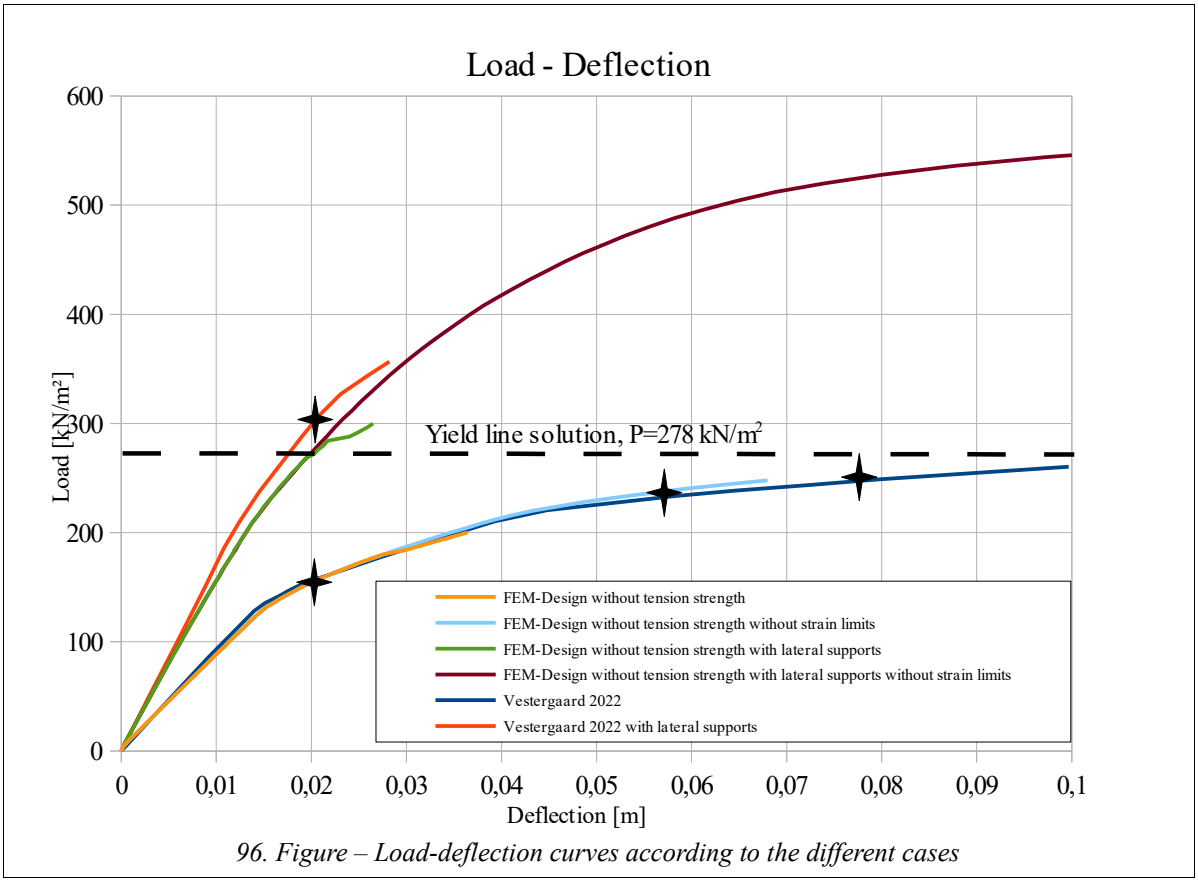

96. Figure – Load-deflection curves according to the different cases

The load-displacement curve in Fig. 96 shows the FEM-Design results, the Ref. [22] results and the analytical ultimate load level as well. The black stars in this diagram shows the assumed ultimate loads according to Ref. [22] with different strain limit considerations (nodal value, averaging values) based on limit analysis where the strain check is a post-processing method after the analysis.

There are two sets of numerical analysis here. The first one which shows higher rigidity are the results which belong to that case where the clamped edges were restrained against horizontal displacements as well. The curve by Vestergaard (red) is not fully shown here because the top of the curve was cut off in the publication. These results show globally higher rigidity, because by a reinforced concrete section there will be coupling between bending and in-plane effects and due to the horizontal supports high amount of in-plane forces also occurs.

The second set of numerical analysis shows lower rigidity because in these cases there were no horizontally restrain on the edges. The FEM-Design results are in good agreement with the limit analysis (Ref. [22]) considering that the elasto-plastic calculation could involve the limit strain values as well.

The three different curves in both sets are as follows:

- Limit analysis result based on Ref. [22]
- FEM-Design with strain limit consideration in concrete and reinforcement as well
- FEM-Design without strain limit considerations

The ultimate load levels are as follows where they are available:
In case of horizontal support:

$$p_{horizontal\ support\ Vestergaard\ with\ nodal\ strain\ limit} = 306\ \mathrm{kN/m^2}$$

$$p_{horizontal\ support\ FEM-Design\ with\ strain\ limit} = 300\ \mathrm{kN/m^2}$$

$$p_{horizontal\ support\ FEM-Design\ without\ strain\ limit} = 560\ \mathrm{kN/m^2}$$

Without horizontal supports:

$$p_{Vestergaard\ with\ nodal\ strain\ limit} = 165\ \mathrm{kN/m^2}$$

$$p_{Vestergaard\ with\ average\ strain\ limit\ 1} = 240\ \mathrm{kN/m^2}$$

$$p_{Vestergaard\ with\ average\ strain\ limit\ 2} = 255\ \mathrm{kN/m^2}$$

$$p_{FEM-Design\ with\ strain\ limit} = 200\ \mathrm{kN/m^2}$$

$$p_{FEM-Design\ without\ strain\ limit} = 248\ \mathrm{kN/m^2}$$

The analytical ultimate load limit was 278kN/m^2, but note that it belongs to a perfectly plastic moment capacity. This value is a theoretical limit considering perfectly plastic, symmetric behaviour in positive and negative moment directions.

The FEM-Design results were in good agreement with the analytical result and with the limit analysis results as well. There is 10% difference between the FEM-Design ultimate load result without strain limit check and the analytical solution, but do not forget that the analytical result assumed perfectly plastic moment behaviour without shifting the neutral axis. This is similar to the steel material where the compression and tension behaviour are similar to each other, but here in case of reinforced concrete the neutral axis is shifting because of the non-linear behaviour of concrete and reinforcement steel coupling.

FEM-Design results also follow the limit analysis load-deflection results as well. In case of consideration of the strain limits in FEM-Design, the results and the ultimate load capacity contains the strain check inside the calculation algorithm compared to the limit analysis results, where the limit strain checks and the ultimate load levels depend on a post-processing method. Where the limit strain was considered in the nodes by the limit analysis the ultimate load level was way below the analytical result (40%). In case of limit analysis where the post-processing strain checks were performed along the edge zones (strain limit method 1 considered an averaging zone a=h/4 and strain limit method 2 considered an averaging zone a=h/2) the ultimate load was closer to the theoretical analytical solution. In these two cases the differences are 14% and 8%, see Fig. 96 as well. In case of FEM-Design result where the limit strains were considered, the difference was 28%, thus the “real” ultimate load should be around 200kN/m^2.

6.1.10 In-plane loading of shear walls with perforations and with different reinforcements and loading conditions compared with experimental data

Section and material properties	
Thickness [mm]	h=70
Panel size [mm]	L=890/890 (hole: 150/150)
Compression strength of concrete PC1A [MPa]	f_c=27.9
Compression strength of concrete PC2 [MPa]	f_c=25.5
Compression strength of concrete PC3 [MPa]	f_c=26.8
Compression strength of concrete PC4 [MPa]	f_c=24.9
Compression strength of concrete PC5 [MPa]	f_c=29.0
Compression strength of concrete PC6 [MPa]	f_c=25.7
Compression strength of concrete PC7 [MPa]	f_c=28.7
Compression strength of concrete PC8 [MPa]	f_c=27.3
Compression strength of concrete PC9 [MPa]	f_c=28.0
Strain at peak stress [-]	ε_{c2}=0.00182 (average value)
Ultimate comp. strain [-]	ε_{cu}=0.0035
Concrete Young's mod. [GPa]	E_c=21.58
Poisson's ratio [-]	ν=0.15
Ultimate tens. strength [MPa]	f_t=2.5 (average value)
Reinforcement ratio in x direction [-]	ρ_x= 0.0165
Reinforcement ratio in y direction [-]	ρ_y= 0.00825
Reinf. steel Young's mod. PC1A, PC2, PC3 [GPa]	E_s=196.8
Reinf. steel Young's mod. PC4, PC5, PC6 [GPa]	E_s=202.7
Reinf. steel Young's mod. PC7, PC8, PC9 [GPa]	E_s=195.0
Yield stress of reinforcements PC1A, PC2, PC3 [MPa]	f_y=500
Yield stress of reinforcements PC4, PC5, PC6 [MPa]	f_y=260
Yield stress of reinforcements PC7, PC8, PC9 [MPa]	f_y=390
Ultimate strain of reinforcements [-]	ε_{su}=0.0225

In this verification example in-plane loaded shear panels will be analysed. Three different panel types will be analysed applying three different load conditions. The FEM-Design results will be compared with experimental results from Ref. [28]. The three different panel types can be seen in Fig. 97, the first panel type (Panel Type I) is a regular panel (size 890mm/890mm) with double amount of reinforcements in horizontal direction compared to vertical, the second panel (Panel Type II) has the same outer dimensions and reinforcements but there is a hole in the middle (with size 150mm/150mm), the third panel type (Panel Type III) has the same

perforation at centre area but there is additional reinforcements around the edges of the hole, see Fig. 97. The amount of additional reinforcements around the hole in Panel Type III is equal to what is left out due to holes, see also Fig. 97. The material properties of concrete and reinforcements can be seen in the table above.

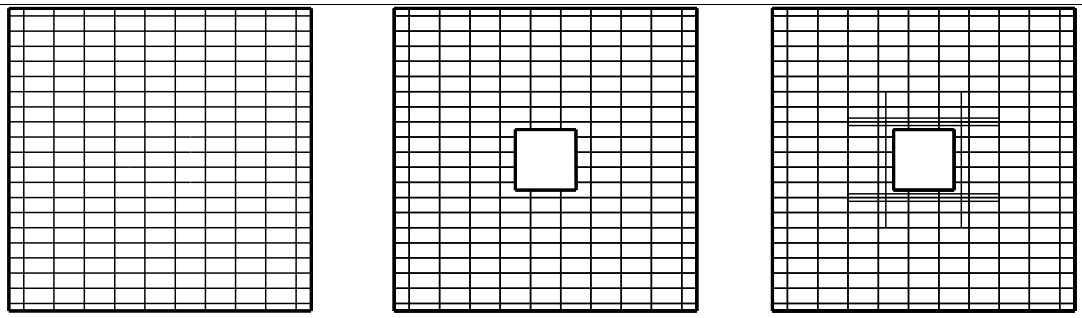

97. Figure - Three different shear panel types with the schematic drawings of the reinforcements Panel Type I, Panel Type II and Panel Type III

In the first loading condition (Load Type I) there is pure shear on the edges, in the second load condition (Load Type II) there is shear force on the edges and there are compression forces along the edges as well in both directions. The third load pattern (Load Type III) contains shear load as well, and additional tension force in both directions along the edges, see Fig. 98.

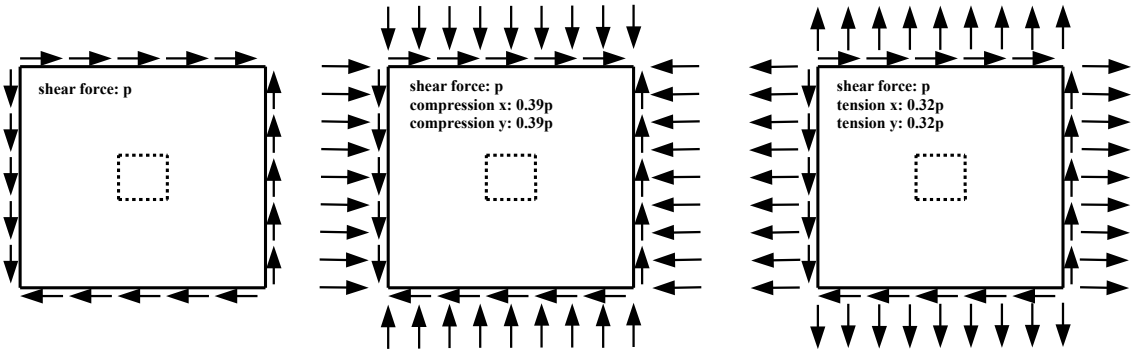

98. Figure - Three different load pattern Load Type I, Load Type II and Load Type III

In the experimental tests 9 different test specimens were analysed:

- PC1A test case: Panel Type I with Load Type I
- PC2 test case: Panel Type II with Load Type I
- PC3 test case: Panel Type III with Load Type I
- PC4 test case: Panel Type I with Load Type II
- PC5 test case: Panel Type II with Load Type II
- PC6 test case: Panel Type III with Load Type II
- PC7 test case: Panel Type I with Load Type III
- PC8 test case: Panel Type II with Load Type III

– PC9 test case: Panel Type III with Load Type III

In FEM-Design three different calculation settings were considered in every 9 cases. In the first settings the tension stiffening rule was the Hinton rule with parameter 0.7. In the second settings the tension stiffening rule was the Vecchio rule with parameter 500 and in the third settings the tension strength of the concrete was excluded from the model, see Fig. 99.

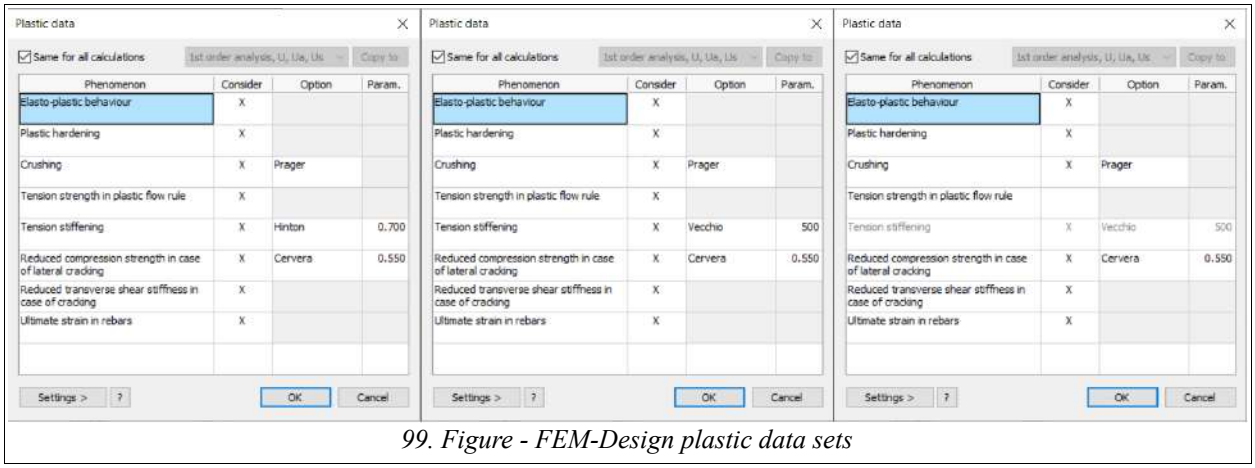

99. Figure - FEM-Design plastic data sets

In the next paragraphs the experimental test results and the ultimate load capacities of the different panels will be described and compared with FEM-Design results.

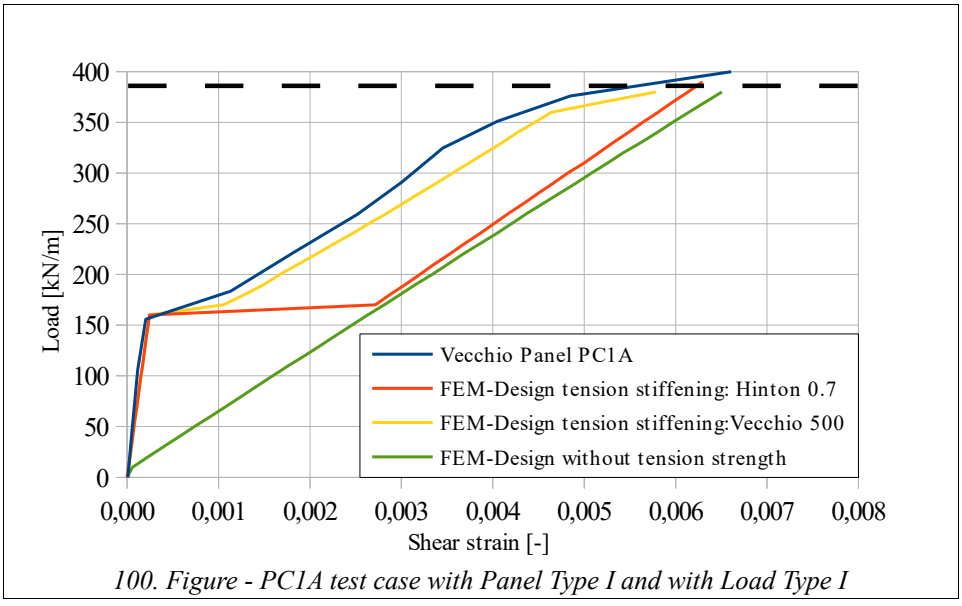

100. Figure - PC1A test case with Panel Type I and with Load Type I

Fig. 100 shows the load vs. shear strain diagrams in case of panel PC1A.

Experimental test result ultimate load level:

$p_{PC1A\,test} = 400\ \mathrm{kN/m}$,

FEM-Design ultimate load levels with the different tension stiffening settings:

$p_{PC1A\ FD\ Hinton\ 0.7} = 370\ \mathrm{kN/m}$, $p_{PC1A\ FD\ Vecchio\ 500} = 380\ \mathrm{kN/m}$, $p_{PC1A\ FD\ no\ tens.\ strength} = 370\ \mathrm{kN/m}$

We can say that the ultimate load level based on FEM-Design is very close to the experimental test results (within 5%) as the path of the load vs shear strain diagram in case of Vecchio tension stiffening rule. Before failure the reinforcements are in elastic states in both directions thus the failure occurs in concrete and there are diagonal cracks, see Fig. 101.

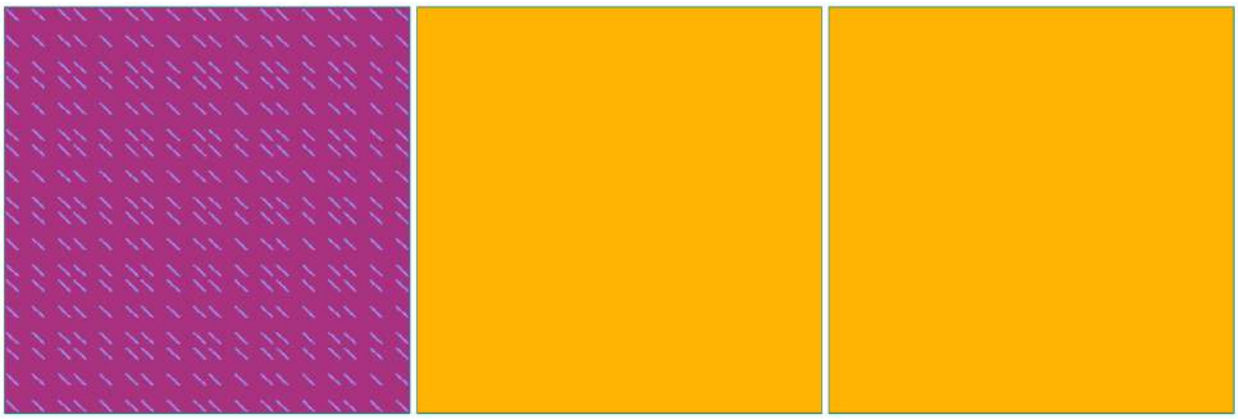

101. Figure - The plastic state of concrete, reinforcement in x and reinforcement in y directions in case of Hinton rule
Panel PC1A Colour palette schema:
Elastic (yellow), Plastic (red),One crack (light purple), Two cracks (dark purple), Crushing/Fracture (blue)

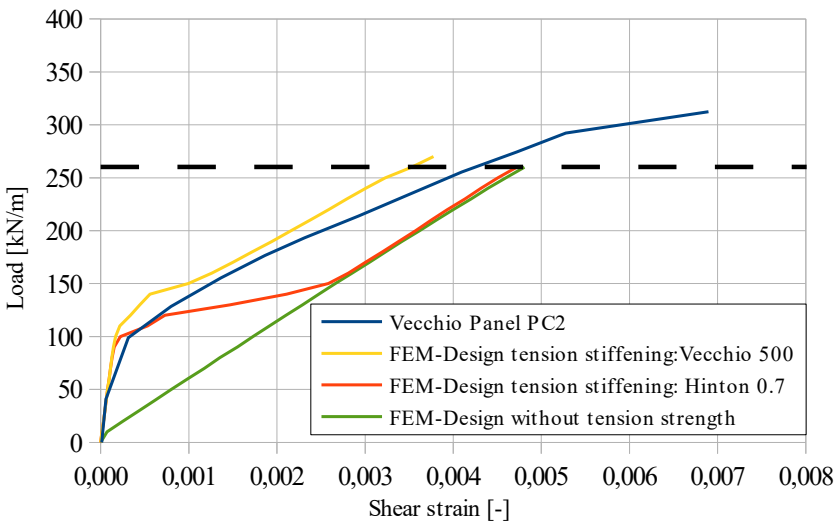

102. Figure - PC2 test case with Panel Type II and with Load Type I

Fig. 102 shows the load vs. shear strain diagrams in case of panel PC2.

Experimental test result ultimate load level:

$p_{PC2\ test} = 310\ \mathrm{kN/m}$,

FEM-Design ultimate load levels with the different tension stiffening settings:

$p_{PC2\ FD\ Hinton\ 0.7} = 260\ \mathrm{kN/m}$, $p_{PC2\ FD\ Vecchio\ 500} = 270\ \mathrm{kN/m}$, $p_{PC2\ FD\ notens.\ strength} = 260\ \mathrm{kN/m}$

We can say that the ultimate load level based on FEM-Design is very close to the experimental test results (within 15%) as the path of the load vs shear strain diagram in case of Vecchio tension stiffening rule. Before failure the concrete and the reinforcements plastic conditions can be seen in Fig. 103. There is failure in concrete around the perforation and its corners. The reinforcements are in yield condition around corners in x and y directions as well.

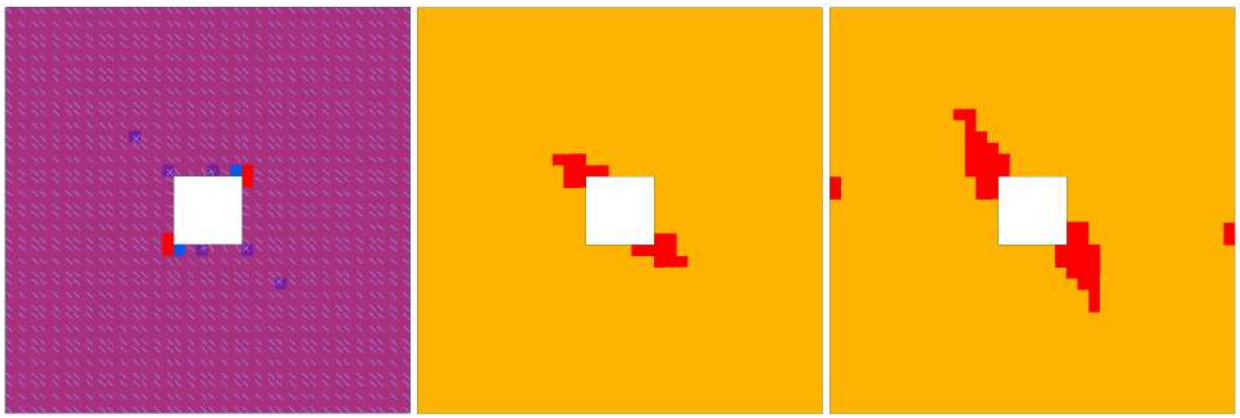

103. Figure - The plastic state of concrete, reinforcement in x and reinforcement in y directions in case of Hinton rule
Panel PC2 Colour palette schema:
Elastic (yellow), Plastic (red),One crack (light purple), Two cracks (dark purple), Crushing/Fracture (blue)

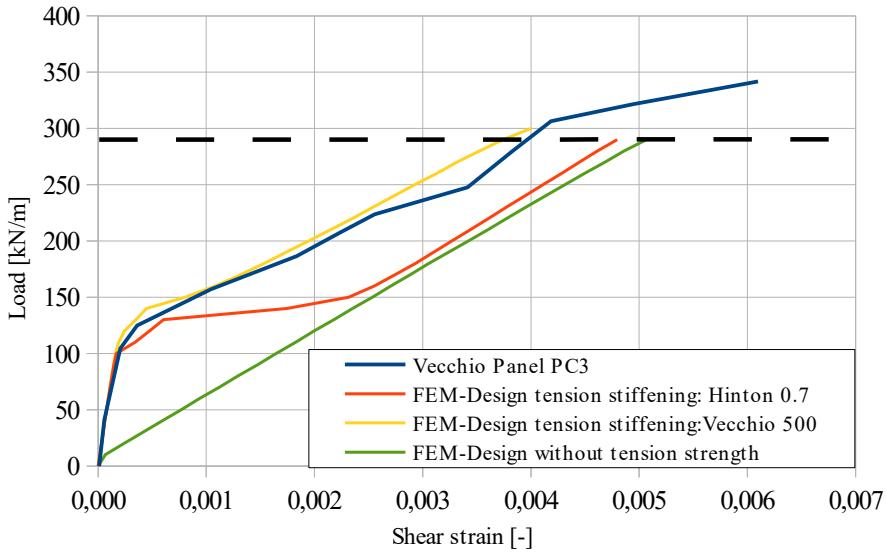

104. Figure - PC3 test case with Panel Type III and with Load Type I

Fig. 104 shows the load vs. shear strain diagrams in case of panel PC3.

Experimental test result ultimate load level:

$p_{PC3\,test} = 340\,\mathrm{kN/m}$,

FEM-Design ultimate load levels with the different tension stiffening settings:

$p_{PC3\,FD\,Hinton\,0.7} = 290\,\mathrm{kN/m}$, $p_{PC3\,FD\,Vecchio\,500} = 300\,\mathrm{kN/m}$, $p_{PC3\,FD\,no\,tens.\,strength} = 290\,\mathrm{kN/m}$

We can say that the ultimate load level based on FEM-Design is very close to the experimental test results (within 12%) as the path of the load vs shear strain diagram in case of Vecchio tension stiffening rule. Before failure the concrete and the reinforcements plastic conditions can be seen in Fig. 105. There is failure in concrete around the perforation and its corners. The reinforcements are in yield condition around corners in x and y directions as well, but due to the additional reinforcements around the perforation the area of the yielding is smaller.

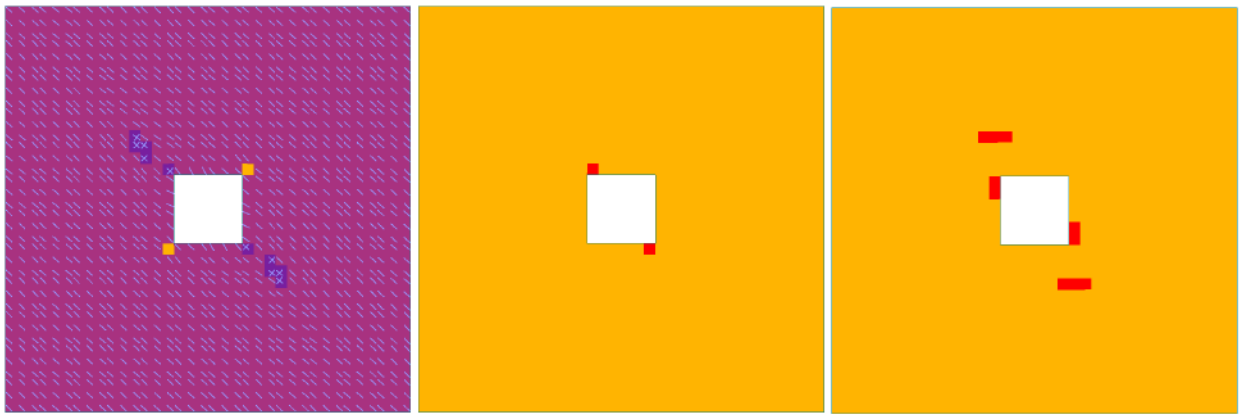

105. Figure - The plastic state of concrete, reinforcement in x and reinforcement in y directions in case of Hinton rule
Panel PC3 Colour palette schema:
Elastic (yellow), Plastic (red),One crack (light purple), Two cracks (dark purple), Crushing/Fracture (blue)

Summary about the Load Type I cases in light of ultimate loads and expectations.

Test results, without perforation, with perforation and perforation with additional reinforcement:

$p_{PC1A\,test} = 400\,\mathrm{kN/m}$, $p_{PC2\,test} = 310\,\mathrm{kN/m}$, $p_{PC3\,test} = 340\,\mathrm{kN/m}$

FEM-Design ultimate load levels with the same sequence:

$p_{PC1A\,FD} = 380\,\mathrm{kN/m}$, $p_{PC2\,FD} = 270\,\mathrm{kN/m}$, $p_{PC3\,FD} = 300\,\mathrm{kN/m}$

The expected ultimate load levels revealed in test results and FEM-Design calculations as well. Panel PC1A needs to have the greatest ultimate load level. The lowest should be in panel PC2, due to the perforation. PC3 panel ultimate load-bearing capacity needs to be between these values thanks to the additional reinforcements. These expectations fulfilled in the experimental data and the FEM-Design results as well, and the ultimate limit loads are close to the test results. We can say that FE calculation follows the non-linear behaviour of these types of panels in a reasonable manner. The figures about the plasticity and failure condition visualize the failure mode perfectly. The ultimate load level is almost independent of the selected tension stiffening rule, see Fig. 100, 102 and 104.

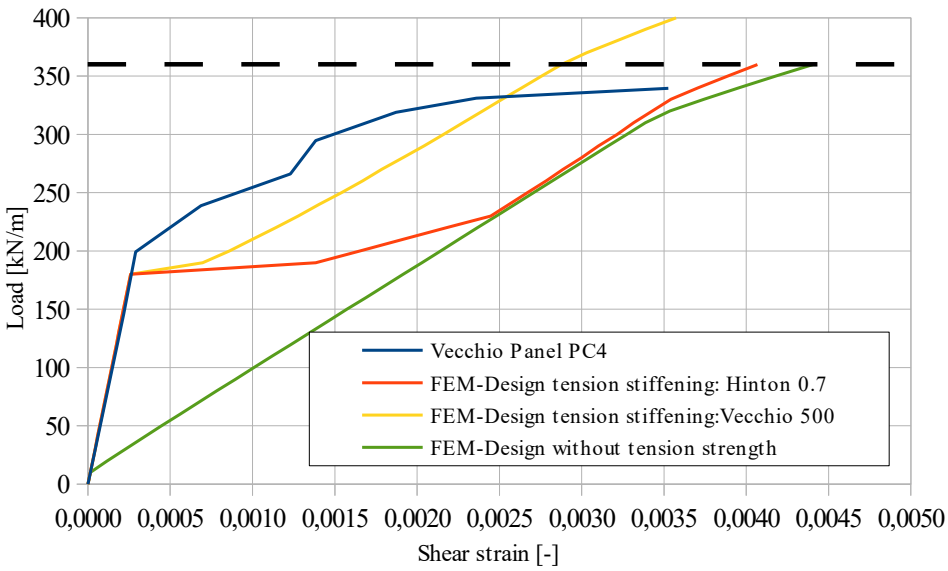

106. Figure - PC4 test case with Panel Type I and with Load Type II

Fig. 106 shows the load vs. shear strain diagrams in case of panel PC4.

Experimental test result ultimate load level:

$p_{PC4\ test} = 340\ \mathrm{kN/m}$,

FEM-Design ultimate load levels with the different tension stiffening settings:

$p_{PC4\ FD\ Hinton\ 0.7} = 360\ \mathrm{kN/m}$, $p_{PC4\ FD\ Vecchio\ 500} = 410\ \mathrm{kN/m}$, $p_{PC4\ FD\ notens.\ strength} = 360\ \mathrm{kN/m}$

We can say that the ultimate load level based on FEM-Design is very close to the experimental test results as the path of the load vs shear strain diagram in case of Vecchio tension stiffening rule. Before failure the concrete and the reinforcements plastic conditions can be seen in Fig. 107. There are diagonal cracks in concrete. The reinforcement in y direction is in yield condition.

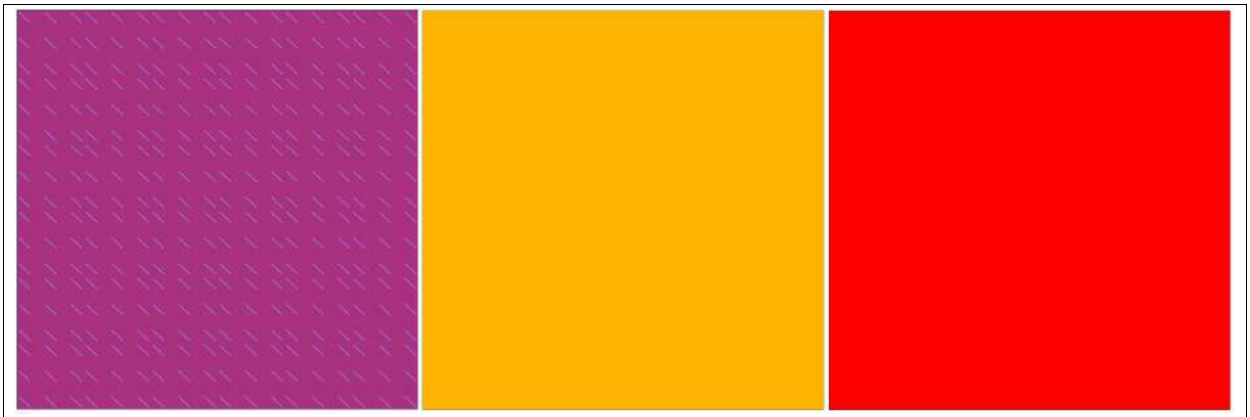

107. Figure - The plastic state of concrete, reinforcement in x and reinforcement in y directions in case of Hinton rule
Panel PC4 Colour palette schema:
Elastic (yellow), Plastic (red),One crack (light purple), Two cracks (dark purple), Crushing/Fracture (blue)

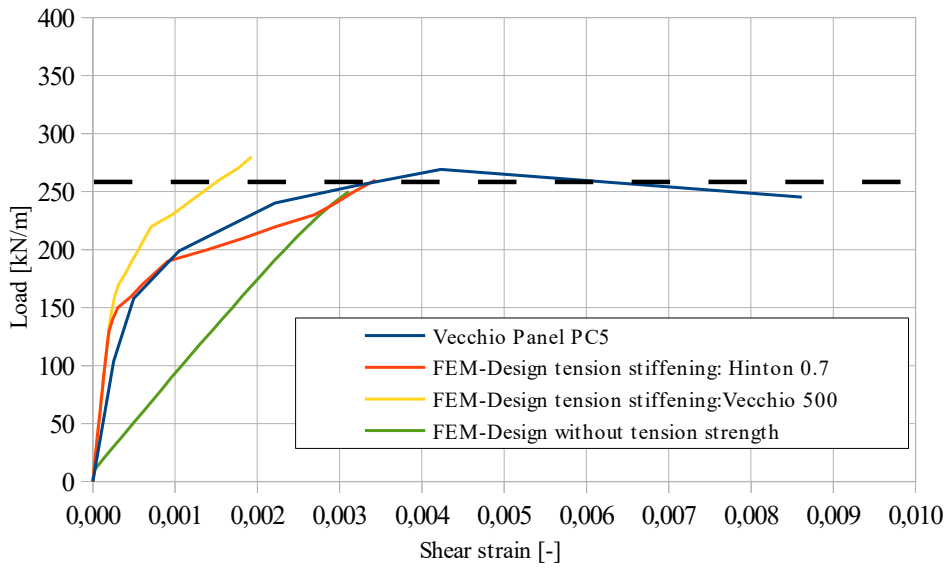

108. Figure - PC5 test case with Panel Type II and with Load Type II

Fig. 108 shows the load vs. shear strain diagrams in case of panel PC5.

Experimental test result ultimate load level:

$p_{PC5\ test} = 269\ \mathrm{kN/m}$,

FEM-Design ultimate load levels with the different tension stiffening settings:

$p_{PC5\ FD\ Hinton\ 0.7} = 260\ \mathrm{kN/m}$, $p_{PC5\ FD\ Vecchio\ 500} = 280\ \mathrm{kN/m}$, $p_{PC5\ FD\ notens.\ strength} = 250\ \mathrm{kN/m}$

We can say that the ultimate load level based on FEM-Design is very close to the experimental test results as the path of the load vs shear strain diagram in case of Vecchio tension stiffening rule. Before failure the concrete and the reinforcements plastic conditions can be seen in Fig. 109. There is failure in concrete around the perforation and its corners. The reinforcements are in yield condition around corners in x and y directions as well. The area of the yielding in the reinforcement much larger compared to panel PC2 (see Fig. 103) because in this case here there was additional compression force on the edges.

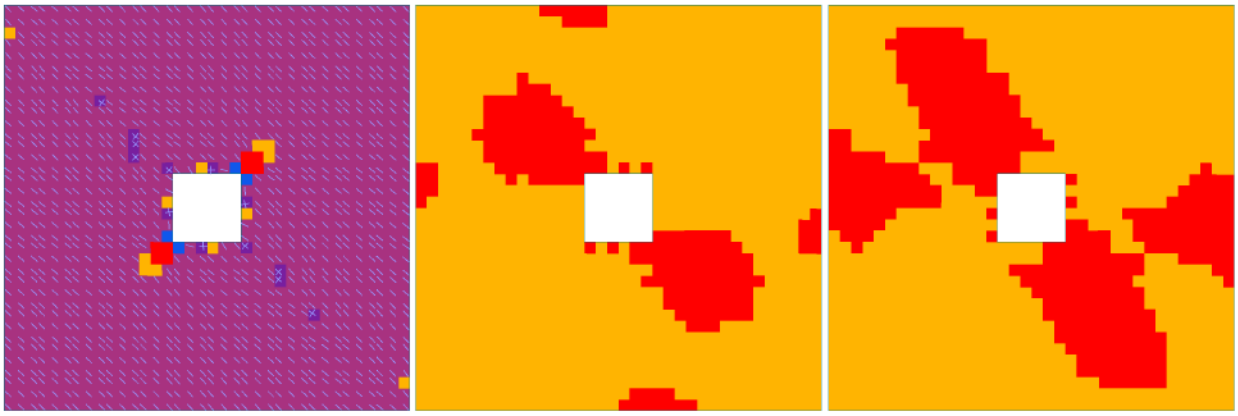

109. Figure - The plastic state of concrete, reinforcement in x and reinforcement in y directions in case of Hinton rule
Panel PC5 Colour palette schema:
Elastic (yellow), Plastic (red),One crack (light purple), Two cracks (dark purple), Crushing/Fracture (blue)

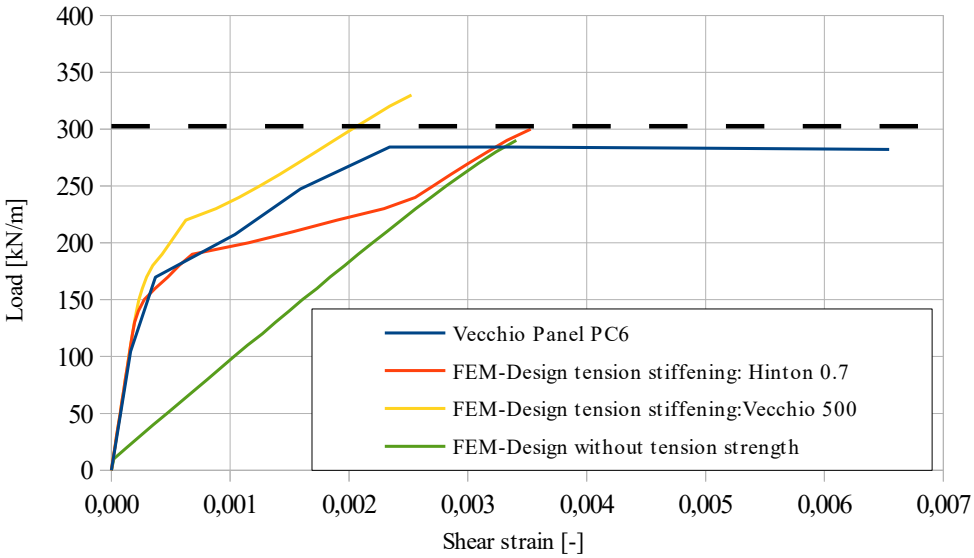

110. Figure - PC6 test case with Panel Type III and with Load Type II

Fig. 110 shows the load vs. shear strain diagrams in case of panel PC6.

Experimental test result ultimate load level:

$p_{PC6\,test} = 284\,\mathrm{kN/m}$,

FEM-Design ultimate load levels with the different tension stiffening settings:

$p_{PC6\,FD\,Hinton0.7} = 300\,\mathrm{kN/m}$, $p_{PC6\,FD\,Vecchio\,500} = 330\,\mathrm{kN/m}$, $p_{PC6\,FD\,no\,tens.\,strength} = 290\,\mathrm{kN/m}$

We can say that the ultimate load level based on FEM-Design is very close to the experimental test results as the path of the load vs shear strain diagram in case of Vecchio tension stiffening rule. Before failure the concrete and the reinforcements plastic conditions can be seen in Fig. 111. There is plasticity in concrete around the perforation and its corners. The reinforcements are in yield condition around corners in x and y directions as well. The area of the yielding in

the reinforcement is a bit smaller compared to panel PC5 (see Fig. 109) because in this case here there was additional reinforcements along the edges.

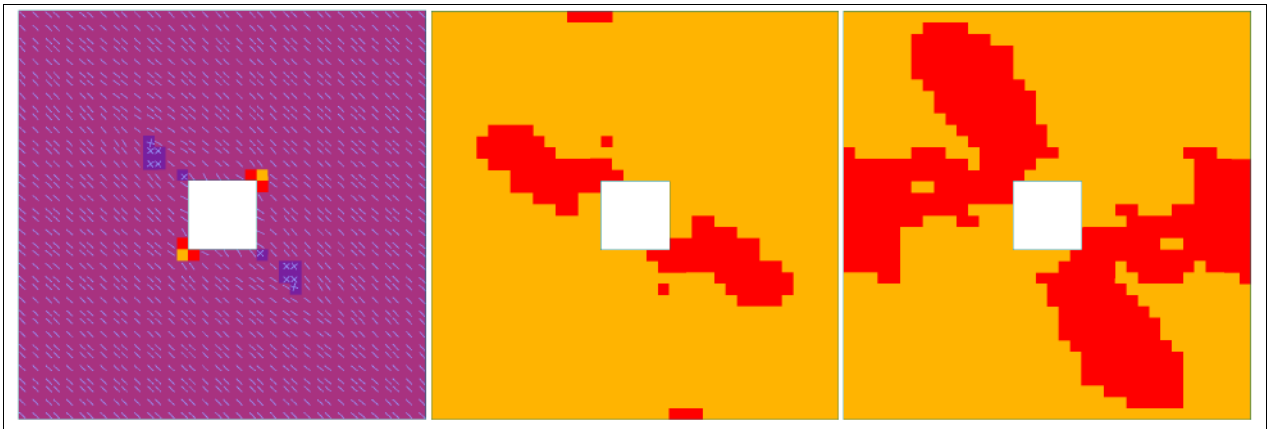

111. Figure - The plastic state of concrete, reinforcement in x and reinforcement in y directions in case of Hinton rule

Panel PC6 Colour palette schema:

Elastic (yellow), Plastic (red),One crack (light purple), Two cracks (dark purple), Crushing/Fracture (blue)

Summary about the Load Type II cases in light of ultimate loads and expectations.

Test results, without perforation, with perforation and perforation with additional reinforcement:

$p_{PC4\,test} = 340\,\mathrm{kN/m}$, $p_{PC5\,test} = 269\,\mathrm{kN/m}$, $p_{PC6\,test} = 284\,\mathrm{kN/m}$

FEM-Design ultimate load levels with the same sequence:

$p_{PC4\,FD} = 360\,\mathrm{kN/m}$, $p_{PC5\,FD} = 260\,\mathrm{kN/m}$, $p_{PC6\,FD} = 290\,\mathrm{kN/m}$

The expected ultimate load levels revealed in test results and FEM-Design calculations as well. Panel PC4 needs to have the greatest ultimate load level. The lowest should be in panel PC5, due to the perforation. PC6 panel ultimate load-bearing capacity needs to be between these values thanks to the additional reinforcements. These expectations fulfilled in the experimental data and the FEM-Design results as well, and the ultimate limit loads are very close to the test results. We can say that FE calculation follows the non-linear behaviour of these types of panels in a reasonable manner. The figures about the plasticity and failure condition visualize the failure mode perfectly. The ultimate load level is almost independent of the selected tension stiffening rule, see Fig. 106, 108 and 110.

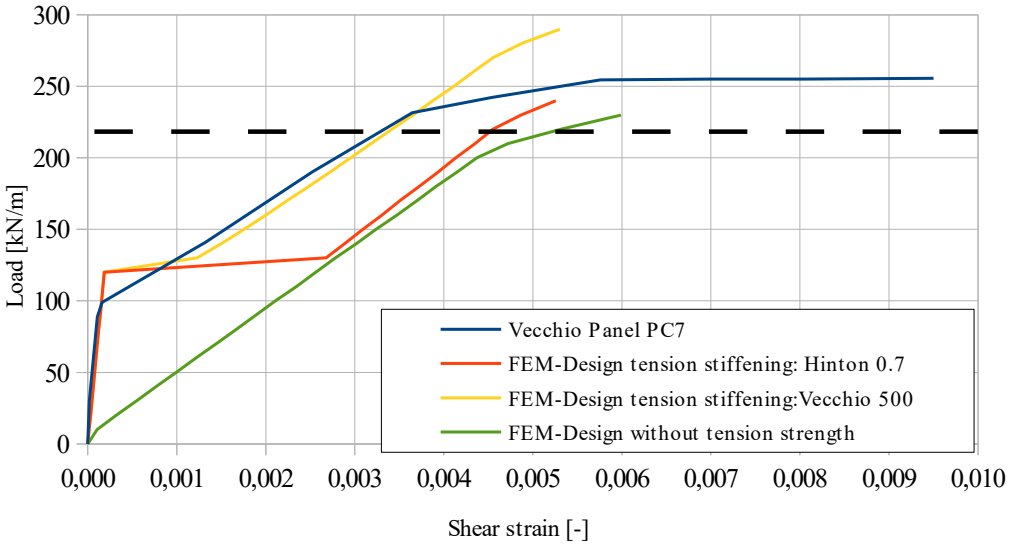

112. Figure - PC7 test case with Panel Type I and with Load Type III

Fig. 112 shows the load vs. shear strain diagrams in case of panel PC7.

Experimental test result ultimate load level:

$p_{PC7\,test} = 255\,\mathrm{kN/m}$,

FEM-Design ultimate load levels with the different tension stiffening settings:

$p_{PC7\,FD\,Hinton0.7} = 240\,\mathrm{kN/m}$, $p_{PC7\,FD\,Vecchio\,500} = 290\,\mathrm{kN/m}$, $p_{PC7\,FD\,no\,tens.\,strength} = 230\,\mathrm{kN/m}$

We can say that the ultimate load level based on FEM-Design is very close to the experimental test results as the path of the load vs shear strain diagram in case of Vecchio tension stiffening rule. Before failure the concrete and the reinforcements plastic conditions can be seen in Fig. 113. There are diagonal cracks in concrete. The reinforcement in y direction is in yield condition.

113. Figure - The plastic state of concrete, reinforcement in x and reinforcement in y directions in case of Hinton rule
Panel PC7 Colour palette schema:
Elastic (yellow), Plastic (red),One crack (light purple), Two cracks (dark purple), Crushing/Fracture (blue)

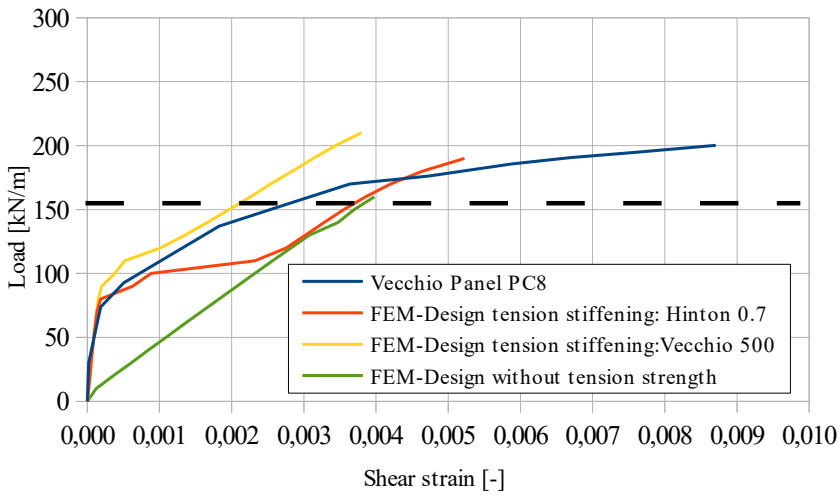

114. Figure - PC8 test case with Panel Type II and with Load Type III

Fig. 114 shows the load vs. shear strain diagrams in case of panel PC8.

Experimental test result ultimate load level:

$p_{PC8\,test} = 200\,\mathrm{kN/m}$,

FEM-Design ultimate load levels with the different tension stiffening settings:

$p_{PC8\,FD\,Hinton\,0.7} = 190\,\mathrm{kN/m}$, $p_{PC8\,FD\,Vecchio\,500} = 210\,\mathrm{kN/m}$, $p_{PC8\,FD\,notens.\,strength} = 160\,\mathrm{kN/m}$

We can say that the ultimate load level based on FEM-Design is very close to the experimental test results as the path of the load vs shear strain diagram in case of Vecchio tension stiffening rule. Before failure the concrete and the reinforcements plastic conditions can be seen in Fig. 115. There are diagonal cracks in concrete. The reinforcements are in yield condition around corners in x and y directions as well.

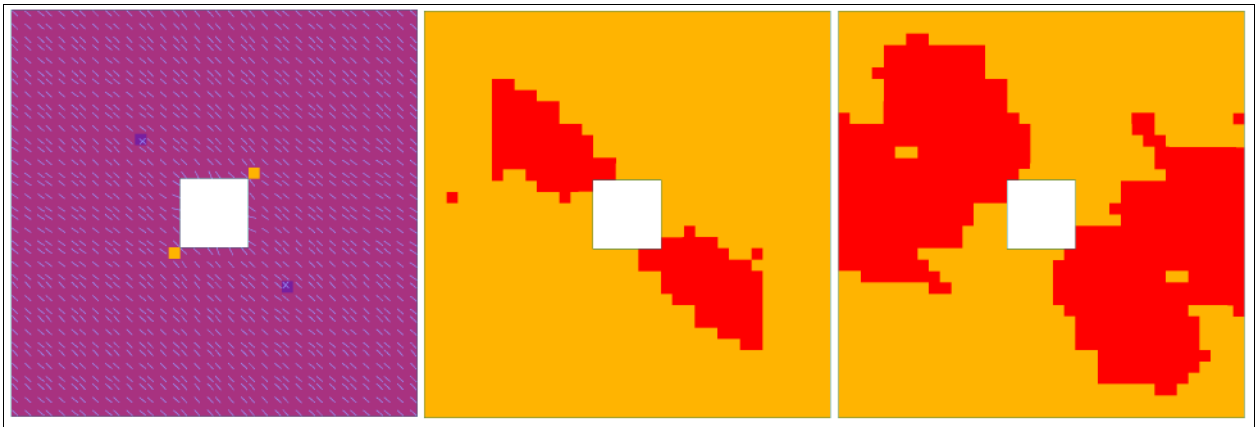

115. Figure - The plastic state of concrete, reinforcement in x and reinforcement in y directions in case of Hinton rule
Panel PC8 Colour palette schema:
Elastic (yellow), Plastic (red),One crack (light purple), Two cracks (dark purple), Crushing/Fracture (blue)

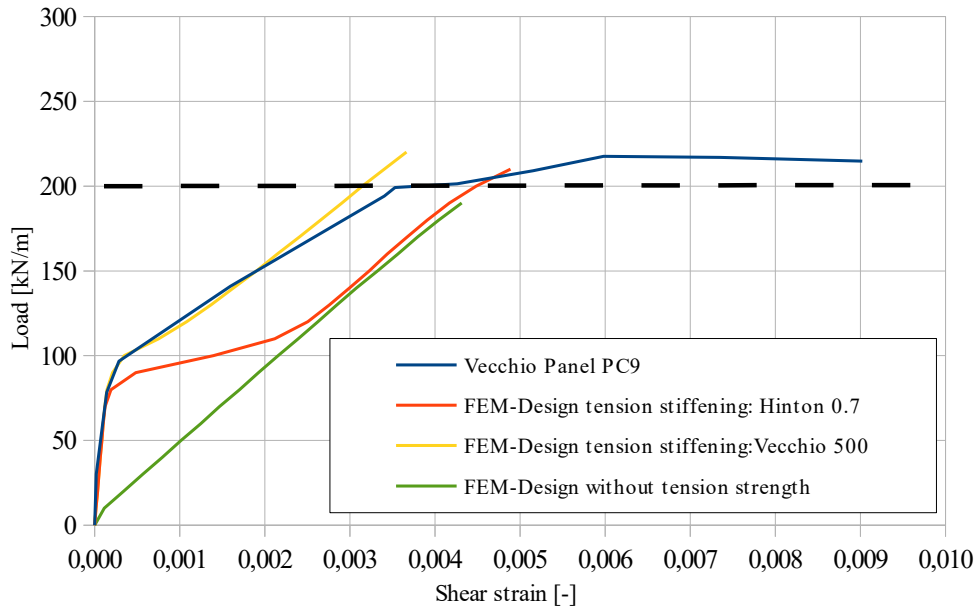

116. Figure - PC9 test case with Panel Type III and with Load Type III

Fig. 116 shows the load vs. shear strain diagrams in case of panel PC9.

Experimental test result ultimate load level:

$p_{PC9\,test} = 217\,\mathrm{kN/m}$,

FEM-Design ultimate load levels with the different tension stiffening settings:

$p_{PC9\,FD\,Hinton\,0.7} = 210\,\mathrm{kN/m}$, $p_{PC9\,FD\,Vecchio\,500} = 220\,\mathrm{kN/m}$, $p_{PC9\,FD\,notens.\,strength} = 190\,\mathrm{kN/m}$

We can say that the ultimate load level based on FEM-Design is very close to the experimental test results as the path of the load vs shear strain diagram in case of Vecchio tension stiffening rule. Before failure the concrete and the reinforcements plastic conditions can be seen in Fig. 117. There is plasticity in concrete around the perforation and its corners. The reinforcements are in yield condition around corners in x and y directions as well. The area of the yielding in the reinforcement is a bit smaller compared to panel PC8 (see Fig. 115) because in this case here there was additional reinforcements along the edges.

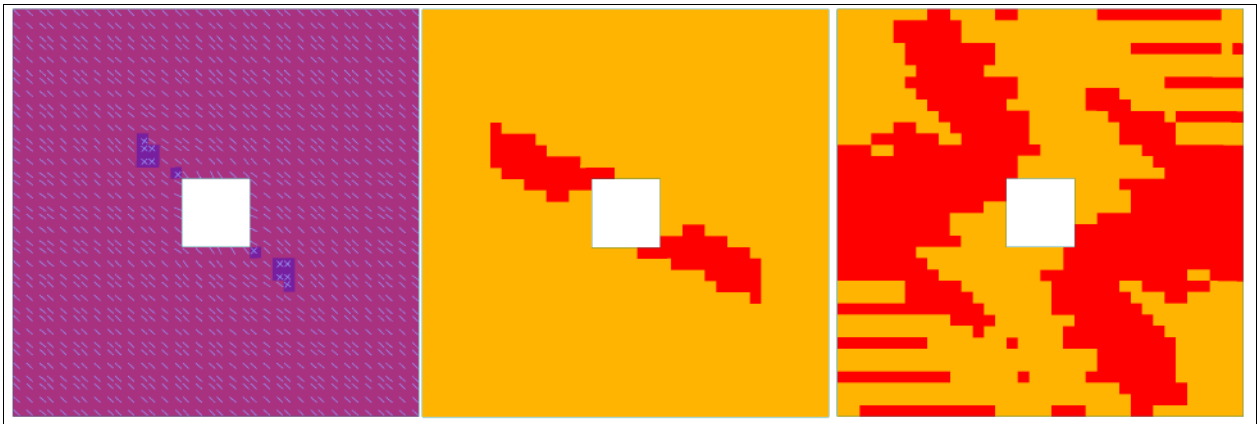

117. Figure - The plastic state of concrete, reinforcement in x and reinforcement in y directions in case of Hinton rule
Panel PC9 Colour palette schema:
Elastic (yellow), Plastic (red),One crack (light purple), Two cracks (dark purple), Crushing/Fracture (blue)

Summary about the Load Type III cases in light of ultimate loads and expectations.

Test results, without perforation, with perforation and perforation with additional reinforcement:

$p_{PC7\,test} = 255\,\mathrm{kN/m}$, $p_{PC8\,test} = 200\,\mathrm{kN/m}$, $p_{PC9\,test} = 217\,\mathrm{kN/m}$

FEM-Design ultimate load levels with the same sequence:

$p_{PC7\,FD} = 240\,\mathrm{kN/m}$, $p_{PC8\,FD} = 190\,\mathrm{kN/m}$, $p_{PC9\,FD} = 210\,\mathrm{kN/m}$

The expected ultimate load levels revealed in test results and FEM-Design calculations as well. Panel PC7 needs to have the greatest ultimate load level. The lowest should be in panel PC8, due to the perforation. PC9 panel ultimate load-bearing capacity needs to be between these values thanks to the additional reinforcements. These expectations fulfilled in the experimental data and the FEM-Design results as well, and the ultimate limit loads are very close to the test results. We can say that FE calculation follows the non-linear behaviour of these types of panels in a reasonable manner. The figures about the plasticity and failure condition visualize the failure mode perfectly. The ultimate load level is almost independent of the selected tension stiffening rule, see Fig. 112, 114 and 116.

6.1.11 Four-Story stairwell with openings and coupling effect between bending and membrane effects

Section and material properties	
Thickness [mm]	h=180
Effective depth, both in x and y direction [mm]	d=150
Effective depth, both in x and y direction [mm]	d'=30
Reinf. bottom x and y direction [mm^2/m]	a_s=335 (ϕ8/150)
Reinf. top x and y direction [mm^2/m]	a'_s=335 (ϕ8/150)
Concrete Young's mod. [GPa]	E_c=33
Poisson's ratio [-]	ν=0.0
Ultimate comp. strength [MPa]	f_c=30.0
Ultimate tens. strength [MPa]	f_t=3.0
Strain at peak stress [-]	ε_{c2}=0.002
Ultimate comp. strain [-]	ε_{cu}=0.0035
Reinf. steel Young's mod. [GPa]	E_s=200
Yield stress [MPa]	f_y=550
Ultimate strain [-]	ε_{su}=0.049

In this example the FEM-Design plastic shell applicability for modelling large structures is demonstrated for a four-story RC stairwell with openings, see Fig. 118. The example was analysed by Ref. [22]. In the mentioned reference the used numerical method to obtain the ultimate load level was the limit state analysis where the combined behaviour of membrane and bending effect was considered as well. The individual walls are simply supported at the base, and the structure is subjected to uniform shear load along the top of the wall with the openings, see Fig. 118. The stairwell width, depth, and height are taken as 3.6 m, 6.6 m, and 16 m, see Fig. 118. The openings with width 0.9 m and height 2.1 m are positioned 0.3 m from the wall edge. The walls have uniform thickness 180 mm. The reinforcements are two-layered orthogonal schema, see the table above with the details. The material properties also can be found in the table above. In the benchmark example the tension strength of the concrete was excluded from the calculation. Two different calculations were performed in the mentioned reference, first the load-top displacement curve was calculated considering only membrane effect in the structure, second the combined membrane-bending effect was taken into account in the calculation of the load-top displacement curve. In FEM-Design the first case - where only the membrane effect was considered - was approximated with hinged connection along the edges of the wall. This is not exactly the same modelling technique but serves an adequate result in this case because in FEM-Design the combined behaviour of membrane and bending always considered. The second case was modelled with fixed rigid connection between the edges to perform a moment bearing joints along the edges just like in the mentioned reference. In FEM-Design two different plastic shell settings were considered for both structural cases. In the first one the tension strength was neglected as in the reference but in the second case a tension stiffening rule with Hinton rule and parameter 0.7 was used, see Fig. 119.

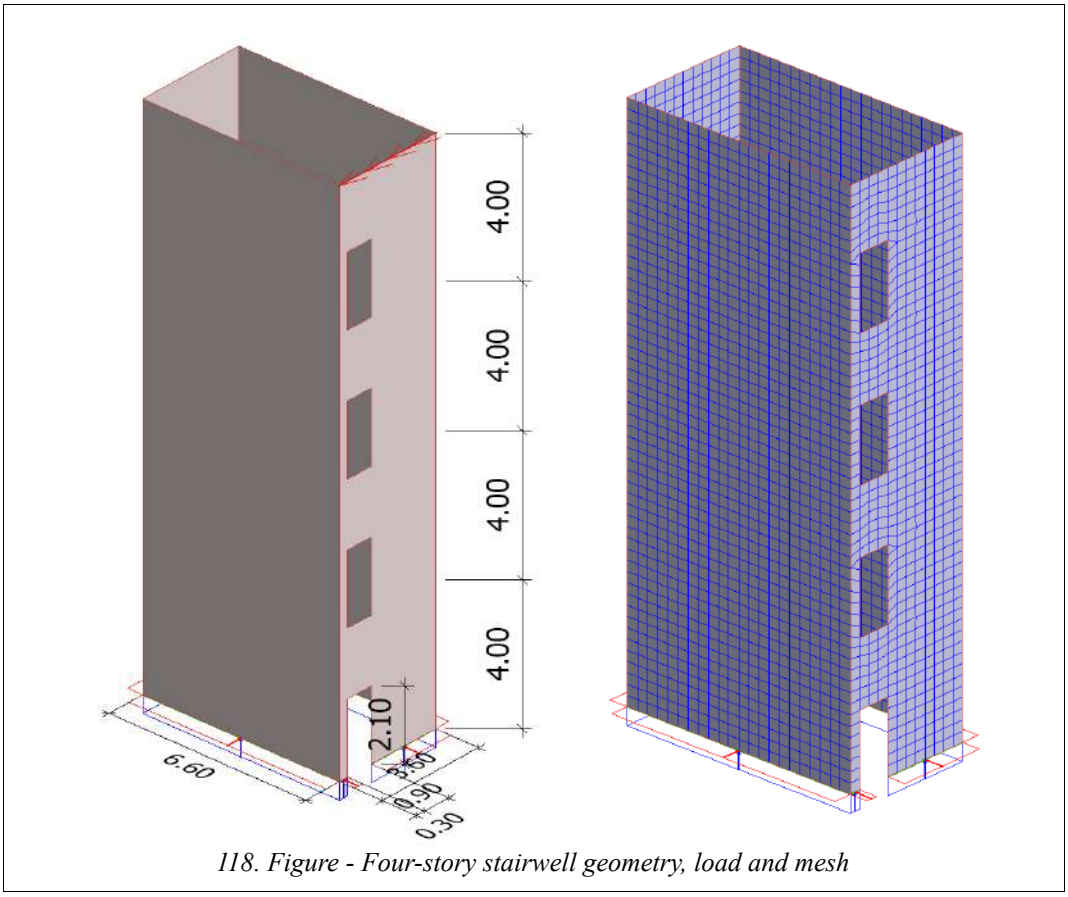

118. Figure - Four-story stairwell geometry, load and mesh

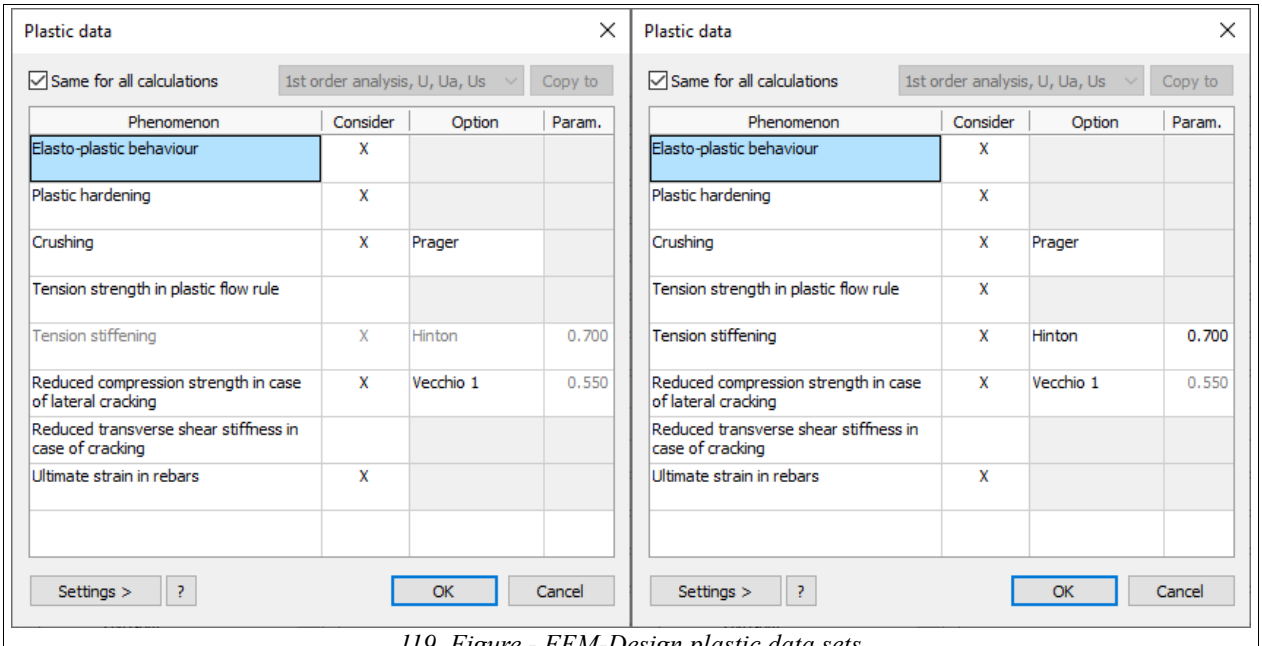

119. Figure - FEM-Design plastic data sets

The following four different calculations were performed in FEM-Design:

- Case A: Concrete without tension strength + continuous fixed wall edges against moment
- Case B: Concrete without tension strength + hinged edge connections
- Case C: Concrete with tension stiffening + continuous fixed wall edges against moment
- Case D: Concrete with tension stiffening + hinged edge connections

In these analysis 10 concrete layers and x and y directional reinforcement on top and bottom surfaces were considered. The average mesh size was 0.3 m, see Fig. 118.

Fig. 120 shows the benchmark results based on Ref. [22] and the four different FEM-Design results. However it should be noted here that the ultimate load-bearing capacity is NOT provided in the mentioned reference only the load-displacement curve based on limit analysis. In limit analysis the ultimate strain check is a result of post processing, therefore the load displacement curves don't really show the ultimate load-bearing capacity in these cases. In FEM-Design the ultimate strain check is involved into the non-linear calculation process, thus the ultimate load can be read from the load-displacement curves.

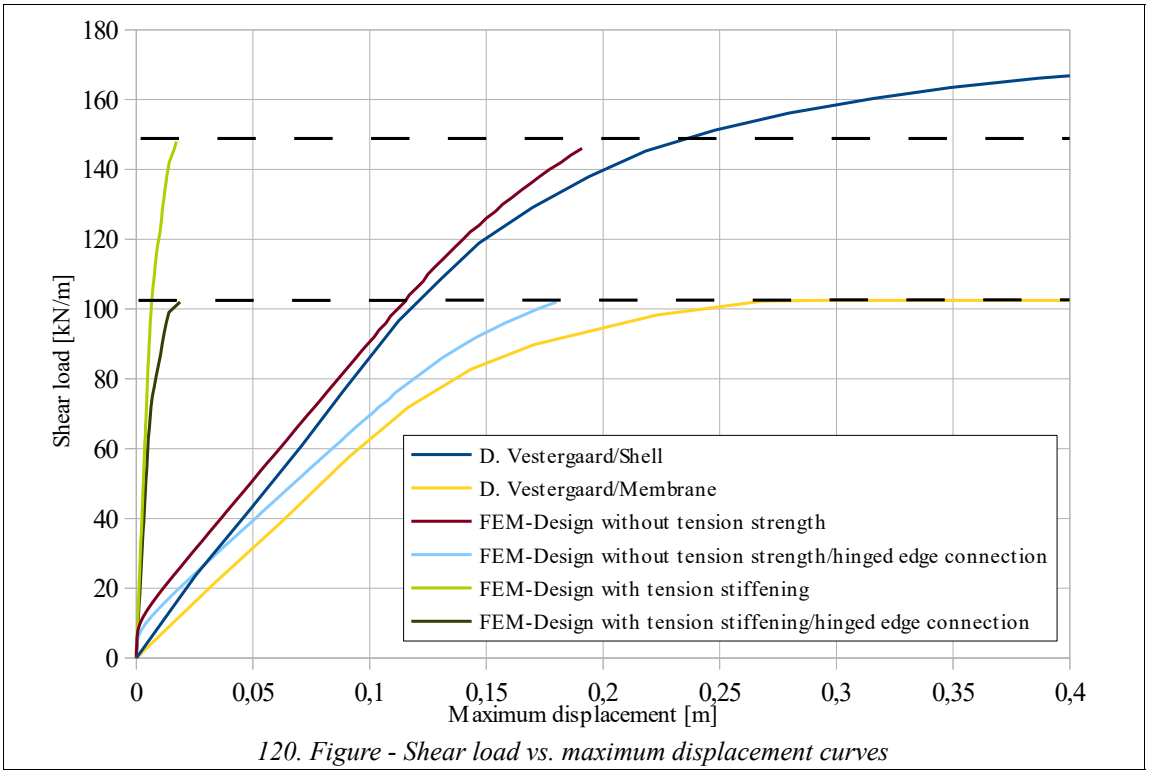

120. Figure - Shear load vs. maximum displacement curves

Fig. 121 shows the displacements in Case A and C based on FEM-Design calculation at the ultimate load levels.

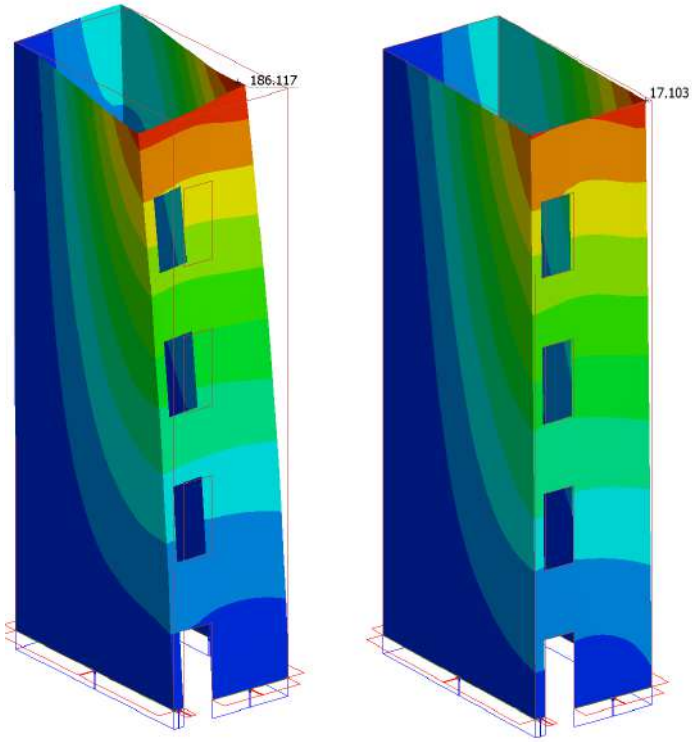

121. Figure - The total displacements [mm]

Fig. 122 shows the first principal normal forces (N1) in Case A and C based on FEM-Design calculation at the ultimate load levels.

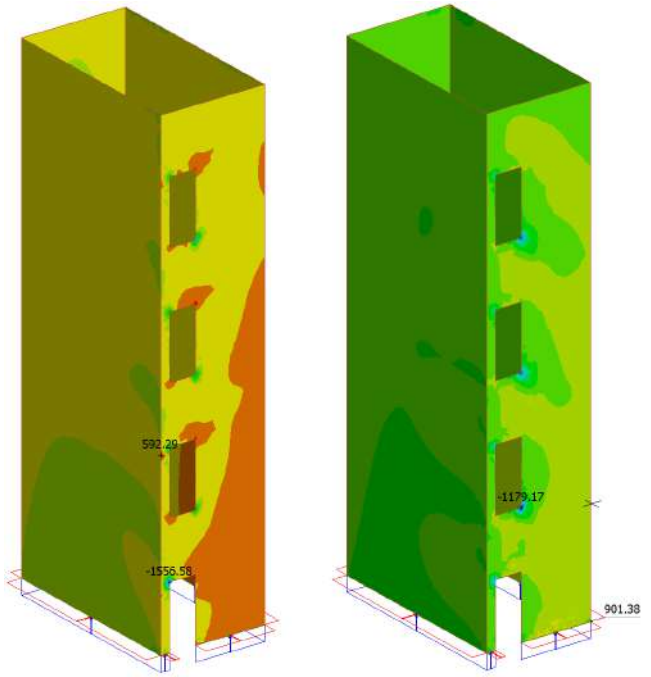

122. Figure - First principal normal forces (N1 – [kN/m])

Fig. 123 shows the second principal normal forces (N2) in Case A and C based on FEM-Design calculation at the ultimate load levels.

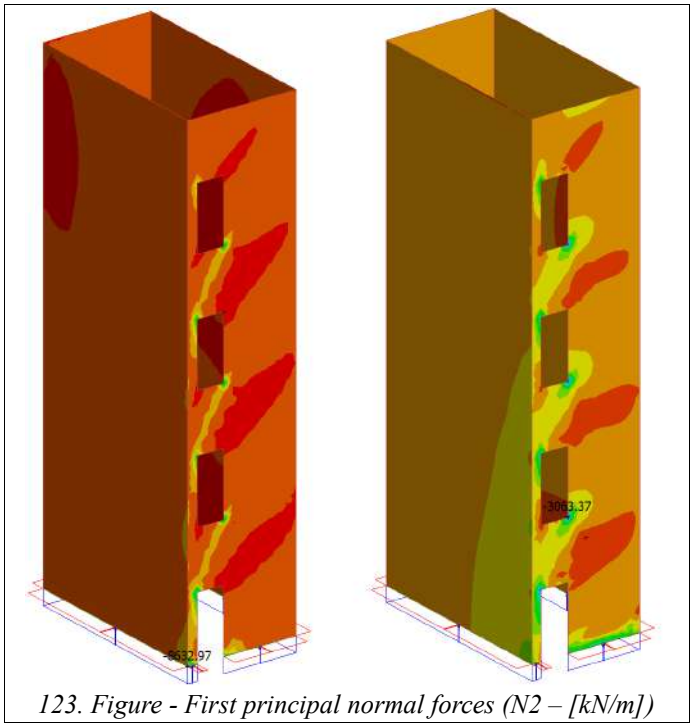

123. Figure - First principal normal forces (N2 – [kN/m])

Fig. 124 shows the first principal moments (M1) in Case A and C based on FEM-Design calculation at the ultimate load levels.

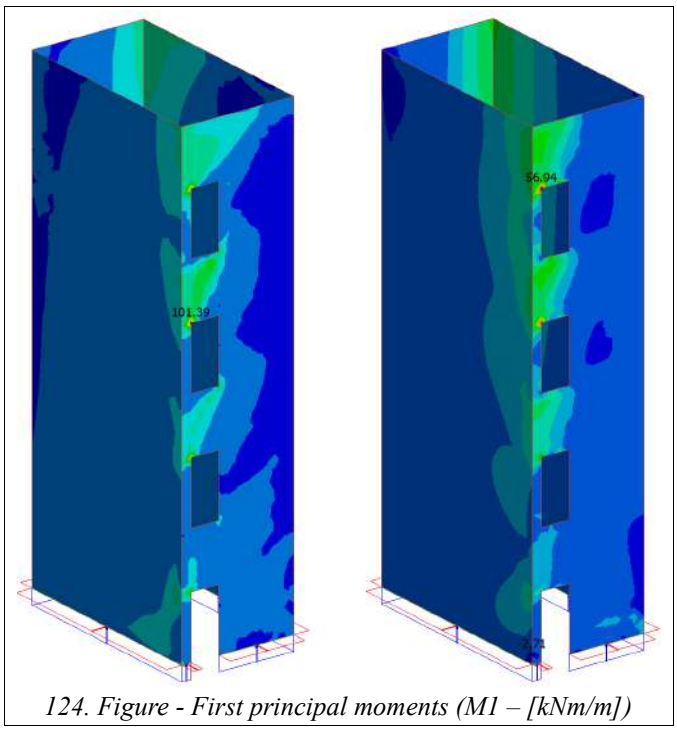

124. Figure - First principal moments (M1 – [kNm/m])

Fig. 125 shows the second principal moments (M2) in Case A and C based on FEM-Design calculation at the ultimate load levels.

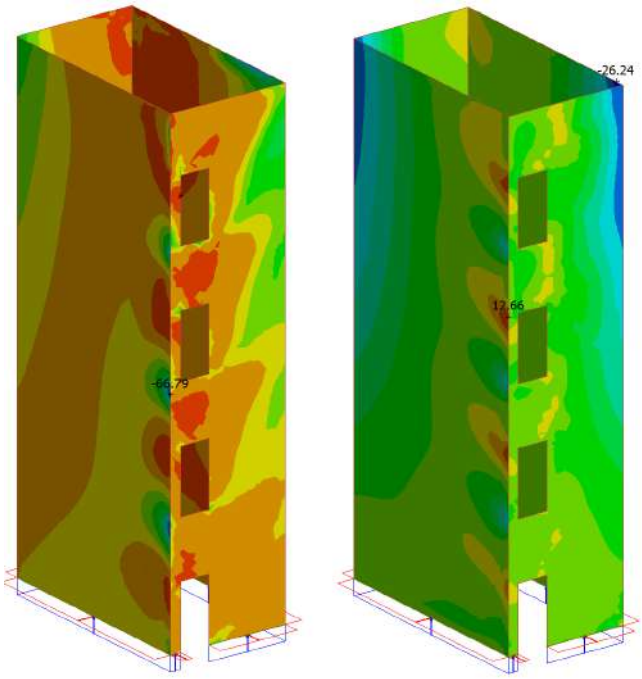

125. Figure - Second principal moments (M2 – [kNm/m])

Fig. 126 shows the bottom concrete layer plastic condition results in Case A and C based on FEM-Design calculation at the ultimate load levels.

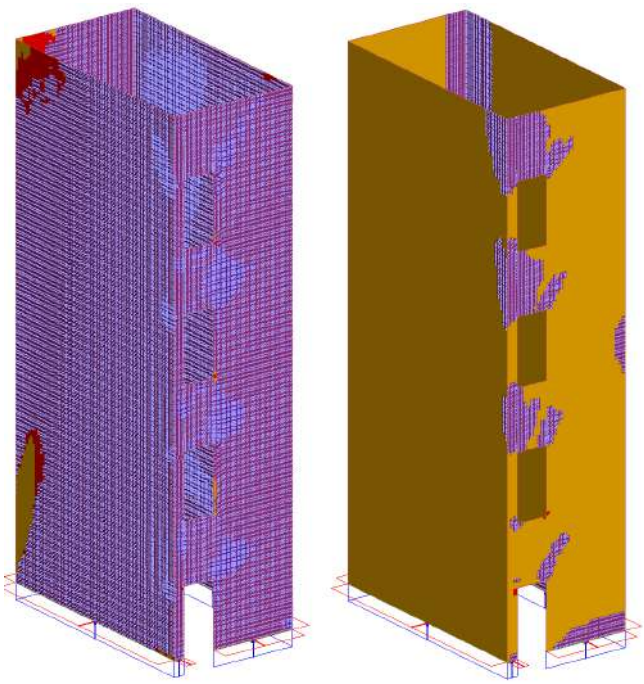

126. Figure - Bottom concrete layer plastic condition results

Fig. 127 shows the top concrete layer plastic condition results in Case A and C based on FEM-Design calculation at the ultimate load levels.

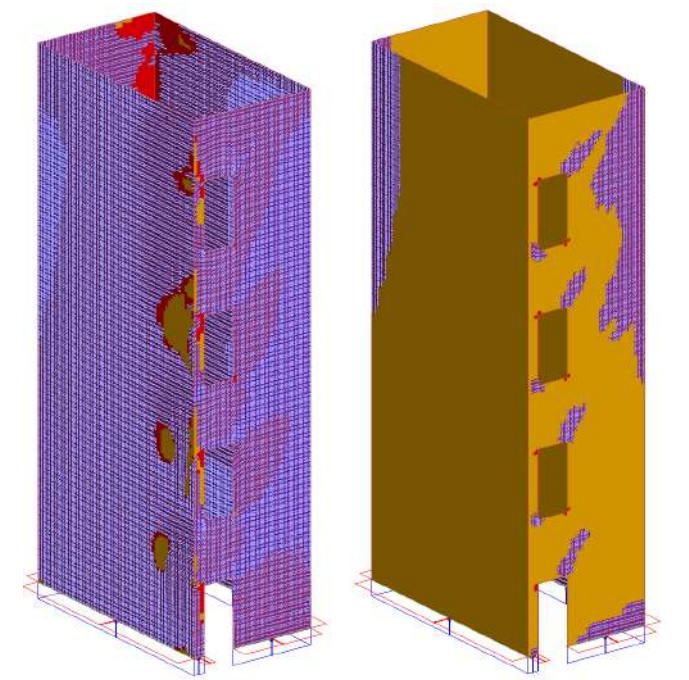

127. Figure - Top concrete layer plastic condition results

Fig. 128 shows the bottom x directional reinforcement layer plastic condition results in Case A and C based on FEM-Design calculation at the ultimate load levels.

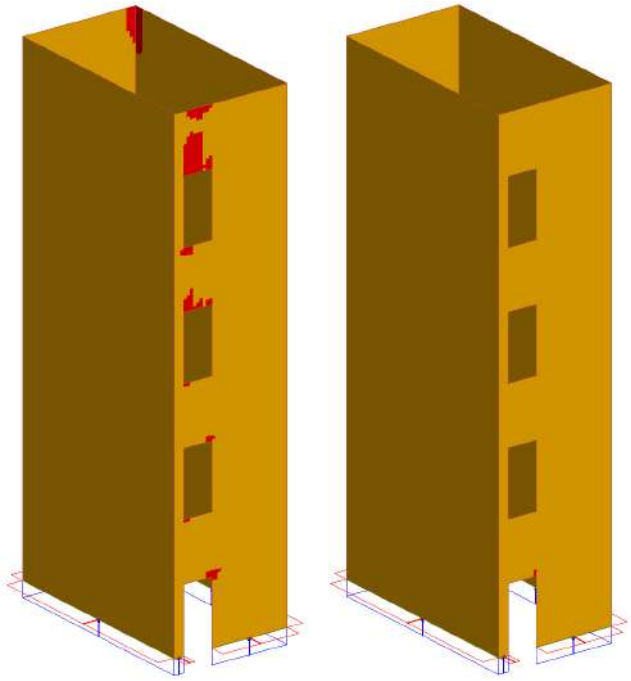

128. Figure - The bottom x directional reinforcement layer plastic condition

Fig. 129 shows the top x directional reinforcement layer plastic condition results in Case A and C based on FEM-Design calculation at the ultimate load levels.

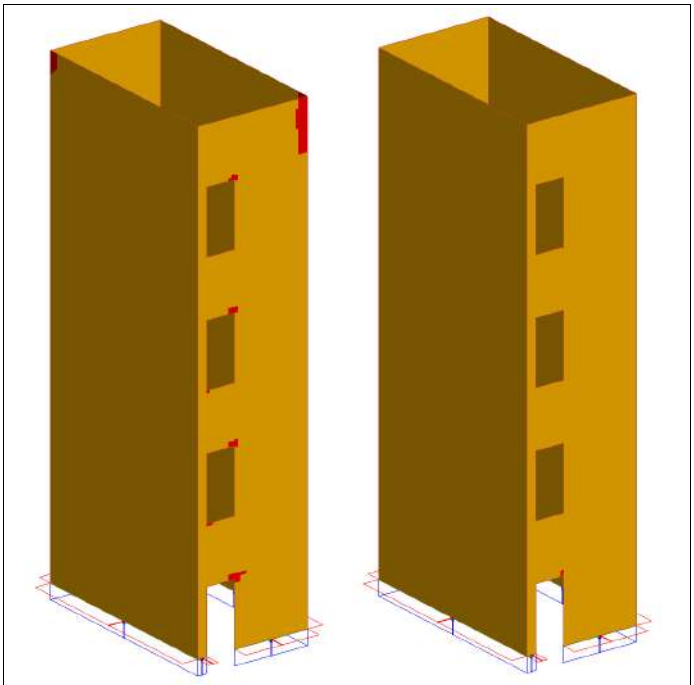

129. Figure - The top x directional reinforcement layer plastic condition

Fig. 130 shows the bottom y directional reinforcement layer plastic condition results in Case A

and C based on FEM-Design calculation at the ultimate load levels.

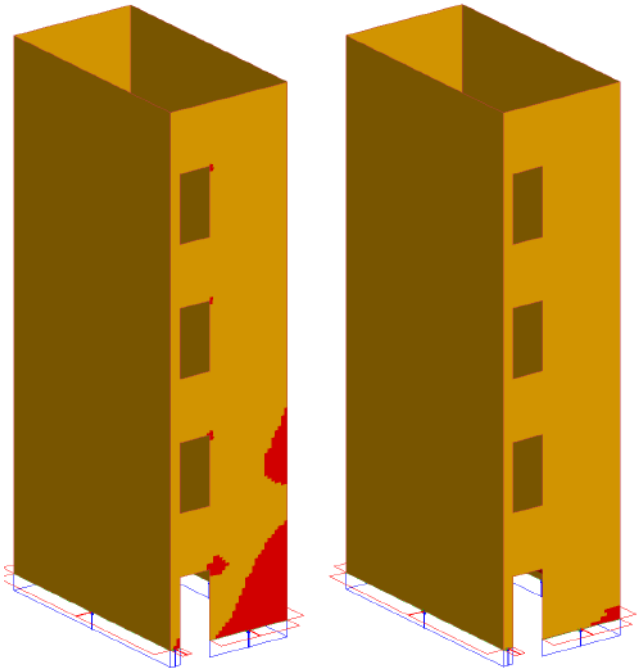

130. Figure - The bottom y directional reinforcement layer plastic condition

Fig. 131 shows the top y directional reinforcement layer plastic condition results in Case A and C based on FEM-Design calculation at the ultimate load levels.

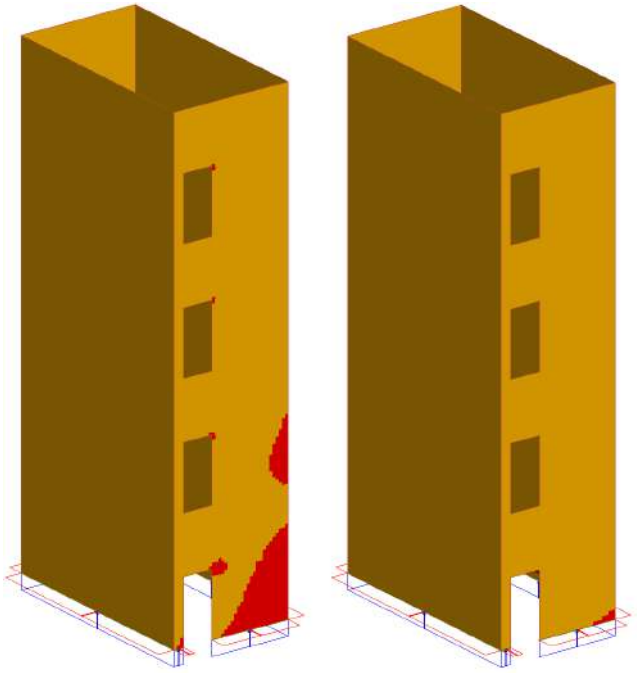

131. Figure - The top y directional reinforcement layer plastic condition

The ultimate shear load level of the structure based on FEM-Design calculation is:

$p_{shear\ FD} \approx 150\,\mathrm{kN/m}$

$p_{shear\ FD,\ hinged} \approx 102\,\mathrm{kN/m}$

The load displacement curve from FEM-Design with the proper settings follows the Ref. [22] values and taken into account that the benchmark doesn't provide exactly the ultimate load level considering strain check, the ultimate load level of the structure should be around the value what FEM-Design provided due to the fact that in FEM-Design the ultimate strains were considered in the calculations. In the different FEM-Design calculations the ultimate load levels are the same regardless the tension stiffening rules. The hinged case calculation result exactly matches with the membrane type calculation of the mentioned reference. In this case the strain limit was not the critical part, as you can see in Fig. 120. In the fixed continuous edge case the ultimate load based on FEM-Design is adequate, because it considers the strain limits as well, see Fig. 120 The reference result shows the load-displacement curve without the proper strain limit check that is why it gives higher load-bearing capacity on the curve but that is only theoretical without the strain limit checks according to the limit analysis!

Thus we can say that FEM-Design provided the proper load-bearing capacity in the simplified case and in the advanced case as well, where the strain limits were considered properly in the calculation.

References

[1] E. Hinton, D.R.J. Owen , Finite element software for plates and shells, Department of Civil Engineering, University College of Swansea, U.K.: Pineridge Press Limited, 1984
[2] D. R. J. Owen , E. Hinton, Finite Elements in Plasticity: Theory and Practice, Department of Civil Engineering, University College of Swansea, U.K.: Pineridge Press Limited, 1980
[3] J.A. Figueiras, D.R.J. Owen (supervisor), "Ultimate load analysis of anisotropic and reinforced concrete plates and shells", PhD Thesis, University of Wales, 1983
[4] M. Cervera, E. Hinton and O. Hassan, "Nonlinear analysis of reinforced concrete plate and shell structures using 20-noded isoparametric brick elements", Computers & structures, vol.25, no. 6, pp. 845-869, 1987
[5] J. N. Reddy, "An evaluation of equivalent-single-layer and layerwise theories of composite laminates", Composite structures, vol.25, no. 1-4, pp. 21-35, 1993
[6] RD Midlin, "Influence of Rotary Inertia and Shear on Flexural Motions of Elastic Plates", Trans. ASME. J. of Applied Mechanics, vol.18, no. 0, pp. 31-38, 1951
[7] K. Yeongbin, PS. Lee, KJ. Bathe, "The MITC4+ shell element and its performance", Computers and Structures, vol.169, no. 0, pp. 57-68, 2016
[8] PS. Lee, KJ.Bathe, "Development of MITC isotropic triangular shell finite elements", Computers & Structures, vol.82, no. 11-12, pp. 945-962, 2004
[9] M.A. Crisfield, Non-Linear Finite Element Analysis of Solids and Structures, Essentials, Volume 1, London, UK: John Wiley & Sons, 1991
[10] M.A. Crisfield, Non-Linear Finite Element Analysis of Solids and Structures, Advanced Topics, Volume 2, London, UK: John Wiley & Sons, 1997
[11] J.N. Reddy, Mechanics of laminated composite plates and shells: theory and analysis, : CRC press, 2003
[12] K.J. Bathe, Finite Element Procedures, Upper Saddle River, NJ: Prentice-Hall, 1982
[13] Chen, Wai-Fah and Han, Da-Jian, Plasticity for structural engineers, : J. Ross publishing, 2007
[14] H. Kupfer, H. Hilsdorf and H. Rusch, "Behavior of concrete under biaxial stresses", Journal proceedings, vol.66, no. 8, pp. 656-666, 1969
[15] G. Hofstetter, G. Meschke, Numerical modeling of concrete cracking, : Springer Science & Business Media, 2011
[16] F.J. Vecchio, M.P. Collins, "The Modified Compression-Field Theory for Reinforced Concrete Elements Subjected to Shear", , vol.83, no. 2, pp. 219-231, 1986
[17] P.K. Mehta, P JM Monteiro, Concrete: microstructure, properties, and materials, : McGraw-Hill Education, 2014
[18] Walter Kaufmann et al., Compatible Stress Field Design of Structural Concrete, Compatible Stress Field Design of Structural Concrete: ETH Zurich, Institute of Structural Engineering, 2020
[19] F.J. Vecchio, "Disturbed stress field model for reinforced concrete: formulation", Journal of structural engineering, vol.126, no. 9, pp. 1070-1077, 2000
[20] N. Friedman, Z. Huszár, K. Rita, K. Klinka, T. Kovács, I. Völgyi, Reinforced Concrete Structures Example Book, Budapest, Hungary: ISBN 978-963-420-903-4, 2007
[21] B. Bresler, A.C. Scordelis, "Shear strength of reinforced concrete beams", ACI Journal, vol.60, no. 1, pp. 51-73, 1963
[22] D. Vestergaard, "Design-Oriented Nonlinear Modeling of Reinforced Concrete Wall Structures for Numerical Limit State Analysis", PhD Thesis, Technical University of Denmark, 2022
[23] H. Duddeck, G. Griebenow, G. Schaper, "Auszuge aus dem sechsten arbeitsbericht zum

forschungsvorhaben stahlbetonplatten mit nichlinearen stoffgesetzen", , vol., no. , pp. , 1976
[24] G. Mueller, "Numerical problems in nonlinear analysis of reinforced concrete", , vol., no. , pp. , 1977
[25] H. Duddeck, G. Griebenow, G. Schaper, "Material and time dependent nonlinear behaviour of cracked reinforced concrete slabs", , vol., no. 1, pp. 101-113, 1978
[26] R. Taylor, D.R.H. Maher, B. Hayes, "Effect of the arrangement of the reinforcement on the behaviour of reinforced concrete slabs", , vol.18, no. 55, pp. 85-94, 1966
[27] E.N. Fox, "Limit analysis for plates: the exact solution for clamped square plate of isotropic homogeneous material obeying the square yield criterion and loaded by unifrom pressure", , vol.277, no. 1265, pp. , 1974
[28] F.J. Vecchio, C.C.L. Chan, "Reinforced Concrete Membrane Elements with Perforations", Journal of Structural Engineering, vol.116, no. 9, pp. 2344-2360, 1990

8 Notes